An Experimental Study on the Inflation of Non-Elastic Tubes

by

Jack Wurster Pazin

Bachelor of Science in Mechanical Engineering, University of Virginia, 2022

Submitted to the Graduate Faculty of the

Swanson School of Engineering in partial fulfillment

of the requirements for the degree of

Master of Science in Mechanical Engineering

University of Pittsburgh

2024

UNIVERSITY OF PITTSBURGH

SWANSON SCHOOL OF ENGINEERING

This thesis was presented

by

Jack Wurster Pazin

It was defended on

April 29, 2024

and approved by

David Schmidt, PhD, Professor, Department of Mechanical Engineering and Materials Science

Patrick Smolinski, PhD, Professor, Department of Mechanical Engineering and Materials Science

Thesis Advisor: Sachin Velankar, PhD, Professor, Department of Chemical and Petroleum Engineering

An Experimental Study on the Inflation of Non-Elastic Tubes

Jack Wurster Pazin, MS

University of Pittsburgh, 2024

Rubber tubes may experience localized bulging during inflation with one familiar example being the inflation of long rubber ballons. Assuming hyperelastic behavior, the presence of a pressure maximum in the pressure-volume response predicts the initiation of bulging instabilities during inflation. Furthermore, the hyperelastic material's strain hardening behavior can be used to predict the evolution of the bulge with continued inflation. However, research on bulging instabilities in non-elastic tubes is limited. In this thesis, polyurethane elastomer and low-density polyethylene (LDPE) tubes were subjected to volume-controlled inflation with no constraints on axial elongation. The polyurethane tubes upon inflation showed an axisymmetric bulging instability with numerous differences as compared to the behavior expected from hyperelastic tubes: appearance of irregularly bulged shapes, gradual (rather than abrupt) bulge growth, a maximum in the pressure-volume curve even when tube inflates homogeneously, a greater degree of bulging at low inflation rates, and irreversible inflation. Qualitatively, a least some of these behaviors can be explained based on material viscoelasticity. The behavior of the LDPE tubes deviated from hyperelastic tubes even qualitatively: a nonaxisymmetric bulge appeared followed by rupture shortly after. The behavior was only weakly sensitive to inflation rate, but the bulge deformation was almost completely irreversible, with little or no shape recovery upon deflation. Additional experiments were conducted with an external cylindrical shell ("limiter") to simulate the sudden onset of strain hardening. With such a limiter, the nonaxisymmetric bulge propagated

axially in a stable fashion. Cross sections of these samples showed that the nonaxisymmetric bulges resembled necking instabilities in the tangential direction. To our knowledge, this is the first documented example of a non-axisymmetric propagating bulge instability. The dependence of the propagation characteristics on limiter diameter were also studied.

Table of Contents

List of Tables

List of Figures

1.0 Introduction

Cylindrical tubes are used in many applications including the transport of fluids, the storage of pressurized materials, and soft robotics [1]. Tubes often need to be able to handle high pressures without rupturing. They can be made of many different types of materials including metals, rubbers, and plastics. Pressurized metal tubes such as pipes and gas cylinders typically fail at relatively small strains experienced. If kept below the yield strength, Hooke's Law is applicable and the wall stresses can be found using relatively simple equations. In these tubes, the stresses are generally highest in the tangential (hoop) direction. If the wall thickness is much less than the diameter, the stress in the tangential direction is twice that of the axial direction and the radial stress becomes negligible. Furthermore, deformations remain relatively small even beyond the yield strength and failure is commonly accompanied by a crack in the axial direction due to the high tangential stresses. An example of a pipe cracked in this manner can be seen in Figure 1.1.

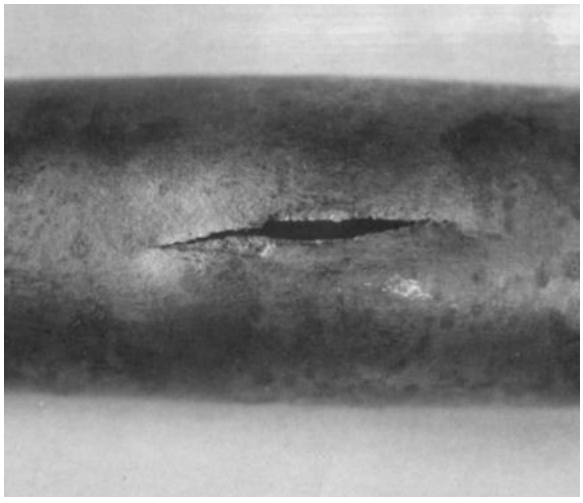

Figure 1.1 Burst Copper Tube. Note that the deformations are relatively small even after failure. The split occurred in the axial direction due to the high tangential stress [8]

Although tubes made in many traditional engineering materials such as metals experience small deformations and can be treated as linearly elastic when below the yield point, the same cannot be said for some other materials including plastics and rubbers. The failure of rubbers usually requires large deformations. This results in Hooke's Law breaking down even when the material does not yield. As a result, nonlinear elasticity is applied to examine their deformation behavior prior to failure. Hyperelastic models come from the idea that all elastic materials store energy when deformed and release all of that stored energy when allowed to return to their original configurations. These models can be used to calculate the stress experienced during deformation and can be applied to the inflation of rubber tubes. Rubber tubes often experience bulging behavior when inflated to high enough pressures due to the presence of mechanical instabilities. These bulges are axisymmetric and can propagate axially or indefinitely expand radially depending on the amount of strain hardening. An example of a propagating bulge is an inflating balloon and is shown in Figure 1.2. Their behavior has been successfully modeled in previous literature [5-6].

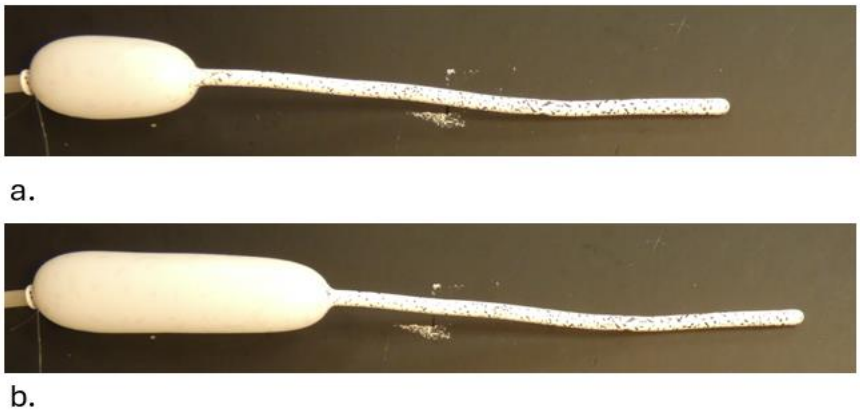

Figure 1.2 a. Balloon inflation shortly after localization. b. Balloon inflation during propagation.

Although elastic tubes experiencing both small and large deformations have been modeled successfully, factors beyond elasticity have been neglected [2] [3] [5] [6]. The effect of yielding on inflation behavior has not been determined. Also, many materials such as plastics have properties that vary with strain rate. Plastics often become stiffer if deformed at higher rates [9]. Another factor not previously studied is strain history dependence. Although rubbers experience a decrease in stiffness over their first few loading cycles, this effect has not been studied extensively but previous literature studying the inflation of rubber tubes involved "preconditioning" the tubes before inflation by stretching them repeatedly [5] [6]. This was not done to study history dependence but instead to erase it so and hence ensure consistent results [5-6]. Yet another factor not previously studied is the effect of stress relaxation on localization. Many plastics experience a decrease in stress when held at constant strain and testing this effect on localization could be done by inflating a tube to a set volume and holding it at that volume for an extended period [36] [38]. Previous literature has found that holding polyethylene pipes at a constant pressure causes creep which eventually leads to either a ductile or brittle fracture depending on the specific resin used [37]. Although previous literature covers instabilities in elastic tubes well, it fails to account for plasticity, strain rate dependence, history dependence, and stress relaxation. In this thesis, polyurethane and low-density polyethylene (LDPE) tubes will be inflated to evaluate situations where hyperelasticity fails.

Following this Introduction, this document contains five additional chapters. Chapter 2 reviews previous research on the mechanical behavior of hyperelastic isotropic tubes undergoing inflation. This section evaluates previous research on tubes undergoing both small and large deformations. The tubes undergoing small deformations are evaluated using linear elasticity with

separate subsections discussing thin and thick-walled tubes. The subsection discussing large deformations considers the Neo-Hookean and Ogden models. It also mentions the formation of localized bulges during inflation and talks about the conditions required for them to form.

Chapter 3 reviews the materials and the experimental methods used. The experimental methods section discusses how the tubes in this document were inflated as well as problems that were addressed along the way.

Chapter 4 describes the inflation of polyurethane tubes with small deviations from purely elastic behavior. This section discusses the general behavior of polyurethane tubes during inflation including the pressure-volume curves. It also looks at how the behavior changes with flow rate, previous loading history, and other factors.

Chapter 5 describes the inflation of low-density polyethylene (LDPE) tubes with severe deviation from elastic behavior. Specifically, these tubes show yielding behavior followed by large permanent deformation which affects their inflation behavior. This chapter analyzes inflation with and without an external limiter, general remarks on the pressure-volume curves, and how quickly bulges propagate. Variables such as external limiter diameter and flow rate were changed to evaluate their effects on the pressure-volume curve and bulge shape.

Chapter 6 presents a summary and comment on directions for future work.

2.0 Physics of Tubes Undergoing Inflation

2.1 Linearly Elastic Thin-Walled Tubes

The principal stresses are as follows: the radial stress $\boldsymbol{\sigma_r}$, the tangential stress $\boldsymbol{\sigma_\theta}$, and the axial stress $\boldsymbol{\sigma_z}$. If the tube is linearly elastic and isotropic, mechanics can be derived using assumptions regarding thin-walled geometry and by simple force balance. These equations were derived in [2-3]. Equations **2-1** through **2-3**

define the principal stresses experienced in thin-walled linearly elastic isotropic tubes**.**

Table 2.1 Defining variable symbols.

Variable symbol	Variable description
σ_r	Radial stress
σ_θ	Hoop stress
σ_z	Axial stress
E	Elastic modulus
P	Internal pressure
R	Radius (thin-walled tube, initial configuration)
R_1	Inner radius (thick-walled tube, initial configuration)

R_2	Outer radius (thick-walled tube, initial configuration)
r_2	Outer radius (thick-walled tube, current configuration)
ν	Poisson's Ratio
ϵ_r	Radial strain
ϵ_θ	Hoop strain
ϵ_z	Axial strain
r	Radial coordinate of point being evaluated (thick-walled tube)
$R_{1,\ narrow}$	Inner radius of unexpanded section
$R_{1,\ wide}$	Inner radius of bulged section
$R_{2,\ narrow}$	Outer radius of unexpanded section
$R_{2,\ wide}$	Outer radius of bulged section
f	Volumetric flow rate
L	Tube length
v	Propagation velocity
T	Wall thickness
t	Time

$$\sigma_r = 0 \qquad \textbf{2-1}$$

$$\sigma_\theta = \frac{PR}{T} \quad \textbf{2-2}$$

$$\sigma_z = \frac{PR}{2T} \quad \textbf{2-3}$$

When the equations for σ_θ and σ_z are substituted and simplified, the final equations for the principal strains are written below.

$$\epsilon_r = \frac{-3\nu PR}{2ET} \quad \textbf{2-4}$$

$$\epsilon_\theta = \frac{(2-\nu)PR}{2ET} \quad \textbf{2-5}$$

$$\epsilon_z = \frac{(1-2\nu)PR}{2ET} \quad \textbf{2-6}$$

If the tube is assumed to be incompressible ($\nu = 0.5$), it can readily be seen that the axial strain reduces to 0.

2.2 Linearly Elastic Thick-Walled Tubes

Calculating the stresses within thick-walled tubes is more complex even when assuming the material of the tube to be linearly elastic and isotropic. The equations for the radial, tangential, and axial stresses are shown below.

$$\sigma_r = \frac{PR_1^2}{R_2^2 - R_1^2}\left(1 - \frac{R_2^2}{r^2}\right) \quad \textbf{2-7}$$

$$\sigma_\theta = \frac{PR_1^2}{R_2^2 - R_1^2}\left(1 + \frac{R_2^2}{r^2}\right) \quad \textbf{2-8}$$

$$\sigma_z = \frac{PR_1^2}{R_2^2 - R_1^2} \quad \textbf{2-9}$$

The strains can be readily calculated if E and ν are also known. When the values for the stresses are substituted, the equations for the strains become

$$\epsilon_r = \frac{(1-2\nu)PR_1^2}{E(R_2^2 - R_1^2)} - \frac{(1+\nu)R_2^2}{Er^2} \quad \textbf{2-10}$$

$$\epsilon_\theta = \frac{(1-2\nu)PR_1^2}{E(R_2^2 - R_1^2)} + \frac{(1+\nu)R_2^2}{Er^2} \quad \textbf{2-11}$$

$$\epsilon_z = \frac{(1-2\nu)PR_1^2}{E(R_2^2 - R_1^2)} \quad \textbf{2-12}$$

If the tube is incompressible, the equations reduce to

$$\epsilon_r = -\frac{3PR_2^2}{2Er^2} \quad \textbf{2-13}$$

$$\epsilon_\theta = \frac{3PR_2^2}{2Er^2} \quad \textbf{2-14}$$

$$\epsilon_z = 0 \quad \textbf{2-15}$$

Like thin-walled tubes, linearly elastic isotropic thick-walled tubes have no axial strain when incompressible and experience positive axial strain when compressible.

2.3 Large Elastic Deformations (Neo-Hookean Model)

When large deformations are considered, the Neo-Hookean Model is the simplest model used for hyperelastic isotropic materials. It involves the use of a strain energy density function.

$$W = C_1(I_1 - 3) \quad \textbf{2-16}$$

In equation Large Elastic Deformations (Neo-Hookean Model)

, $I_1 = \lambda_1^2 + \lambda_2^2 + \lambda_3^2$ and I_1 is known as the first principal invariant. The two other invariants are $I_2 = \lambda_1^2\lambda_2^2 + \lambda_2^2\lambda_3^2 + \lambda_1^2\lambda_3^2$ and $I_3 = \lambda_1^2\lambda_2^2\lambda_3^2$ where the λs are the principal stretches. This model predicts that the pressure inside an inflating tube initially rises sharply, peaks, and decreases asymptotically to zero. In Figure 2.1, a pressure-volume curve for a Neo-Hookean tube is shown while assuming homogeneous expansion. However, this prediction assumes that the tube expands

uniformly which does not happen in practice due to the tube becoming unstable due to the presence of a pressure maximum. Instead, a bulge suddenly forms at the peak pressure causing a sudden drop in the pressure. An example of this will be discussed in Chapter 4.

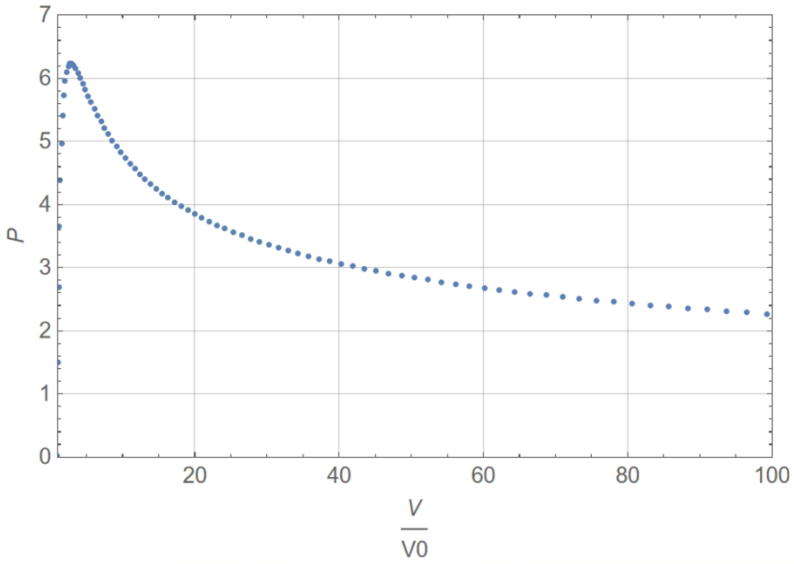

Figure 2.1 Example pressure-volume curve for a Neo-Hookean tube assuming uniform expansion. Calculated curve provided by Fatemeh Rouhani.

2.4 Large Elastic Deformations (Ogden and Other Models)

As briefly mentioned in the previous subsection, some cylindrical tubes and other inflatable devices experience bulging during inflation [5-7]. Examples include the bulging of tires and balloons [7]. Inflating a tube may cause one part of the tube to suddenly expand despite the pressure staying constant throughout the tube. In theory, a perfectly cylindrical tube could bulge at any arbitrary location but bulging usually occurs at defects in practice [5-6]. So far, most of the research done on bulging during tube inflation has only involved hyperelastic tubes [5-6]. Bulging can be predicted from the degree of strain hardening of the material. The amount of strain hardening can

be qualitatively evaluated by plotting the pressure-volume curve while assuming homogeneous expansion. A monotonic increase in pressure would predict uniform expansion and a high amount of strain hardening. A dip followed by an increase would predict localization with propagation and moderate strain hardening. Finally, pressure that rises followed by asymptotically approaching zero would imply localization with only radial expansion and low strain hardening [6]. Propagation pressure can be predicted through an equal-area construction [5-6] as illustrated in Figure 2.2. The pressure-volume curve on the equal-area plot is the theoretical curve expected if no bulge appears. The horizontal line corresponding to the equal area construction minimizes the energy needed to inflate the tube after bulging and therefore predicts the propagation pressure [5-6]. Also, this means that after the tube follows the loading path up to the peak pressure, the pressure abruptly drops to the propagation pressure. During that process, a bulge forms and propagates once inflated further. The propagating bulge results in a tube with two coexisting diameters as seen in Figure 1.2.

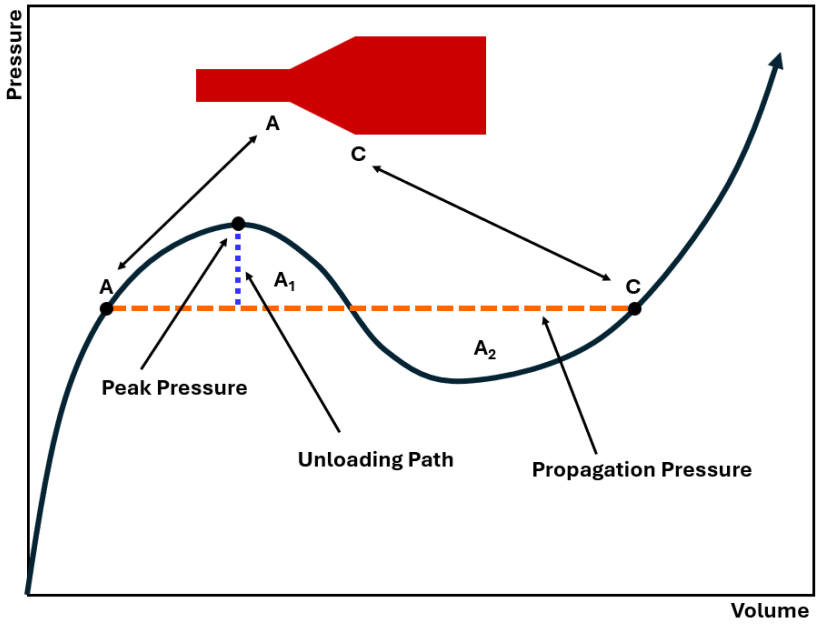

Figure 2.2 Equal-area plot superimposed on pressure-volume curve that assumes uniform expansion.

Previous research has shown that the ability for a tube to localize depends on the amount of strain hardening [6]. Assuming no axial stretch, one would expect a linearly elastic tube to only bulge in the radial direction. In Figure 2.3, theoretical pressure-volume curves are plotted using the Ogden Model and assume uniform expansion. In these curves, a low amount of strain hardening implies that an instability will form once the pressure maximum is reached and that the bulged region will keep expanding radially due to the lack of strain hardening. A moderate amount of strain hardening results in the formation of a bulge at the pressure maximum but forces the bulge to stop growing radially once sufficiently large. The bulge will propagate axially with further inflation. A monotonic increase in pressure implies that the strain hardening is high enough to prevent the formation of an instability.

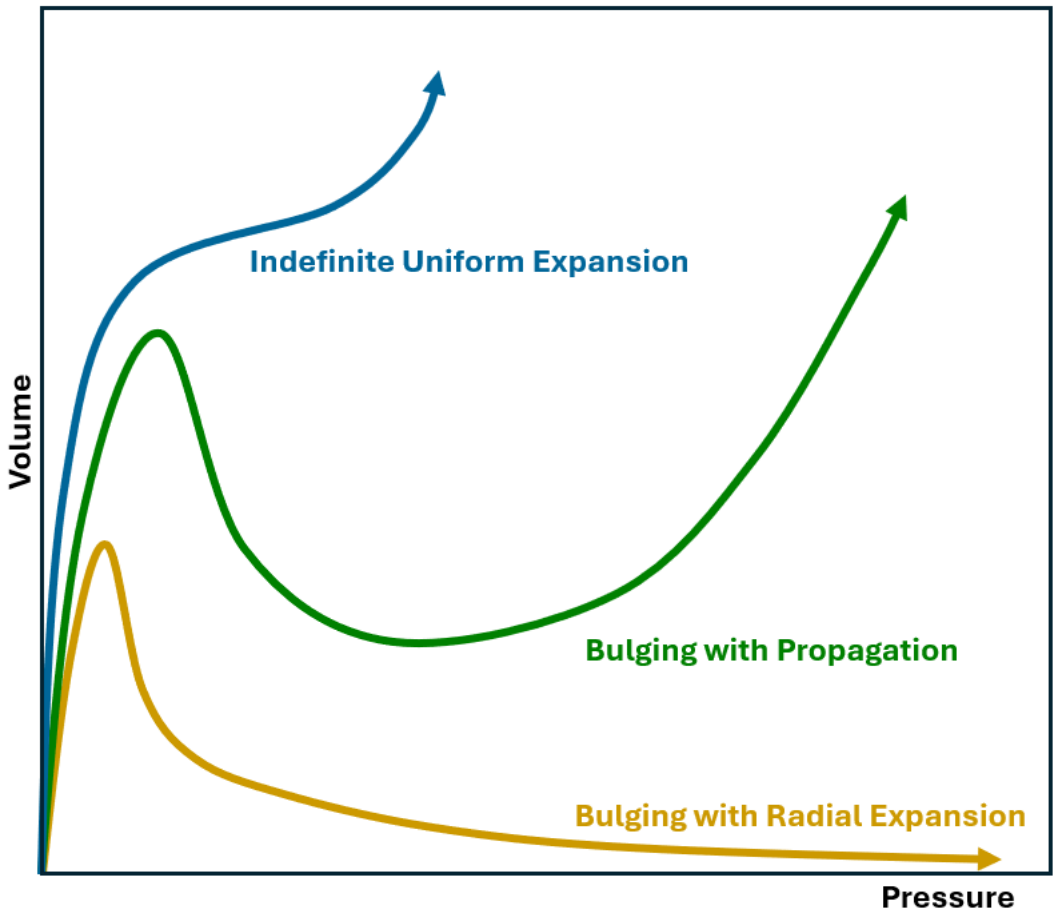

Figure 2.3 Strain hardening conditions required for uniform expansion, localization with propagation, and localization with radial expansion.

Some previous research was based on the Ogden Model to model the behavior of latex tubes under inflation [5-6]. Calculated pressure-volume curves with the parameters adjusted for different amounts of strain hardening were used to predict the bulging behavior of the tubes.

2.5 Large Non-Elastic Deformations

Although the research on large inelastic deformations is limited, there is still some literature describing the effects of inflation on materials that cannot be modeled as hyperelastic. Previous literature has modeled the inflation of aluminum alloy tubes and found necking in the tangential direction occurred shortly after the pressure was maximized. Fracture occurred in the axial direction [8]. Similar behaviors were seen in copper tubes although the necking was less pronounced [8]. Literature evaluating the inflation of anisotropic aluminum tubes also found necking shortly before rupture with parts of the tube walls experiencing localized thinning by as much as 13%. These tubes were inflated at a constantly increasing manner while also being axially loaded such that the axial stress was ¾ of the hoop stress [42]. Fracture also occurred along the axial direction as seen previously [8] [42].

The inflation of viscoelastic materials has been studied. One such paper evaluates the inflation of rodent bladders with a constant flow rate of 100μL/min until a pressure of 25mmHg was reached. The pump was then shut off while the fluid was kept inside the bladder. A pressure-time plot was then provided. The pressure-time plot showed a rise in pressure during inflation and the rate of increase in pressure was greater as the pressure increased. Once the pump was stopped, the pressure dropped rapidly at first and appeared to reach a plateau [35]. However, the bladders were roughly spherical and did not appear to show any mechanical instabilities during inflation.

Another paper evaluated the effect of plasticity in tubes undergoing inflation. Simulations involving an elastic-viscoplastic model and material parameters similar to polycarbonate were run. These simulations were run at a constant rate of pressure increase until yielding and were then run at a constant increase in volume. Necking happened in the tangential direction shortly after yielding which was expected since stresses were the highest in that direction [26]. Although work

has been done with simulations describing how plasticity affects the formation of inflation instabilities, limited experimental research has been conducted on large deformation plasticity during inflation. Also, the strains in the necked regions were smaller than what was seen in the experiments in this thesis.

3.0 Setup and Procedure

The main components of the setup are a water source, a positive displacement pump, a pressure gauge, a tube sample, two cameras, and two valves. The positive displacement pump receives water from the source and forces a set flow rate. Steel tubing connects the pump to the tube and the pressure gauge. Steel tubing was chosen to reduce compliance in the system and reduce the chance of rupture when pressurized. A soft, clear plastic pipe guides water from the top valve back to the source and this was chosen to allow for air bubbles to be visible when evacuating air from the system while allowing enough compliance to rotate the system. Both valves are on-off ball valves as early tests found significant leakage when other types of valves were used.

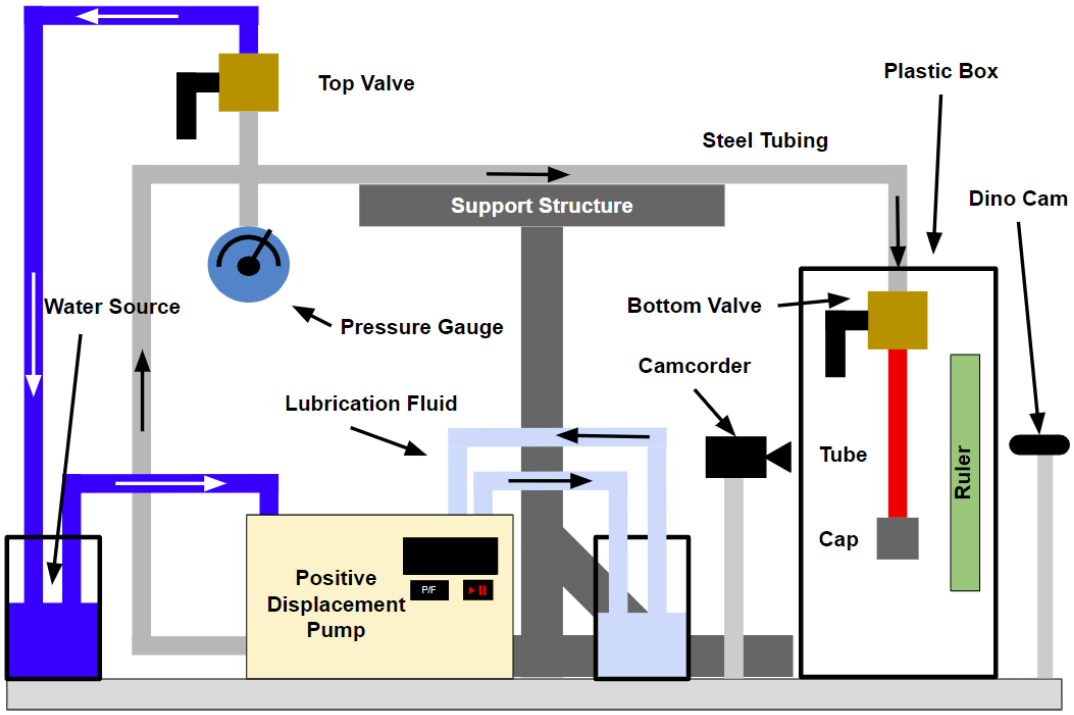

Figure 3.1 Experimental setup

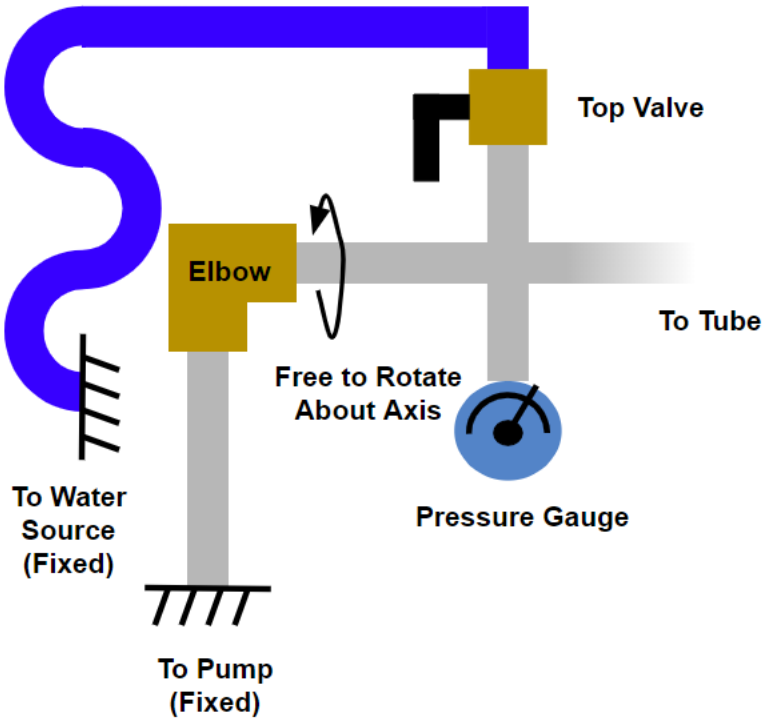

Figure 3.2 Being able to freely rotate the pipe that connects to the pressure gauge and the tube makes it easier to remove air before a test .

3.1 General Procedure: Closed Valve Tests

These tests were done to test the compliance of the testing setup itself. This compliance must be subtracted from the compliance of the tube (next paragraph) in cases when the tube is relatively stiff. The air had to be evacuated out of the system before running the test. Evacuating the air was done by turning portion of the system indicated in Figure 3.2 upside down, closing the top valve, opening the exit valve, and providing a fast flow rate. The system was kept this way until a steady stream of water was flowing out the valve for several seconds. Turning the system upside down is simply done by rotating the top part of the steel tubing while keeping the other

components right side up since there is a pipe elbow behind the pressure gauge that only allows rotation along the pipe's axis. The pump was shut off and the bottom valve was closed while the system was still upside down. The system was then turned right side up and the top valve was opened. The pump was restarted at a fast flow rate and kept running until there were no bubbles above the top valve for at least several seconds. The pump was shut off and the top valve was closed. The flow rate was then set to 0.2mL/min before starting. The pump and pressure gauge were started simultaneously and the system was pressurized to 2.5MPa before the pump and pressure gauge were shut off at the same time. The top valve was then opened to depressurize the system and conclude the trial.

3.2 General Procedure: Tube Pressurization Tests

The general procedure involved inflating plastic tubes with water at a constant flow rate and measuring the pressure versus time. The experiments were initiated by choosing a fast flow rate, rotating the testing device so the bottom valve is pointed upwards. This was continued until a steady stream of water eluted out the open valve for several seconds. The valve was closed and the pump was shut off. The system was rotated right side up before opening the top valve. The pump was restarted to bleed air out of the top before being shut off again. The tube was marked with ink dots or with small glitter particles and then attached to the top valve with the defect being near the top of the tube. Two cuffs were added to prevent deformation near each valve to prevent leaks. The system was turned upside down again with the bottom valve open and the pump turned on again to drain the air out of the tube. While the system was still upside down, the cap for the

end of the tube was filled with water and the pump was shut off before attaching the cap to the tube. The testing device was flipped back to its normal orientation again. The desired flow rate was set on the pump and the camcorder was started. These two cameras allowed for views at two different magnifications. The pressure gauge and pump were then started simultaneously. Once the propagation front approaches bottom cuff, the pump and pressure gauge were simultaneously shut off and the top valve was opened to depressurize the system. Both valves were then closed before releasing the tube while minimizing the leakage. The process for evacuating the air had to repeated every time a tube was changed since air leaked into the system every time a tube was changed.

4.0 Mildly Plastic Polyurethane Tubes

4.1 Introduction

When a long elastomeric tube such as a rubber hose is inflated, it can exhibit two limiting behaviors: homogeneous expansion maintaining a cylindrical shape (not shown), or coexistence between two cylindrical regions one of which is much more inflated than the other (Figure 4.1a). The latter behavior is often called a *propagating instability* because as the tube is inflated, the more-inflated region propagates axially with no change in pressure or diameter of either region [1]–[8]. A third behavior – a localized bulge that expands to bursting [9], [10]– may be regarded as a special case of Figure 4.1a where the more-inflated region of the tube ruptures before coexistence between the two states is achieved. These behaviors can be captured by hyperelastic models of material behavior where the degree of strain hardening and the tube geometry (i.e. ratio of inner to outer diameter) determine which of these behaviors appear. Previous articles by Fu and coauthors have provided a succinct summary of the sequence of research from the 1960s understanding bulging of elastic tubes [7], [11].

However, these limiting cases are overly simplistic and more complex behavior may appear, as illustrated in Figure 4.1b-d. Even though all three specimens were cut from the same spool of polyurethane tubing and inflated identically, they show distinct inflations. These behaviors do not cleanly resemble either homogeneous inflation or the bulge propagation instability of Figure 4.1a; instead, the tubes inflated in an irregular fashion, sometimes with multiple bulges separated by less-inflated regions. More strikingly than the irregular inflation, the bulges in the polyurethane tubes grow over timescales of minutes to hours, whereas in hyperelastic tubes bulge growth is almost instantaneous. These tubes also show rate dependent inflation behavior, permanent deformation upon unloading, and loading-reloading hysteresis, all of which will be discussed below. None of these complexities can be captured by existing theories based on hyperelastic material models.

This paper is an experimental study of tube inflation that includes mechanical behaviors

beyond hyperelasticity. We examine the role of inelastic deformation, viscoelasticity, and strain-induced damage (i.e. permanent changes in properties upon first inflation) on the inflation behavior of polyurethane elastomer tubes. These tubes were selected to be approximately elastic, i.e. their behavior resembles that of hyperelastic tubes at least qualitatively. In a later article [12], [13] we will also examine large deformation inflation of polyethylene "plastic" tubes which inflate in a non-axisymmetric manner which is qualitatively different from hyperelastic tubes [14]–[18].

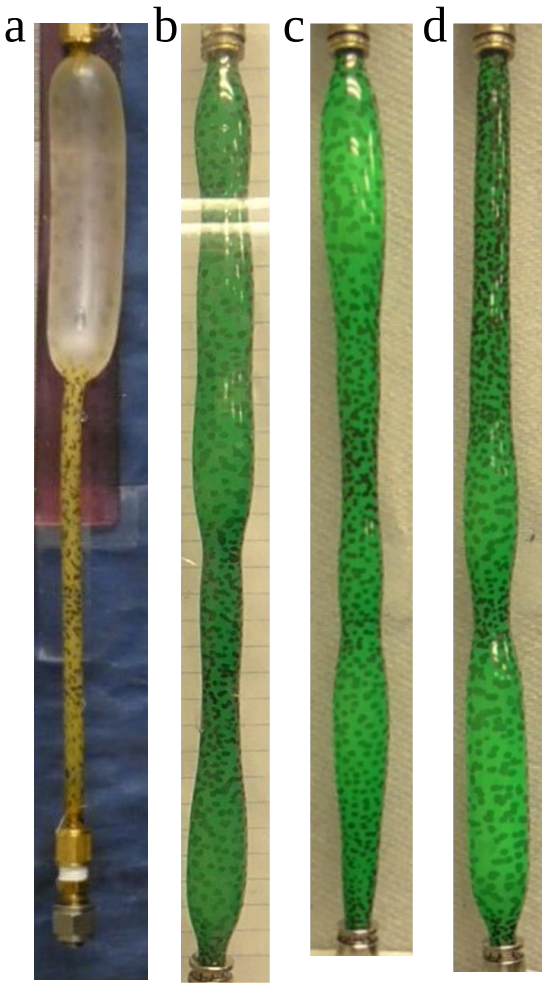

Figure 4.1 Bulge propagation in a natural rubber tube in which a more-bulged region coexists with a less-inflated region, As fluid is pumped in, the bulged region propagates axially with no change in diameter. b-d. Irregular expansion of three polyurethane tubes inflated under the same conditions. All three were cut from the same spool of tubing had

similar initial length. The dark splotches on each tube are ink marks to help visualize the local area changes.

Incidentally we note that even ordinary rubber balloons – which are often cited in the literature on inflation instabilities of hyperelastic tubes – can sometimes show some of these complexities. For example, inflating a rubber balloon into the bulge propagation regime such as Figure 4.1a and then deflating it induces a permanent increase in diameter. A second inflation can then yield three coexisting diameters, the smallest of which corresponds to the portion of the balloon that has never experienced large inflation (Appendix Figure 4). Such complexities are rarely discussed in the literature. Indeed experimental papers on inflation instabilities sometimes mention that they "preconditioned" their samples by stretching them repeatedly prior to inflation [19]–[22], and it is only this preconditioning that allows them to be modeled as hyperelastic.

4.2 Experiments

Tensile testing: Polyurethane tubes, with an outer diameter of 1/4 inch (6.35 mm) and an inner diameter of 5/32 inch (3.97 mm), were purchased from McMaster-Carr Supply Co. The tubes were available in the form of rolled spools and hence were bent to a radius of curvature of 120-130 mm in their stress-free configuration. This inherent curvature had no noticeable effect on the inflation behavior.

Uniaxial tests were conducted using an Instron model 34TM-30 tensile testing machine equipped with a 30 kN load cell. The clamp to clamp length of the samples was 50 mm, and they were stretched at 25 mm/min (i.e. a nominal rate of 50% per minute) to various strains. The corresponding tensile data (Figure 4.2a) give a tensile modulus of 56 MPa. As with many polymeric materials, the material is strongly strain hardening at strains exceeding 200%.

The tubes had readily visible permanent deformation upon deflation if inflated to at least 10mL. To test for inelastic behavior, the same specimens were also unloaded at the same speed. Pronounced loading-unloading hysteresis was noted in Figure 4.2a. A marker of inelastic deformation is that the force during unloading reduces to zero when the nominal strain is still non-

zero. By this criterion, significant inelastic behavior (e.g. permanent strain exceeding 10%) appeared when the strain exceeded about 50%.

The effect of elongation rate, ranging from nominal rate of 20%/min to 250%/min is shown in Appendix Figure 13. The tensile behavior remains qualitatively similar to that in Figure 4.2, with a modest decrease in stress at lower rate.

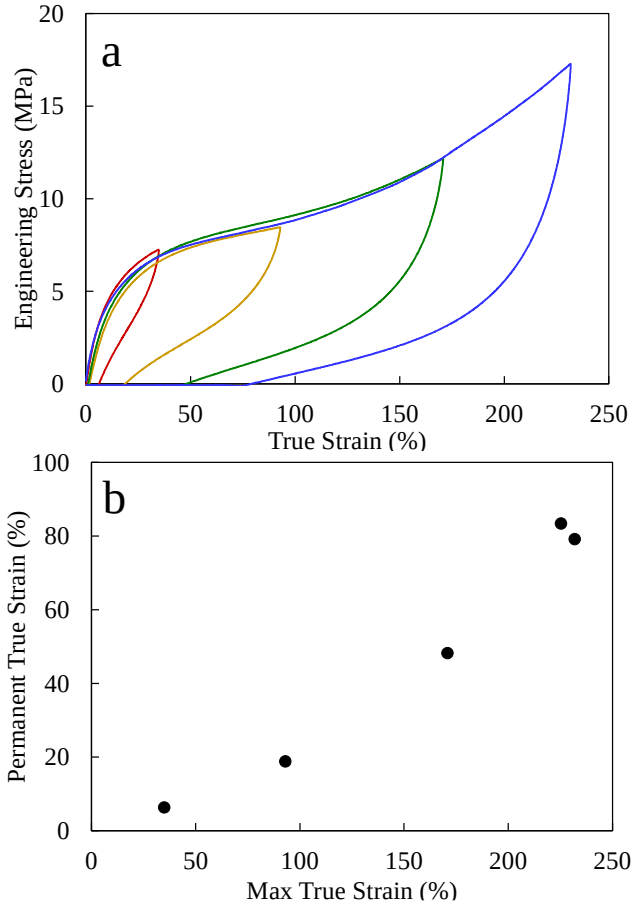

Figure 4.2 a. Uniaxial tensile testing data for polyurethane tubes during loading and unloading at a nominal strain rate of 50% per minute up to various values of maximum strain. b. Inelastic strain obtained from the data in a.

Inflation testing: The experimental setup is shown in Figure 3.1 and in simplified form in Figure 4.3. Tubes were inflated using a constant-flow rate piston pump (Isco Reaxys LS). A pressure gauge (Ralston LC10-GR2M) was used to continuously monitor pressure at 1 Hz frequency. The entire inflation process was imaged, either using a video camcorder (Panasonic HC-V180

operating at 60 frames/s) or a camera (Panasonic DC-FZ80 operating with a 1 - 10 s duration between successive photos).

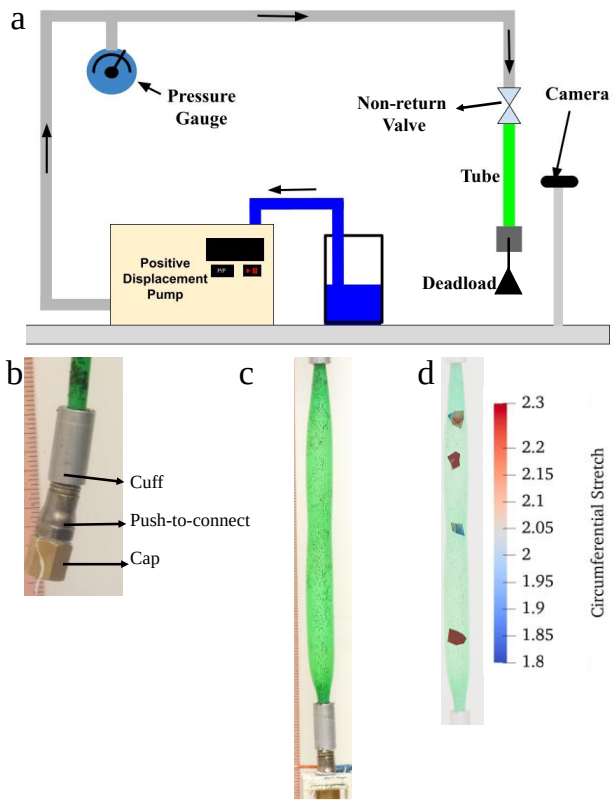

Figure 4.3 a. The inflation setup which includes positive displacement pump, pressure gauge, camcorder, and camera. A more detailed version of this figure was shown in Figure 3.1. b. Tube connections shown at higher magnification. c& d. Example of the snapshot and circumferential stretch of the tube at *DV*=20 mL calculated from tracking markers on the tube surface.

All tubes were cut to a length of 200 mm, and the water was supplied from the top of the tube, whereas the bottom was capped. The fittings on both ends were of the push-to-connect type. To reduce the chance of leakage at the connections, the end section immediately adjacent to the connectors was restrained by snugly fitting aluminum “cuffs” (Figure 4.3b). The section within the cuffs could only inflate axially, not radially. Thus, accounting for the cuff lengths and the

length at each end that is inserted into the push-to-connect fittings, the section of the undeformed tube that could inflate freely was 115 mm long, corresponding to an undeformed aspect ratio *L/R* of 52.7, and an initial internal volume of 1.42 mL. Inflation rates ranged from 0.1 to 20 mL/min, with a majority of the experiments being conducted at 2 mL/min. Incidentally, if the tubes expanded homogeneously and isotropically (i.e. equal expansion along circumferential and axial direction), the rate of 2 mL/s corresponds to an initial expansion rate of 46% per minute on the inner surface of the tube, which is comparable to the tensile testing rate.

All experiments were conducted with a load of 2.44 N suspended from the bottom of the tube, which served to keep the tube approximately taut even before inflation was started. While previous experiments and theory show that inflation behavior can change with axial load [10], [12], [28], [32], in fact the axial load used here is negligible. This may be judged by two criteria. First, the stress corresponding to this load is 0.128 MPa, which is too small to induce significant axial strain as judged from the uniaxial tensile data (Figure 4.2a). Second, typical pressures during inflation are on the order of 3 MPa, which (even using the cross-sectional area of the uninflated tube diameter) corresponds to an "internal" axial force of 37.7 N, which far exceeds the 2.44 N weight suspended from the ends.

Prior to conducting the test, the tube was sprayed with droplets of paint, or with flakes of black "glitter" to serve as markers for motion-tracking. Subsequently, the displacement of these markers was monitored using digital correlation software (Blender). The radial and axial stretch at any point could then be calculated from these displacement fields as shown in Figure 4.3c.

As a measure of sample-to-sample variability, we note that at an inflation rate of 2 mL/min (which was used for most of the experiments in this paper), a total of 24 experiments were conducted. These showed a peak pressure of 2.93 MPa with a standard deviation of 0.16 MPa, which corresponds to a 5% variation in peak pressure. Tests conducted in succession, i.e. from adjacent sections of tubing, tended to show higher reproducibility suggesting that at least a part of the variation may be due to small variations or imperfections in the geometry or in the mechanical properties of the tube over long lengths.

4.3 Results and Discussion

We first illustrate an exemplary inflation of a polyurethane tube at a rate of 2 mL/min, with *DV* denoting the increase in volume of the tube. The corresponding video is shown as Supplementary Information, and individual snapshots are shown in Figure 4.4a. Figure 4.4b shows a rise in pressure at low inflation volumes, followed by a peak at a volume of roughly *DV*=3 mL and a pressure of roughly 2.8 MPa. Subsequently, the pressure decreases gradually towards a plateau value of about 1.8 MPa. This decrease in pressure is denoted *pressure-unloading* in the rest of this paper. During this inflation, the macroscopic length of the tube increased monotonically. At the final volume of *DV*=40 mL, the increase in length corresponds to an average axial strain of roughly 80% based on the length of the uncuffed tube at the beginning of the experiment.

The evolution of pressure and tube length during inflation is qualitatively similar to that of hyperelastic tubes undergoing stable propagation of an inflated region, and similar to hyperelastic tubes, the tube develops a distinct bulge after the pressure maximum. Yet, there are some key differences. First, the pressure-unloading is gradual, occurring over several mL of volume inflation, i.e. a period of 3-5 minutes. This is in sharp contrast to the behavior of rubber tubes where the pressure-unloading is nearly instantaneous [29], [30], [33] (also Figure 4.8 discussed later). The second is that the inflation is irregular as was mentioned in the Introduction. In the case of Figure 4.1a, the mid-section of the tubing inflated less than the ends, and this was seen most frequently. In some cases, the inflation approximately resembled a bulge propagation instability where a more-bulged region coexists with a less-inflated region (Figure 4.6). Furthermore, although repeated trials on identical specimens had significant variations in shape, they all had very similar pressure evolutions suggesting that the pressure is primarily related to material behavior rather than the geometric details of bulging.

To quantify the irregular deformation, Figure 4.4c and d shows the circumferential and the axial stretches at four distinct locations along the tube. Up to a *DV* of roughly 5 mL, all marker positions show similar deformation, indicating uniform expansion. However, following the emergence of the bulge, deformations at the various locations first steeply deviate from each other. Later during the inflation, the least-deformed region does “catch up” with the more deformed

regions, but at the final volume, there is still a difference of almost 0.8 unit in the circumferential stretch of the most vs least inflated region.

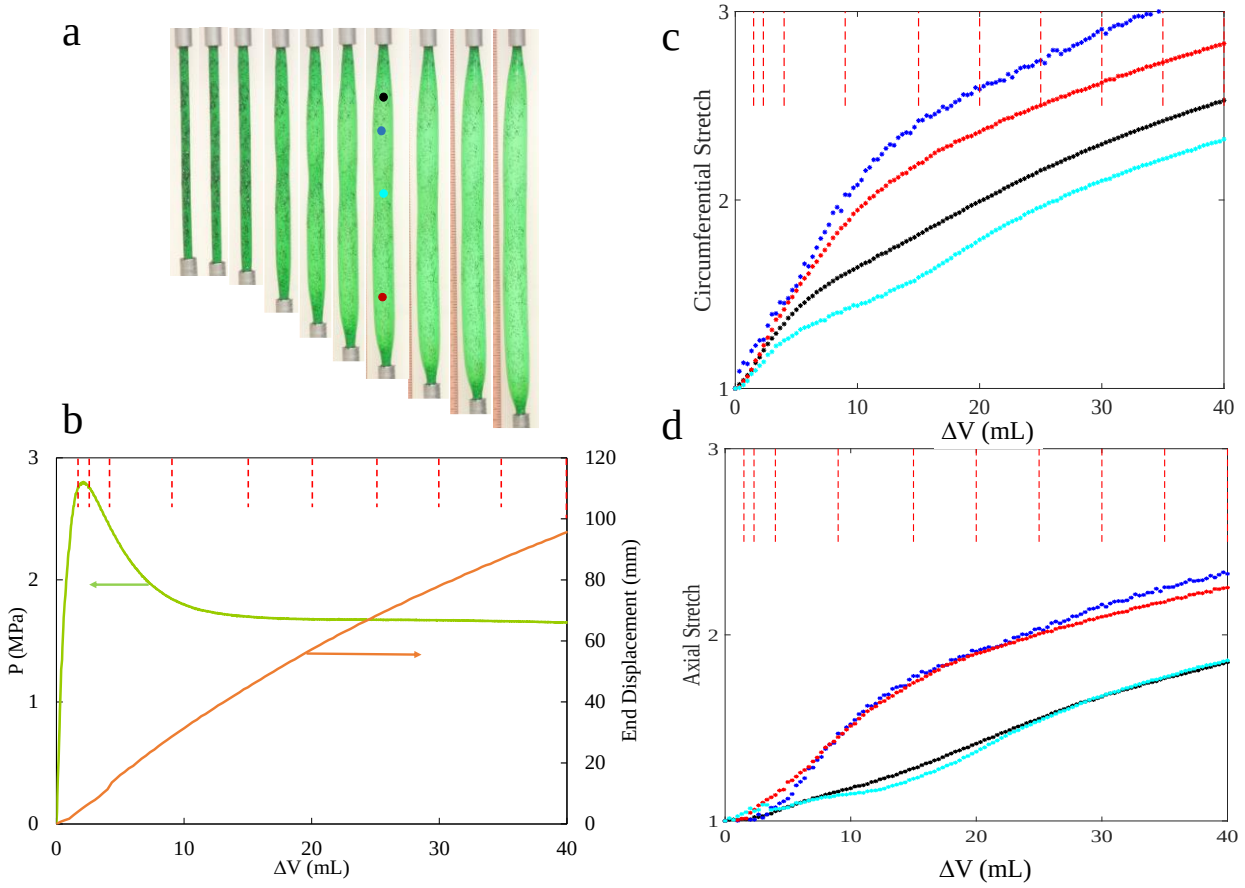

Figure 4.4 a. Appearance of the tube at various points during inflation. b. Pressure vs volume during the same experiment. c&d. Quantification of the two stretches at the four locations marked in one of the images in a. The vertical dashed lines in b-d correspond to the sequence of images in a.

Upon deflating the tube of Figure 4.5**Error! Reference source not found.**, it was found to be distinctly distorted. Accordingly, we examined inelastic deformation in more detail. Several tube specimens were inflated at 2 mL/min to various volumes, deflated, and then imaged. In Figure 4.5, the initial configuration (without inflation) appears bent due to the intrinsic curvature of the tube as mentioned at the beginning of Section 4.2. Beyond inflation volumes *DV* of 10 mL, significant

permanent deformation appears, both as a gradual straightening of the tube, as well as a permanent change in diameter. It is noteworthy that deflation after *DV*=6 mL, which well-exceeds that at the pressure maximum, does not induce noticeable permanent deformation. This is consistent with Figure 4.2 and Figure 4.4: Figure 4.4c and d show that at the peak volume of 2.5 mL, the axial stretch is close to 1, and the circumferential stretch is no more than 1.3, and at this stretch, Figure 4.3b confirms that significant permanent deformation is not expected.

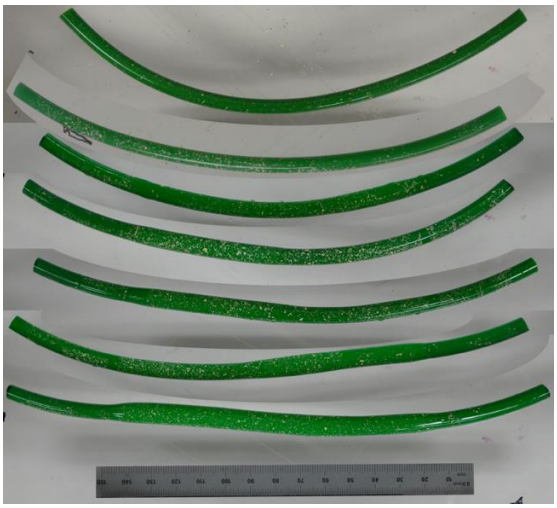

Figure 4.5 Inelastic deformation of tubes after being inflated to volumes of (top to bottom) 0 mL (i.e, undeformed), 6, 10, 20, 30, 40, and 60 mL. The ruler at the bottom is 150 mm long.

Next we examine the role of inflation rate. Tube specimens were inflated at rates ranging from 0.1 to 20 mL/min. Figure 4.6a shows that the peak pressure and the plateau pressure both increase modestly with increasing flow rate. At the lowest rates examined, the pressure does not show a true plateau, but instead continues to reduce gradually with continued inflation. This gradual decrease can be seen more clearly in Appendix Figure 12 which the same data are shown with log(time) on the x-axis. The inflation rate strongly affects the tube shapes, with low rates promoting a greater degree of localized bulging, but high rates inducing smaller deviations from homogeneous inflation. It is noteworthy that the volume required for pressure-unloading remains roughly 5 mL regardless of rate, and by implication, the time required for pressure-unloading increases sharply as the flow rate reduces. For the lowest flow rate examined, the duration from the peak to the end of the experiment (when the pressure had still not plateaued) exceeded 1 hour.

A remarkable observation from Figure 4.6 is that despite the diverse inflation behaviors, all cases share similar pressure-volume curves. Even the cases of 6 mL/min and 20 mL/min, which happens to show nearly homogeneous inflation, still show a clear maximum in the PV curve followed by pressure-unloading. This is contrast to hyperelastic tubes for which homogeneous inflation is associated with monotonically increasing PV data. This will be discussed further below.

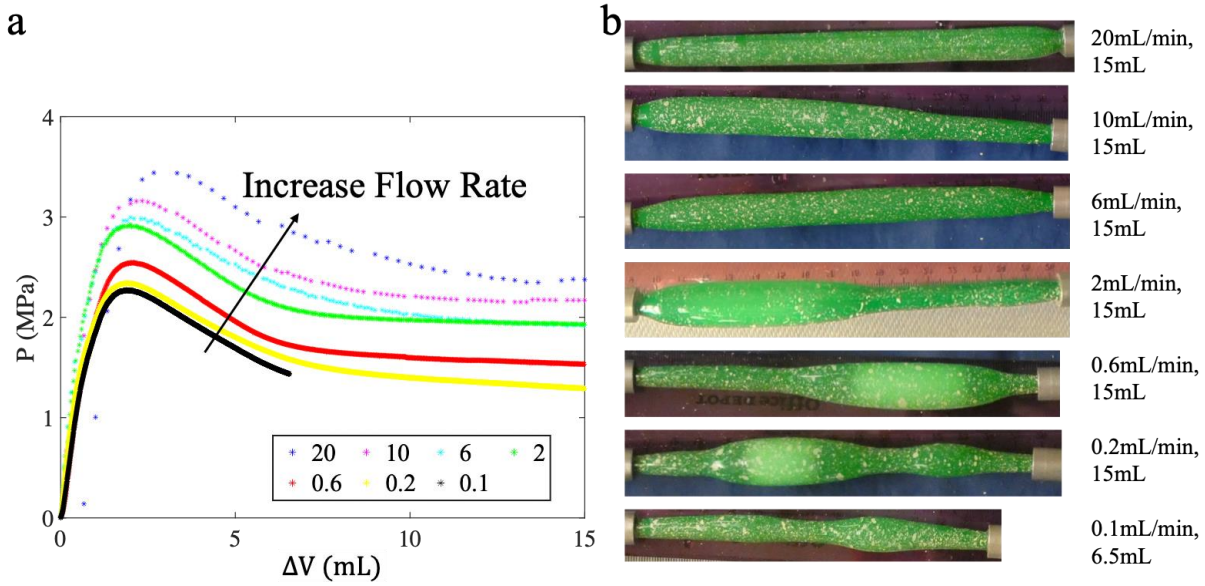

Figure 4.6 a. Pressure vs. volume curve for the various listed in the legend (all in mL/min). b. Images of tubes during deformation. All the images were taken when the tubes had been inflated with 15 mL water, except the last one which was inflated to 6.5 mL. Although the tubes were vertical during experiments, images have been rotated for convenience, with the sequence of images following the sequence of pressure-volume data.

Finally, we examine the extent to which inflation induces irreversible softening (henceforth called *strain-induced damage*) of the material such that a second inflation is different from the first. This was tested in loading-unloading-reloading experiments where tubes were inflated by various volumes DV_1 (ranging from 1.5 mL to 15 mL), then deflated to atmospheric pressure and reinflated. Figure 4.7a shows the images of the samples at three stages: at the volume DV_1 during the first inflation, at zero pressure after deflation, and at volume DV_1 during the second inflation.

Figure 4.7b shows the pressures during the second inflation. Increasing DV_1 first reduces, and then eliminates, the pressure peak during inflation. Notably, a DV_1 value of 6 mL eliminates the pressure peak, whereas Figure 4.5 shows that this same inflation volume does not induce significant permanent deformation, i.e. strain-induced damage precedes inelastic deformation.

Turning to the tube shapes, at first glance, the first and the second inflation appear similar, i.e. images in the third column of Figure 4.7a are almost identical to those in the first column. However closer examination reveals that for volumes exceeding 6 mL, the regions that were more (or less) inflated after the first inflation become even more inflated (or even less inflated) during the second. This is quantified Figure 4.7c which shows the difference in the profile between the first and second inflation for the 6 mL case.

This issue of loading-unloading-reloading behavior was tested more thoroughly (shown in Appendix A) [10], [12], [28], [32]. Briefly, tubes were repeatedly cycled between two states: inflation by DV = 6 mL, and zero pressure. Over 10 cycles, the bulge grew steadily suggesting a slow but incremental damage that caused an increasing degree of bulge localization.

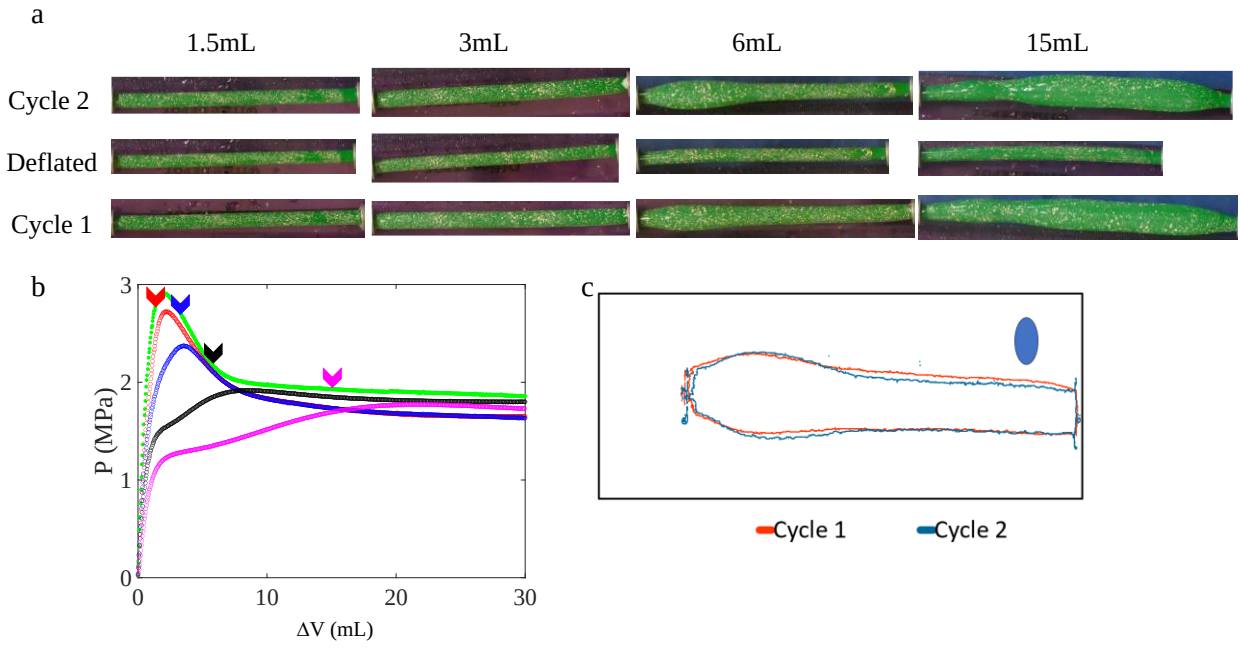

Figure 4.7 a. Images of samples during inflation-deflation-reinflation experiments. Although the tubes were vertical during experiments, images have been rotated for convenience. b. Pressure vs. volume curve during the reinflation step with various values of DV_1 for the first

cycle. c. A superposition of the profiles of the tube during the first and second cycle, both at *DV*=6 mL. Note that the axes of c are distorted so that the tube dimensions in the radial direction are magnified 2-fold, and the blue ellipse represents the initial, undeformed, circular cross section of the tube.

4.4 Discussion

4.4.1 Interpretation based on theory of hyperelastic tubes

A fellow student, Fatemeh Rouhani, examined whether hyperelastic models can successfully describe the behavior of polyurethane tubes. The Ogden model was fitted to stress-strain data during loading. The corresponding pressure-volume curves increased nearly monotonically and hence did not predict bulge localization. They also predicted that the tubes shortened during initial inflation. To resolve the latter discrepancy, the constraint $\frac{d\lambda_z}{d\lambda_\theta} \geq 0$ was applied to the fitting parameters. In this case, the model predicted the pressure plateau and peak pressure reasonably well, but at the cost of poor fits to the tensile data.

4.4.2 Inelastic effects and one further experiment

We now turn to the two noteworthy aspects of the inflation behavior that strongly differ from past experiments on rubber tubes [10], [28-30]. The first is that multiple specimens cut from the same spool of tubing show distinct behaviors even under identical inflation conditions. For the inflation rate of 2 mL/min, in more than 40 experiments, we have observed several examples of tubes with irregular shapes, Figure 4.1, several examples that approximately resemble bulge

propagation, and occasional examples of nearly-homogeneous inflation. Even tubes that resemble bulge propagation show up to 20% variation in the diameter of the more-bulged and less-inflated regions. In contrast, hyperelastic tubes can only show coexistence of two well-defined strain states. Despite this variability in deformation however, all these specimens show very similar pressure-volume behavior. Especially remarkable are two cases in Figure 4.6 where the inflation proceeds almost homogeneously even though the PV curve shows a prominent maximum. In contrast, for hyperelastic tubes, a pressure-volume curve with a negative slope is necessarily unstable and incompatible with homogeneous inflation. This suggests that pressure-unloading is not only due to bulging but due to material behavior. This notion, that material behavior is a strong contributor to pressure-unloading is also supported by the observation (Figure 4.6) that despite a wide difference in the degree of bulging and a 100-fold difference in experimental timescales, the pressure-unloading remains similar, and always requires roughly 5 mL of inflation volume.

A second noteworthy aspect is the simultaneous inflation of two or more bulges along a single tube. Intuition suggests that once a bulge starts growing, three factors encourage further localization. First, a bulge has a larger diameter and a thinner wall, both of which increase the local wall stress as per Laplace equation. This effect is present even in hyperelastic tubes. Second, if the material has a yield point (or undergoes strain-induced damage), the bulged region becomes more compliant. Third, as a consequence of the prior two factors, the pressure within the tube reduces, thus making it impossible to initiate new bulges. Accordingly, we expect that when a single bulge starts growing, the formation or growth of other bulges must be suppressed. Despite this however, we have noted numerous examples where more than one bulge grows simultaneously (although one always grows more than the others).

We propose that both these unusual aspects, sample-to-sample variability in bulging behavior and multiple bulges, are related to the remarkably slow pressure-unloading behavior of these tubes as compared to hyperelastic tubes. To illustrate this, Figure 4.8a compares the pressure-volume response of the polyurethane tubing with natural rubber tubing of similar diameter and wall thickness. The natural rubber tubing (same as shown in Figure 4.2a) was found to bulge "instantaneously", i.e. the pressure reduces more steeply than can be resolved by the 1 Hz data acquisition rate. Such rapid bulging was also reported in previous studies [29], [30], [33]. In contrast, the decrease in pressure of the polyurethane tubing occurs over several tens of seconds in Figure 4.8a, but might take over an hour at low flow rates.

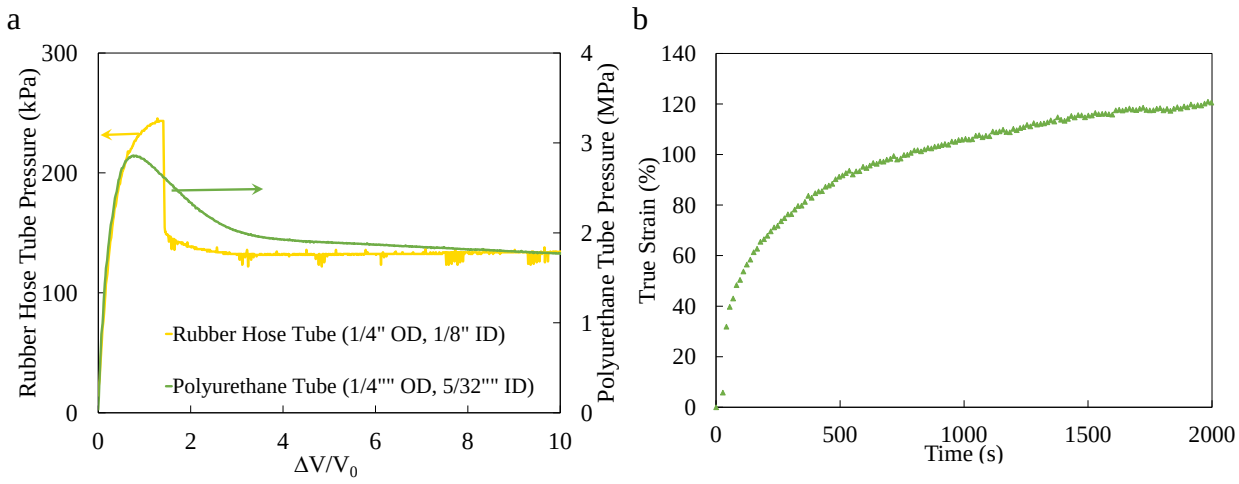

Figure 4.8 Delayed strain response of polyurethane tubes. a. Comparison of pressure-volume curves of polyurethane tubes vs. natural rubber tubes. Note that the right and left y-axes have different scales because the natural rubber tube is much softer. The green data for the polyurethane tube in a is identical to Figure 4.4 Error! Reference source not found.**b. b.The axial strain measured when a tube is subjected to a rapid increase in axial load from 40N to 140N.**

Such slow unloading likely results from an intrinsically slow strain response of the polyurethane material. To quantify this, we conducted an experiment where a polyurethane tube was first loaded with a weight of 40N for several minutes, and then abruptly (within less than 2 s) the weight was raised to 140N. This is conceptually similar to a creep experiment except that the force (rather than stress) is held constant; in fact, in Figure 4.8b the stress increases with time due to a decrease in cross sectional area. The strain evolution was obtained from quantitative analysis of images of ink marks on the tube taken during the experiment. Figure 4.8b shows that strain increases gradually over tens of minutes before reaching a stable value.

The consequence of the slow response to load is that in the inflation experiment, the strain in the tube wall lags behind the instantaneous pressure. Once the pressure reaches the maximum

value expected from homogeneous expansion, the entire tube becomes susceptible to bulging, and at some location (presumably a small defect), a bulge initiates. However, the crucial point is that because this bulge grows slowly, the tube stays at high pressure for a long duration. Thus, locations sufficiently remote from the first bulge can also initiate bulging independently. Only when one or more bulges grows sufficiently does the pressure reduce gradually, and new bulges are no longer viable; beyond this point a single bulge grows more than the others. Nevertheless, some of the other bulges can still continue growing gradually. We suggest that this is because strain-induced damage has already rendered these regions softer and local creep allows a steady increase in strain with time.

Although a slow material response is often deemed to be a viscoelastic effect, we believe that viscoelasticity alone cannot explain the experimental results for the following reasons. To a first approximation, one would expect viscoelastic relaxation to have some characteristic timescale, which would in turn determine the time needed for pressure-unloading. This timescale may depend on stress, yet, experiments conducted at various rates (Figure 4.6) have similar pressures, and hence similar wall stress. Accordingly, we would expect them to have similar viscoelastic relaxation times. Thus, intuition suggests that pressure-unloading should occur over a similar time-scale at all inflation rates. Yet, the same data as Figure 4.6, but with time on the x-axis (Appendix Figure 12) shows that pressure-unloading can occur over timescales as short as few ten seconds and as long as tens of minutes. In fact, previous calculations of the homogeneous inflation of viscoelastic spherical shells show that as the inflation time becomes longer than the viscoelastic relaxation time, the peak pressure reduces (in agreement with our experiments), but the volume at the peak pressure also reduces sharply (in disagreement with our experiments) [35]. Thus, rather than interpreting the results as arising from viscoelasticity alone, it may be better to regard it as also having contributions from inelastic deformation.

In summary, we conclude that the pressure-volume characteristics, which include the initial pressure rise, the peak in pressure, and the subsequent approach to an apparent pressure plateau, appear from a complex coupling of all four phenomena: bulge formation, strain hardening, time-dependent relaxation of the material, and strain-induced damage. The first of these is a purely geometric effect, whereas the other three are material properties. The latter two phenomena are (by definition) absent in hyperelastic materials. For the polyurethane tubes, bulge formation is not essential to the existence of a pressure maximum, since even tubes that inflate homogeneously

show the same pressure-volume characteristics as the other tubes. In contrast, in hyperelastic tubes the pressure maximum is necessarily linked to bulge initiation, and indeed the pressure unloads instantaneously once the maximum is reached. Finally, for polyurethane tubes, the pressure does not reach a true plateau at large volumes, likely due to a combination of the strain hardening characteristics, viscoelasticity and strain-induced damage. In contrast, for hyperelastic tubes that show bulge propagation, there is a true plateau that is determined entirely by the strain hardening characteristics of the material.

4.5 Summary and conclusions

To summarize, this paper explores the inflation behavior of tubes whose material behavior deviates from strict hyperelasticity. Hyperelastic tubes inflated under volume-controlled conditions are known to inflate along three possible pathways: tubes that are sufficiently strain-hardening inflate uniformly, maintaining their cylindrical shape. Tubes that have insufficient strain-hardening develop a bulge, which may either inflate circumferentially to failure with a continuous decrease in pressure, or propagate axially at constant pressure. This paper explores how the inflation behavior changes when the material comprising the tube wall has inelastic behaviors such as rate-dependent mechanical properties, strain-induced damage, and plastic deformation.

We find that during inflation at fixed flow rate, the pressure within the tubes first rises, then shows a maximum, and then reduces towards a plateau. While this behavior is qualitatively similar to that of hyperelastic tubes undergoing axial bulge propagation, in fact there are major differences. First, the decrease in pressure from its peak value towards a plateau value can take from tens of seconds to tens of minutes, depending on the inflation rate. In contrast, hyperelastic tubes inflate almost instantaneously they bulge. Second, the tubes deform into a variety of shapes: uniform inflation maintaining cylindrical shape, irregular axisymmetric shapes with multiple bulges, or axial propagation of a bulge. In all these cases – even when tubes inflate uniformly – the pressure shows a maximum value followed by unloading. In contrast, for hyperelastic tubes at fixed axial force, a peak in pressure is necessary and sufficient condition for bulge formation. Third, after sufficient inflation, tubes are left permanently deformed indicating plastic

deformation. Finally, if tubes are reinflated a second time, the pressure-volume curve does not show a maximum indicating that damaged induced by the first inflation, i.e. a permanent change in mechanical properties due to strain. One observation that underpins some of these observations is that the polyurethane material responds to an applied load relatively slowly, on the order of many minutes. We propose that it is this slow response that causes the pressure to remain high for a long duration during inflation, and hence allow multiple bulges to grow. In contrast, since a single bulge instantaneously reduces the pressure in hyperelastic tubes, growth of multiple bulges is suppressed.

We also tested the extent to which existing hyperelastic models of tube inflation can predict the first-inflation behavior of the tubes. The first-loading uniaxial tensile testing data were fitted to the Ogden model, and the corresponding predictions were tested against the observed behavior. The predictions were found to underpredict the pressure and the deformations. More significant than the quantitative discrepancy, the model does not predict a maximum in pressure, and predicts that the tubes stretch when inflated, contrary to experiments. We show that the Ogden model can make more reasonable predictions, but only at the cost of poorly fitting the initial portion of the uniaxial tensile testing data.

Broadly, we conclude that bulge formation in the polyurethane tubes examined here appear from a coupling between bulge formation, strain-hardening, strain-induced damage, and rate-dependent mechanical properties. The latter two features are necessarily absent from hyperelastic tubes. Perhaps the most interesting qualitative result from this paper is that a pressure peak followed by a pressure plateau – a signature of bulge initiation and propagation in hyperelastic tubes – may appear without bulge formation, and due to mechanical properties alone.

The polyurethane tubes studied here showed only modest deviations from hyperelastic behavior. They retain one key feature of hyperelastic tube inflation, viz. the inflated tubes remain axisymmetric. In contrast, if the tubes have a relatively large yield stress, non-axisymmetric deformations appear. These will be explored in chapter 5 [21].

5.0 Severely Plastic LDPE Tubes

5.1 Theoretical Background

Before discussing how LDPE tubes deform nonaxisymmetrically, it is useful to understand how yielding induces strain localization. When materials with a yield point are subjected to uniaxial tension, they initially experience uniform strain but experience localized thinning once sufficiently stressed. This is caused by localized yielding and the yielded regions soften. The localized yielding is caused by small irregularities in the material acting as stress concentrations. Further increases in strain result in large, localized deformations known as necking. In materials such as aluminum, the necking will proceed to failure as seen in Figure 5.1a. However, if the material has sufficient strain hardening, the strain of the necked region reaches a limit and the necked region grows in length if pulled further. This case is called stable necking and is seen in Figure 5.1b.

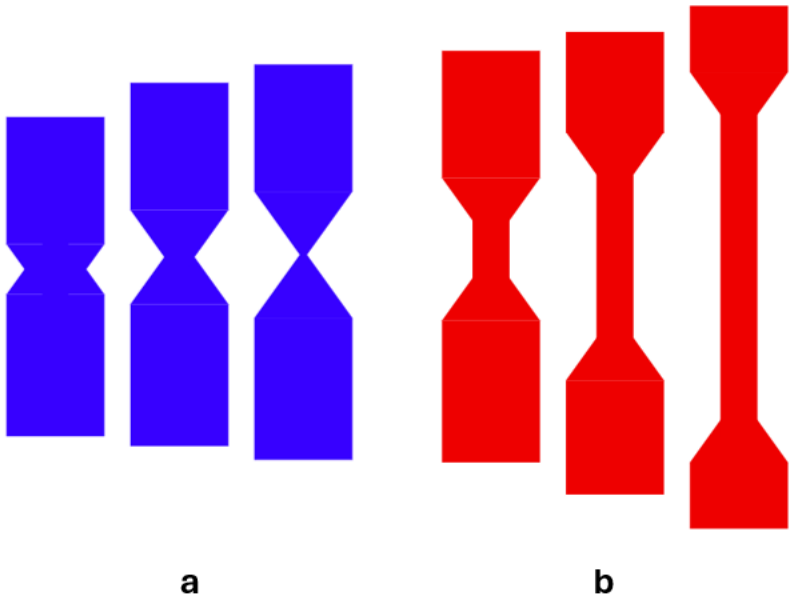

Figure 5.1 a. Unstable necking in uniaxial tension. b. Stable necking in unaxial tension.

When tubes are pressurized, the highest stress appears in the circumferential direction. Analogous to the case of uniaxial tension above, if the tube material has a yield point, it may experience localized necking in the circumferential direction. Depending on the degree of strain hardening, the necked region may be stable or unstable. A stable neck would be expected to propagate tangentially giving a prismatic cross section with one thin and one thick region. In contrast, a material with poor strain hardening is expected to result in localized thinning until rupture. A schematic comparing stable and unstable necking in tubes can be seen in Figure 5.2. These scenarios will be explored in this chapter with experiments on LDPE tubes.

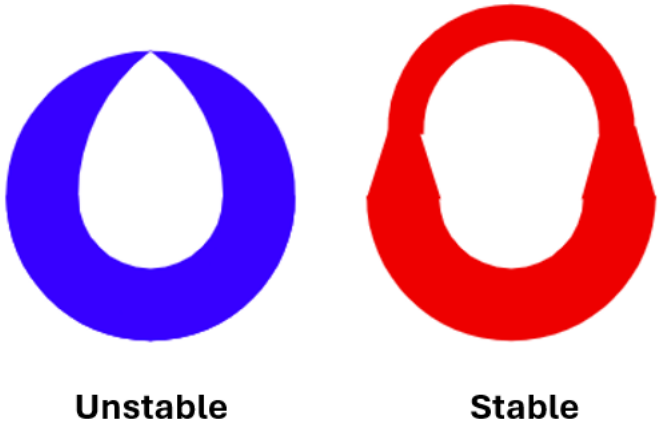

Figure 5.2 Schematic showing stable vs unstable necking in an inflated tube cross section.

5.2 Materials and Tensile Behavior

LLDPE tubes with an outer diameter of 1/4 inch (6.35 mm) and an inner diameter of 5/32 inch (3.97 mm) were purchased from McMaster-Carr Supply Co. The tubes came from rolled spools and therefore had an inherent radius of curvature of 160-170mm. The curvature had no noticeable effect on inflation behavior but a 2.44N load was still applied to the end of the tubes during testing to straighten to tubes for experimental convenience.

Uniaxial tests were done to quantify the mechanical at a 50%/min engineering strain rate and a 40mm clamp to clamp distance. A Panasonic Lumix camera took a timelapse of each test with a frame rate of 1/3fps and ink markings were applied to each sample before testing. After each test, ImageJ was used to measure the distance between the markings in each frame and these measurements were used to calculate the engineering strain in each frame using equation **5-**. The variables within that equation are explained in Figure 5.3.

$$\epsilon = \frac{\left(x_{2,\text{current}} - x_{1,\text{current}}\right) - \left(x_{2,\text{initial}} - x_{1,\text{initial}}\right)}{x_{2,\text{initial}} - x_{1,\text{initial}}} \quad \textbf{5-1}$$

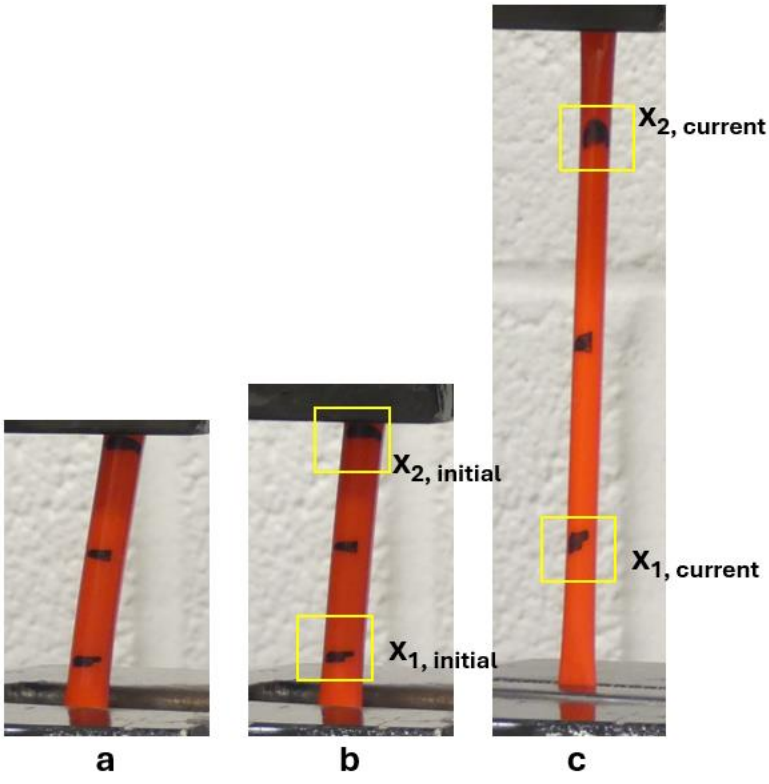

Figure 5.3 a. Sample before pretensioning. b. Initial configuration of uniaxial tensile test (with pretensioning). c. Current configuration. $x_{1,\text{initial}}$ is the height (in pixels) of the botton mark in the initial cofiguration while $x_{2,\text{initial}}$ is the top marker. $x_{1,\text{current}}$ is the height of the bottom marker in the current configuration while $x_{2,\text{current}}$ is the top marker.

The image frame 6 seconds after motion starts (5% engineering strain) was used as the reference configuration and a constant value was subtracted from the loads to make the load 0 at the chosen reference configuration. A correlation between nominal and true strain was found experimentally as follows. A 6^{th} order polynomial fit was performed in the true strain vs

engineering strain plot as shown in Figure 5.4. Unlike the polyurethane tensile tests, there was a large discrepancy between the nominal and true strains due to slight slippage from the grips. Another more significant factor that caused this discrepancy was motion of the clamps during testing due to the use of self-tightening clamps. The clamps primarily tightened during the early stages of the test and moved in the same direction as the crosshead during tightening.

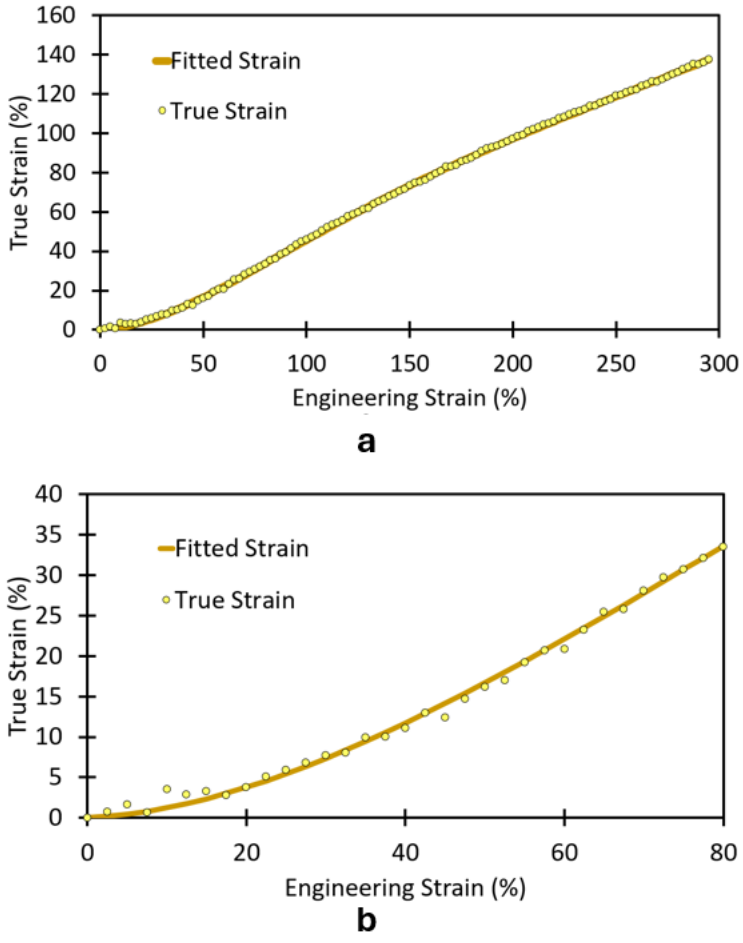

Figure 5.4 a. True strain vs engineering strain plot. b. Zoomed in version of plot a.

The elastic modulus for each test was calculated by plotting the stress vs the true strain up to 5% true strain for both tests and linear fits as seen in Figure 5.5. Values of 74.8MPa and 59.6MPa were found for tests 1 and 2 which gives an average elastic modulus of 67.2MPa. The yield strength

for each test was found by offsetting a line with a slope corresponding to the elastic modulus but with a true strain of 5% as seen in Figure 5.5b. The intersection between the offset line and the stress-strain curve is the yield stress and a zoomed in view of this can be seen in Figure 5.5c. Values of 5.1MPa and 5.4MPa were found, resulting in an estimated yield strength of 5.25MPa. After unloading , large permanent deformation is evident as judged by the over 100% elonggation at which the stress reaches zero indicating significant plasticity.

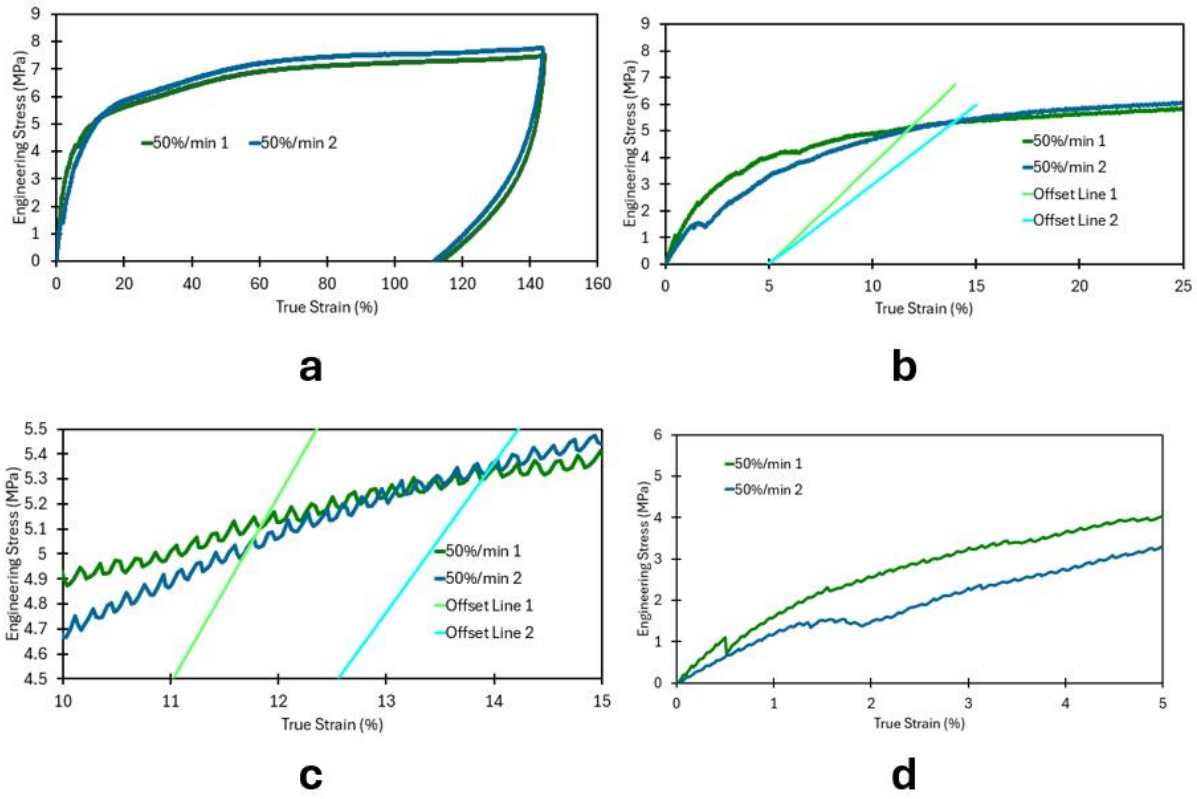

Figure 5.5 a. Stress-strain plots for LDPE tubes loaded and unloaded at a 50% nominal strain rate. b. Zoomed in view showing offset lines used to find yield strength. c. Zoomed in view showing the intersection of the offset lines and stress-strain curves. d. Zoomed in view showing regime where the linear fit was used to find the modulus.

With knowledge of the properties of the tube, equation **2-8** allows predictions of when yielding initiates. When tubes are inflated, yielding typically starts at the inner surface.

$$\frac{\sigma_y}{2} = \frac{PR_2^2}{R_2^2 - R_1^2} \quad \textbf{5-2}$$

Prior to yielding, assuming that the LDPE was linearly elastic, plugging $r = R_1$ and $\sigma = \sigma_y$ into equation **2-8** gives equation **5-2**.

$$P = \frac{\sigma_y(R_2^2 - R_1^2)}{2R_2^2} \quad \textbf{5-3}$$

When the dimensions and yield strengths were substituted into equation **5-3**, the pressure needed for yielding to initiate at the inner surface is calculated to be 1.6MPa. If the tubes are incompressible, equation **2-15** applies which simplifies the calculations for finding the internal volume needed to initiate yielding. Equation **2-14** was used to find the tangential strain. When the average elastic modulus and average pressure at yielding were substituted, the tangential strain at the inner surface was 8.9% at the onset of yielding. The percent change in radius is the same as the tangential strain. This caused the radius to increase from 2mm to 2.18mm. Since the tube has 115mm between the cuffs, the initial internal volume is 1.44mL and increases to 1.71mL at the onset of yielding. This predicts that yielding should initiate on the inner surface at a volume of 0.27mL. Further calculations using $\nu = 0.33$ found a reduction in volume (0.14mL) needed to cause yielding on the inner surface even when axial lengthening is considered. Calculations were derived from equations **2-11** and **2-12**.

5.3 Inflation Test to Rupture

Having established the mechanical properties and the expected mechanical behaviors of LDPE through uniaxial testing, inflation tests were run. As seen in Figure 5.6a, LDPE tubes undergoing inflation initially experienced uniform expansion before undergoing nonaxisymmetric bulging and rupture. Surprisingly, the tube continued to expand uniformly well after reaching its maximum pressure which counters what happens in elastic tubes that experience instabilities [5] [6]. This also contrasts with elastic tube bulging behavior since elastic tubes bulge axisymmetrically [5] [6]. However, bulging resulted in a sudden drop in pressure as expected, and rupture occurred shortly after. An image sequence and a corresponding pressure-volume plot of an inflation test are shown in Figure 5.6a and Figure 5.6b. In the pressure-volume plot, the measured peak pressure and volume are significantly higher than the pressure and volume expected to cause yielding at the inner surface. The uncertainties in the yield strength were relatively small with a 1% change in engineering strain resulting in the yield strength changing by 0.1-0.2MPa. However, choosing the amount of offset was arbitrary due to the curve having no sharp yield point. This would mean that arbitrarily choosing a much larger or smaller offset would have significant effects on the yield strength. After rupture, the tubes showed a large

degree of permanent deformation in the vicinity of the rupture.

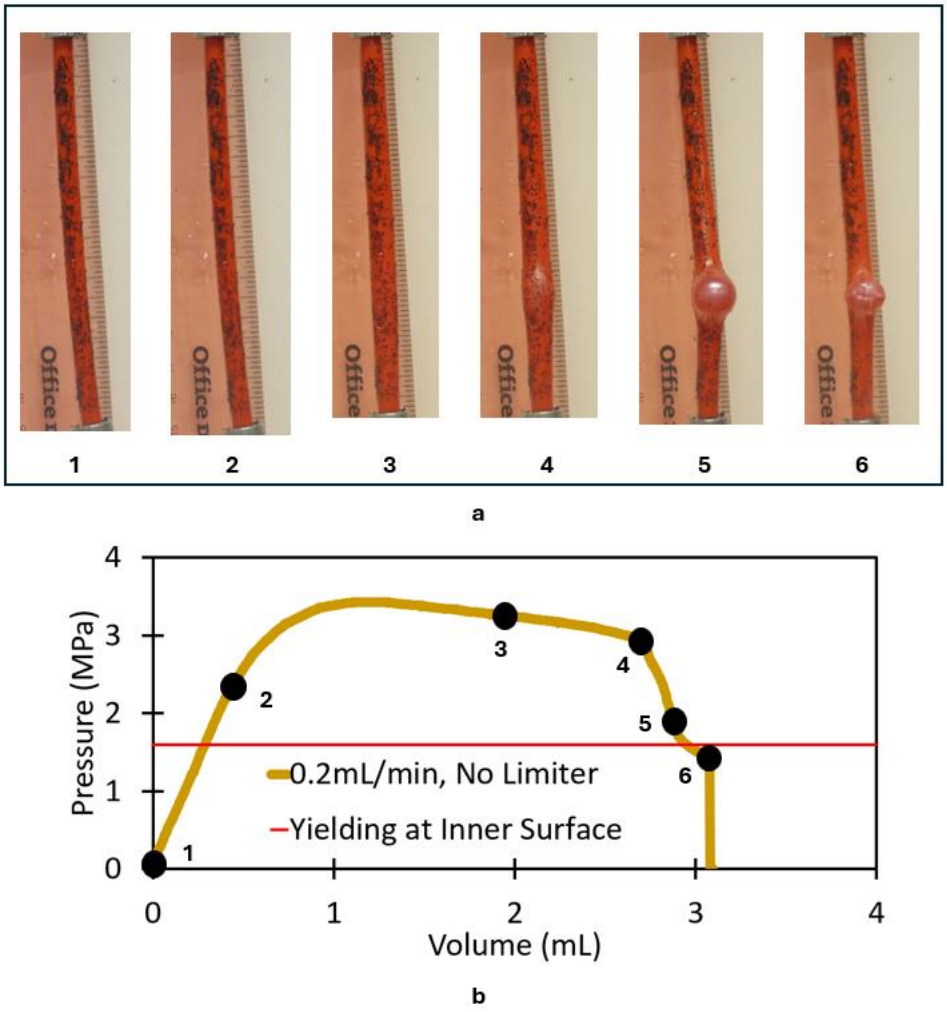

Figure 5.6 a. Snapshots of a tube being inflated at 0.2mL/min. b. Pressure-volume plot of inflation test with markers corresponding to the shape of the tube as shown in part a. Bulging starts when the pressure reduces rapidly and rupture occurs shortly after that. The red line indicates the predicted pressure needed to cause yielding at the inner surface.

Strain hardening may contribute to the formation and propagation of mechanical instabilities during inflation. The inflation tests conducted here showed that the material had enough strain hardening to allow for the bulge to inflate significantly before rupturing, but not

enough to force axial propagation. However, forcing axial propagation may be possible if the strain hardening is high enough to make the deformation of the non-bulged section energetically favorable. This would be difficult since the material outside the bulge has not yielded and is therefore harder to deform. Although strain hardening behavior cannot be changed since it is an intrinsic material property, a stiff cylindrical "limiter" can mimic what happens when the LDPE tubes suddenly experience a very high amount of strain hardening in the circumferential direction. The limiter is much stiffer than the LDPE, so it stops further circumferential expansion of the bulge upon contact.

5.4 Use of External Limiter

As mentioned in the previous paragraph, an external limiter approximates the behavior of strain hardening. The external limiter is a cylindrical shell made of a much stiffer material and prevents the bulge from expanding circumferentially beyond a certain diameter once contact occurs. Adding a limiter as shown in Figure 5.7 is similar to the material suddenly experiencing a large increase in strain hardening in the circumferential direction. When the tube inflates sufficiently in the circumferential direction, it contacts the limiter and is forced to neck in a stable manner just like how a bar under uniaxial tension can have two coexisting widths under the right conditions. Shortly after the neck stabilizes, the bulged section propagates axially as inflation continues.

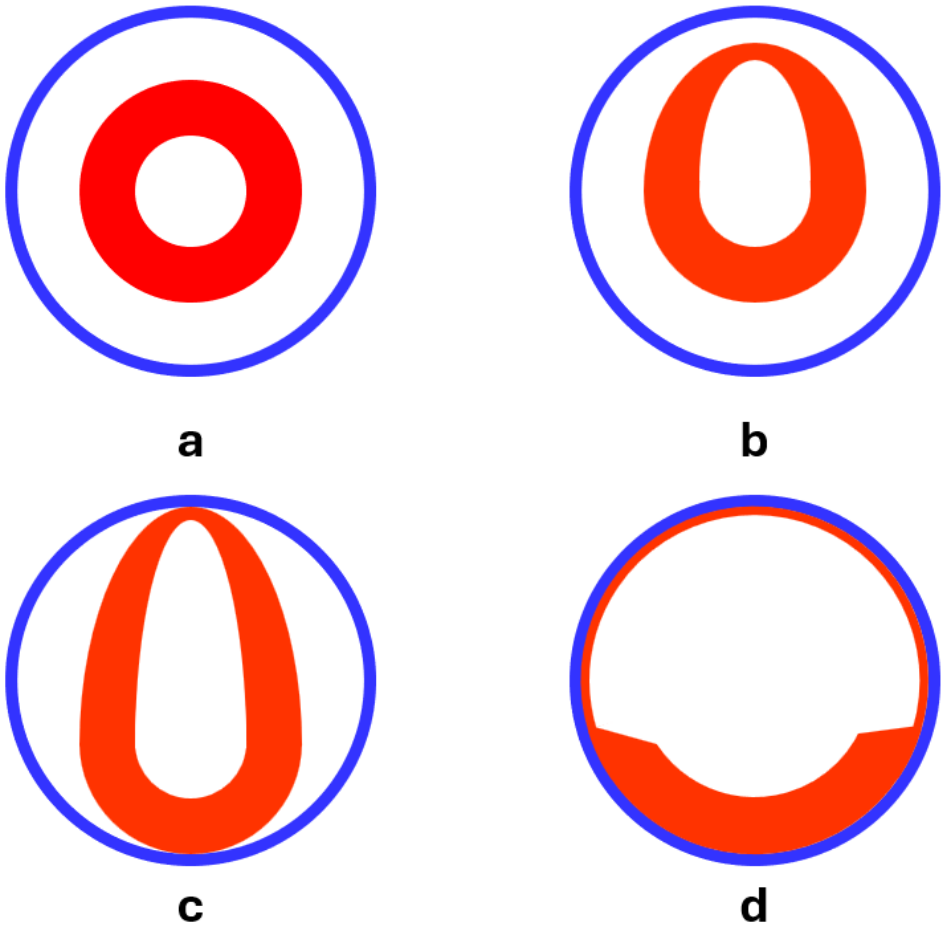

Figure 5.7 a. Uniform inflation. b. Unstable necking. c. Unstable necking right as tube contacts limiter. d. Stable necking long after tube contacts limiter. All views are cross-sectional.

There are multiple variables that may affect inflation behavior. Firstly, varying the limiter diameter would change the onset of sudden "strain hardening" since a larger limiter would allow for larger circumferential strains to be achieved before the onset of high strain hardening. Also, changing the flow rate would examine the viscoelastic properties of LDPE since faster flow rates are correlated with faster strain rates. In the sections below, limiter size and flow rate will be adjusted. Pressure-volume curves, propagation velocity, end displacement, and estimated elastic moduli will be compared across tests.

5.4.1 Detailed Tests with Limiter

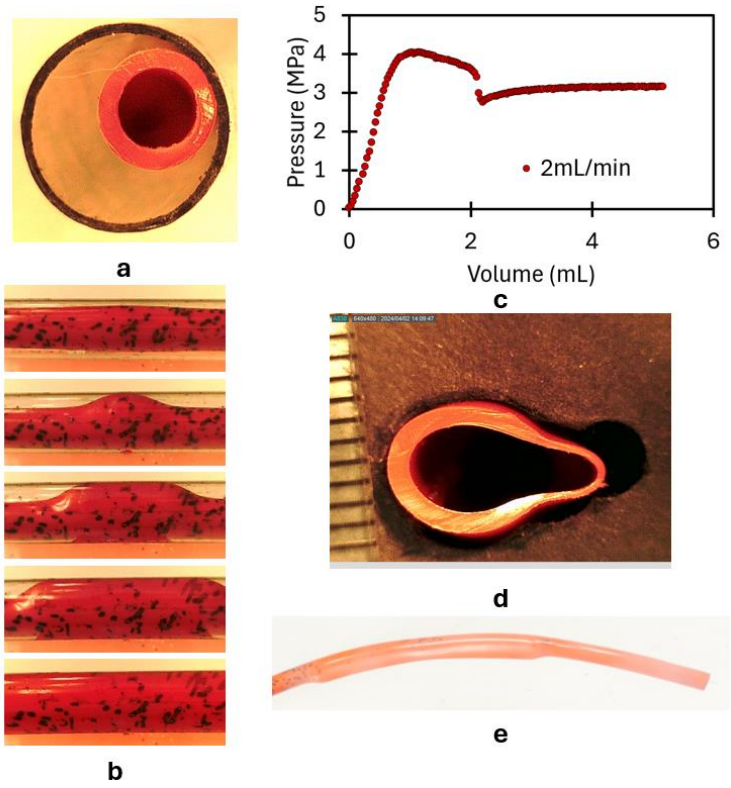

Figure 5.8 2mL/min test with 10.2mm external limiter. a. Top view of uninflated tube inside limiter. b. Zoomed in view of bulge initiation and propagation c. Pressure-volume curve. Flat region shows stable propagation. d. Cross section of bulge shows nonaxisymmetric inflation. e. Permanent deformation after depressurization.

The trial shown above in Figure 5.8 was conducted at 2mL/min with an external limiter. As seen in Figure 5.8c, the pressure-volume curve follows a similar path as the tubes without external limiters. The pressure still rises rapidly, peaks, and initially drops slowly. The pressure then drops rapidly as the bulge initiates but flattens once the bulge contacts the limiter. After contacting the limiter, the bulge propagates axially resulting in a constant pressure as shown in Figure 5.8b. This stage is considered stable propagation due to the constant pressure and the time-

invariant appearance of the bulge as it propagates axially. The cross sections in the bulged section show non axisymmetric inflation as seen in Figure 5.8d. The tube is left permanently bent as shown in Figure 5.8e. To our knowledge, this is the first example of a non-axisymmetric propagating bulge instability.

One complication with this setup is that the bulge initiates in a different location for each experiment and may propagate in either or both directions. Each tube has small random imperfections due to the manufacturing process and the bulge initiates on those defects due to the higher stresses. However, the bulge can be forced to initiate at a consistent location by intentionally adding a defect to each tube before pressurization. The defects were engraved with a laser and were drawn in the circumferential direction to prevent any biases in the θ direction. These biases were considered since the tubes bulged nonaxisymmetrically. The defects were engraved near the end of the tubes to force the bulges to propagate in a single direction.

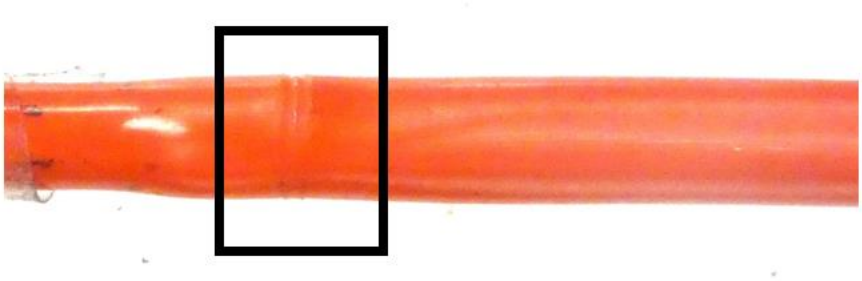

Figure 5.9. Tube with circumferential defect added to control location of bulge initiation. Doing so gives consistitently unidirectional propagation.

One trial at 0.7mL/min was conducted to show how an external limiter can induce stable axial bulge propagation and quantify propagation velocity, end displacement, and end velocity during stable propagation. For this trial, an engraved defect was added in the circumferential direction as shown in Figure 5.9. Similar to Figure 5.8, the propagation is stable as shown in Figure

5.10d since the pressure is constant after the bulge initiates. This same analysis was done for subsequent trials but this first section here shows how the above quantities were extracted. After running this trial, the videos were played on VLC and every tenth frame was saved. The frames were imported into ImageJ to make image sequences for each trial. Markers were drawn to define the number of pixels per cm in the videos using the ruler in the image for reference. Once the scale was set, markers were placed every nth frame at the propagation front to see how far the propagation front had traveled per unit of time. Markers measuring end displacement were applied to the extracted frames starting at the point in the video where one could hear the pump starting. The propagation front measurement markers were applied once the front reached the top limiter since this condition allowed for the front to travel in a single direction during every trial. The interval for how often to mark a frame was chosen through trial and error. Marking too many frames could result in noisy data while marking too few frames could cause valuable information to be missed. The end displacement was plotted versus dispensed volume (calculated by multiplying the time and flow rate) and the propagation front displacement was plotted versus time. The propagation velocity was calculated by taking a linear fit to the propagation displacement vs time data.

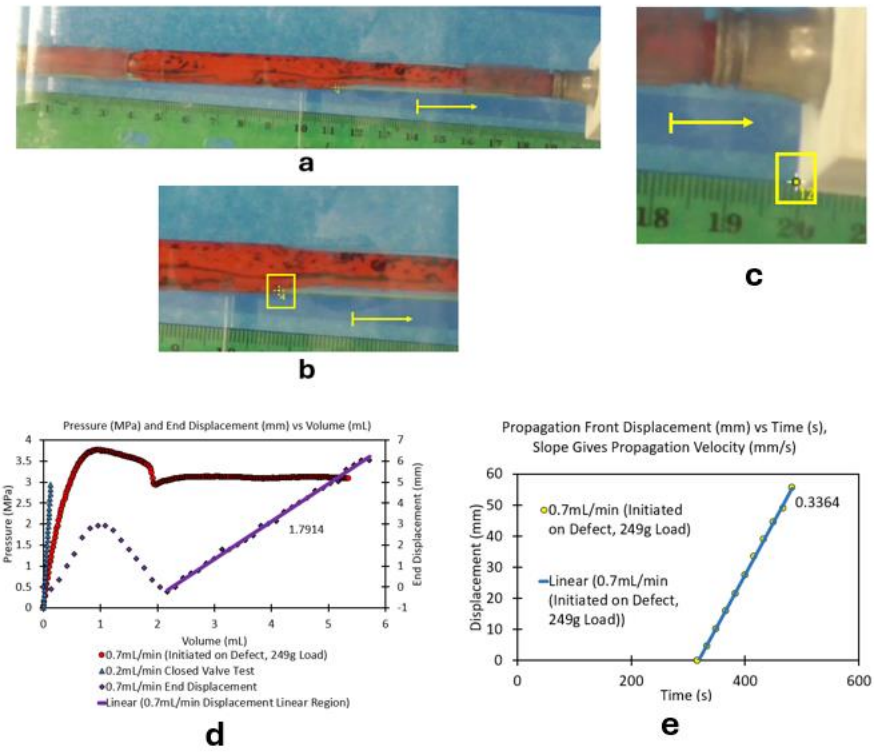

Figure 5.10 a. An example point in ImageJ used for measuring propagation velocity. The yellow arrow shows the direction for positive displacement which implies a lengthening of the bulged zone. b. Zoomed in version of a. c. An example point in ImageJ used for measuring end displacement. Positive displacement as shown by the arrow implies an increase in tube length. d. Pressure-volume plot showing a closed valve test and a 0.7mL/min open valve test (explanations for these are found in Chapter 3). The end displacement grows linearly during the later stages of the test and the trendline shows the rate of growth with respect to volume (slope is labeled). e. Displacement of the propagation front versus time. Slope gives propagation velocity. The "zero displacement" point is arbitrary and has no meaning since only the change in displacement is needed to calculate propagation velocity

An elastic modulus can be estimated from the pressure-volume data and compared against the tensile measurements. The pressure-volume data in for the closed and open valve test appeared mostly linear near the start of the trial. Data up to 2MPa was plotted and linear trendlines were fit to each data set as shown below in Figure 5.11a. The volumes at each pressure were subtracted and this created a pressure vs change in volume plot as shown in Figure 5.11b. This subtraction in the volume is done to remove the added volume due to the compliance within the pump and piping. With the subtracted volume known, it is possible to know the amount of volume involved in inflating the tube and this can be used to estimate the strains the tube experiences.

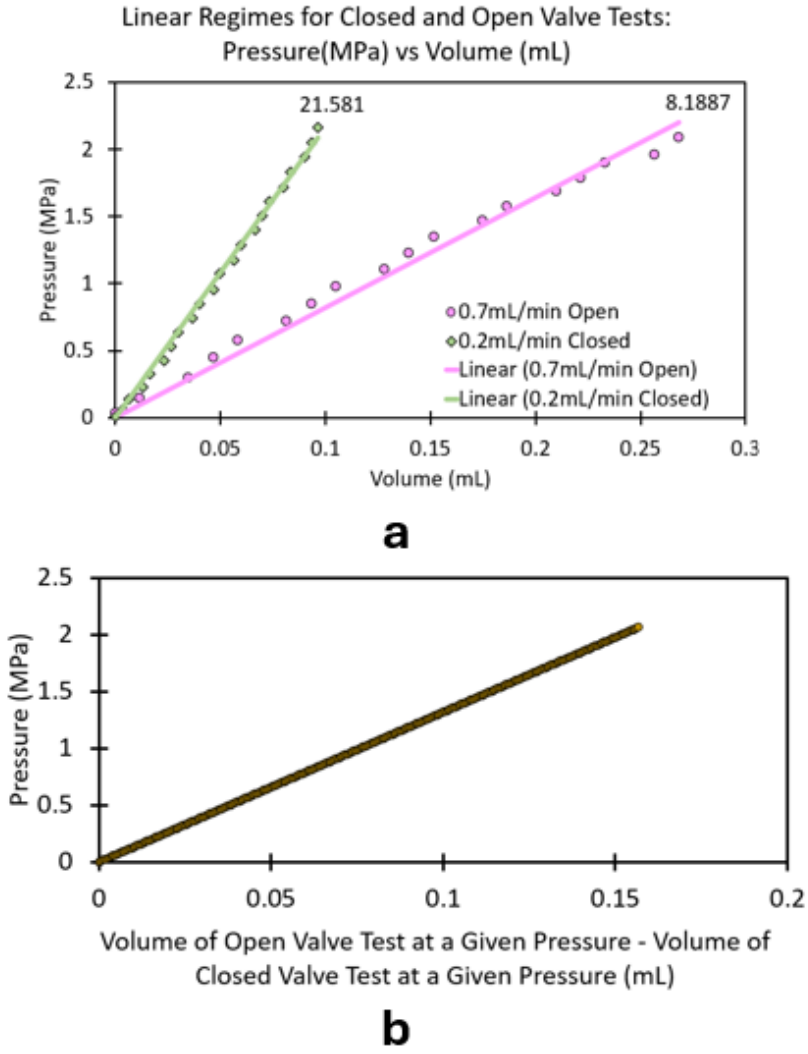

Figure 5.11 a. Pressure versus volume during the initial sharp increase in pressure. Change in volume is calculated by taking two points at the same pressure and subtracting their corresponding volumes from the trendlines. These trendlines were then used to calculate values for a pressure versus change in volume plot. The values for the volumes at set pressures were found on each trendline and these became the values for the pressure versus change in volume plot shown below. b. Estimated pressure versus change in volume plot

for the initial steep rise in pressure. An elastic modulus can be estimated from this combined with the tube dimensions.

After subtracting the volumes of the closed and open valve tests, an elastic modulus can be estimated. Equation **2-15** comes from assuming the tube to be incompressible. This means that length changes are assumed to be 0.

$$\sigma_\theta = \frac{2PR_1^2}{R_2^2 - R_1^2} \qquad \textbf{5-4}$$

σ_θ at r = R_2 was calculated from the pressure-volume plot using equation **5-4** which is derived by substituting R_2 for r in equation **2-8.**

$$A = V/L \qquad \textbf{5-5}$$

Due to the lack of any change in length, a pressure vs cross-sectional area curve can be obtained by using equation **5-5**.

$$r_2 = \sqrt{\frac{A}{\pi}} \qquad \textbf{5-6}$$

The values for r_2 are derived from the calculated cross-sectional areas using equation **5-6.**

$$\epsilon_\theta = \frac{r_2 - R_2}{R_2} \qquad \textbf{5-7}$$

ε_θ was calculated from equation **5-7** and the slope of the σ_θ vs ε_θ curve gave the estimated elastic modulus. These calculations gave an estimated elastic modulus of 154 MPa which does not agree with the results from the uniaxial tensile tests (67.2MPa). Possible explanations for these disagreements are measurement errors, differences in strain rate, and anisotropy due manufacturing processes.

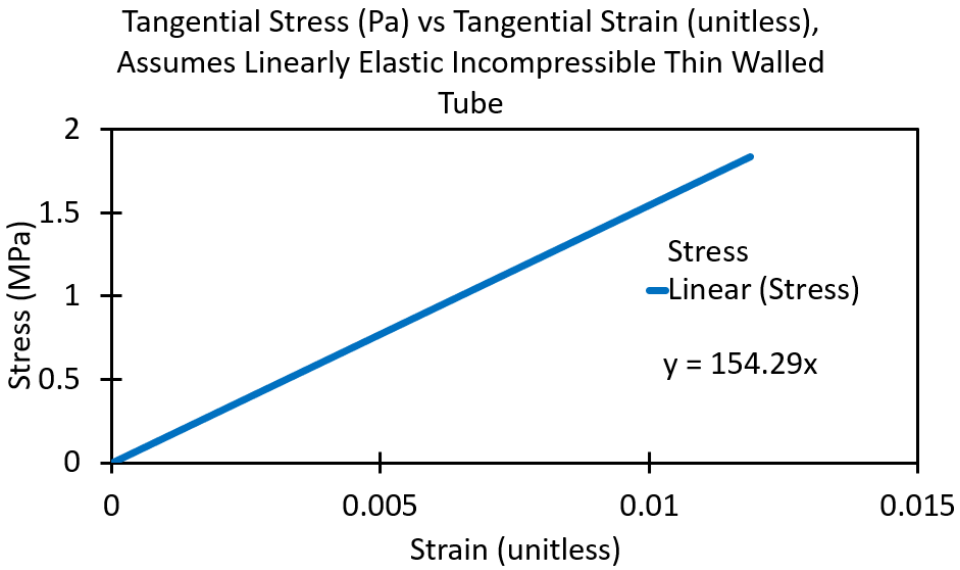

Figure 5.12 An estimated stress-strain curve from a 0.7mL/min open valve test using equations 5-4 and-5-7. The slope gives an estimated elastic modulus.

The axial elongation of the tubes is modest. For example, Figure 5.10d indicates a value of roughly 5%. Due to the limiter, the diameter of the unexpanded section is difficult to measure accurately due to poor image quality. However, if one assumes that the tube wall is incompressible, it is possible to estimate the inner and outer diameters of the unexpanded section during stable propagation. This can be done through the conservation of volume as seen in Figure 5.13. Knowing the propagation velocity and flow rate makes these calculations possible since the volume of the tube at times t_1 and t_2 is known. Knowing the propagation velocity also allows one to calculate the change in propagation front displacement between t_1 and t_2. Both these values can be used to calculate the unexpanded diameter.

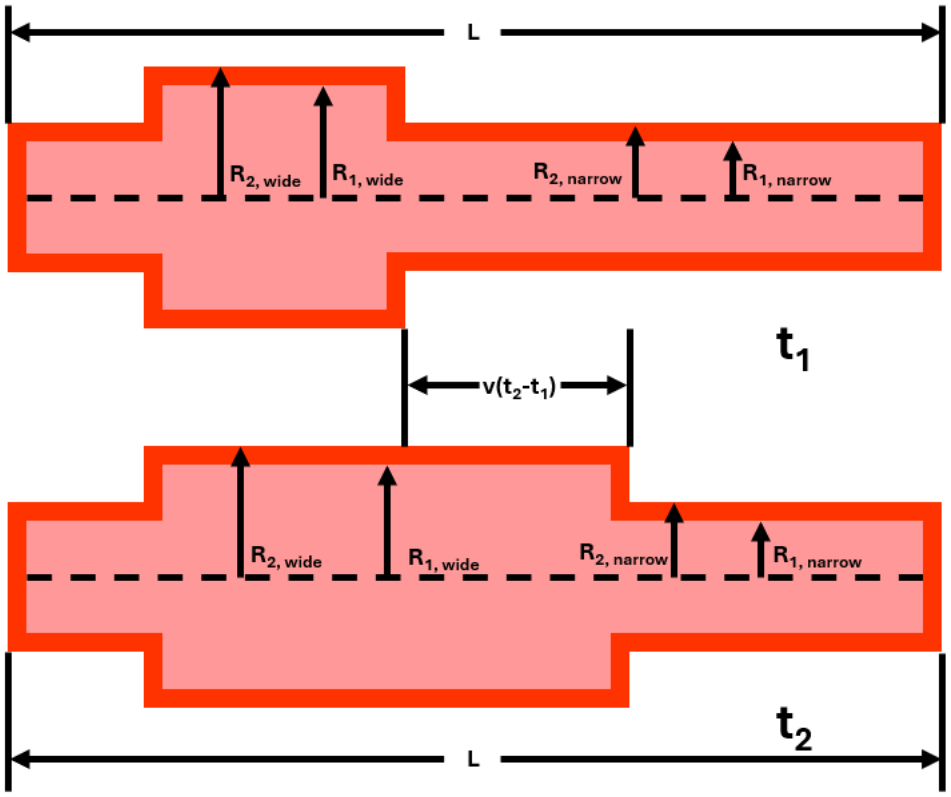

Figure 5.13 cross section of an inflated tube experiencing stable propagation at times t_1 and t_2. Conservation of volume and propagation velocity are used to estimate the diameters of the unexpanded section.

	Volume of propagated section = volume of unpropagated section + flow rate · time	**5-8**

Equation **5-8** comes from the conservation of volume. This can be done since the tube walls and the water being pumped inside are both assumed to be incompressible. In this example, f is 2mL/min, v is 0.909mm/s, and $R_{2,\,wide}$ is 5.1mm since a 10.2mm limiter was used.

$$\pi R_{2,\,wide}^2 vt = \pi R_{2,\,narrow}^2 vt + ft \qquad \textbf{5-9}$$

When eliminating t and solving for $R_{2,narrow}$, the equation becomes

$$R_{2,narrow} = \sqrt{R_{2,wide}^2 - \frac{f}{\pi v}} \quad \textbf{5-10}$$

Assuming the tube walls to be incompressible makes it easy to calculate the unexpanded inner diameter through volume conservation.

$$\text{Inner volume} + \text{wall volume} = \text{total volume} \quad \textbf{5-11}$$

$$\pi R_{1,\,narrow}^2 L + V_{wall} = \pi R_{2,\,narrow}^2 L \quad \textbf{5-12}$$

When solving for the unpropagated outer diameter, the above equation becomes

$$R_{2,\,narrow} = \sqrt{R_{1,\,narrow}^2 + \frac{V_{wall}}{\pi L}} \quad \textbf{5-13}$$

For this sample, $R_{1,narrow}$ is 5.96mm and $R_{2,narrow}$ is 7.74mm. These values imply that the unexpanded section of the tube has a tangential stretch of 1.49 on the inner surface and a tangential stretch of 1.22 on the outer surface. This means that the unexpanded section is still wider than the reference configuration but still significantly narrower than the expanded section which is expected since the tube is still pressurized.

Qualitatively, the bulges left behind significant amounts of plastic deformation as seen in Figure 5.8e. This plasticity was clearly nonaxisymmetric and as expected, the parts of the tube that experienced larger deformations during inflation showed much higher levels of plasticity after being depressurized. Interestingly, the area where the bulge initiated had a thinner ridge when compared to the regions of the tube where bulging happened due to propagation as seen in Figure 5.9. Also, a cross-sectional image showed significant amounts of thinning in the bulged region which agrees with the idea that the bulge was triggered by a localized necking instability and this effect is seen in Figure 5.8c. The necked region had a consistent wall thickness which is visible in Figure 5.8b.

5.5 Limiter Size Effects

Changing the constraint affects many variables. As expected, these changes occur after unloading. Regardless of maximum limiter size, it is expected that the peak pressure would remain the same since the pressure peaks before the instability develops. Once a bulge forms, the pressure drops suddenly until the bulge contacts the limiter. After contacting the limiter, the pressure stabilizes as the bulge starts propagating. It is expected that the propagation pressure will be lower when the limiter diameter is increased since the walls thickness to diameter ratio will be smaller

at larger circumferential strains. Also, it is expected that the propagation velocity will be slower with larger limiters due to the volumetric flow rate being the same while the cross-sectional area is larger. For these experiments the wall thickness of the necked region was determined by taking cross sections of the tubes and taking four measurements within the thinner region. The wall thickness to diameter ratio was calculated by normalizing the wall thickness by the limiter diameter. Measurements for these are shown in Figure 5.17a and Figure 5.17b in section 5.5.1.

During these experiments, limiters with inner diameters of 9.3mm, 10.2mm, 11.4mm, 12.0mm, and 13.6mm were used. The 9.3mm, 11.4mm, and 12.0mm sizes were created by lining larger limiters with thin sheets of plastic wrap on the inside. Detailed results for multiple tests are shown in Appendix B since only a brief summary is discussed here. When the limiter's inner diameter was increased from 10.2mm to 13.6mm, some significant changes occurred after unloading. The pressure decreased and the bulge appeared to propagate for a short distance before bursting. The plastic wrap chosen was a thin sheet to keep the "step" within the wrapping small while also making the wrapping process easier. The limiter was washed with water and ethanol in between each trial to improve visibility. For the experiments with the 13.6mm limiter, the pressure drop during unloading was more pronounced when compared to the tubes constrained by the 10.2mm limiter as seen in Figure 5.14a. Based on the pressure-volume response, stable propagation was not achieved due to the tubes rupturing. End displacement measurements for the 13.6mm tests in Figure 5.14b were of poor quality so conclusions could not be drawn from that data.

5.5.1 Limiter Size Summary

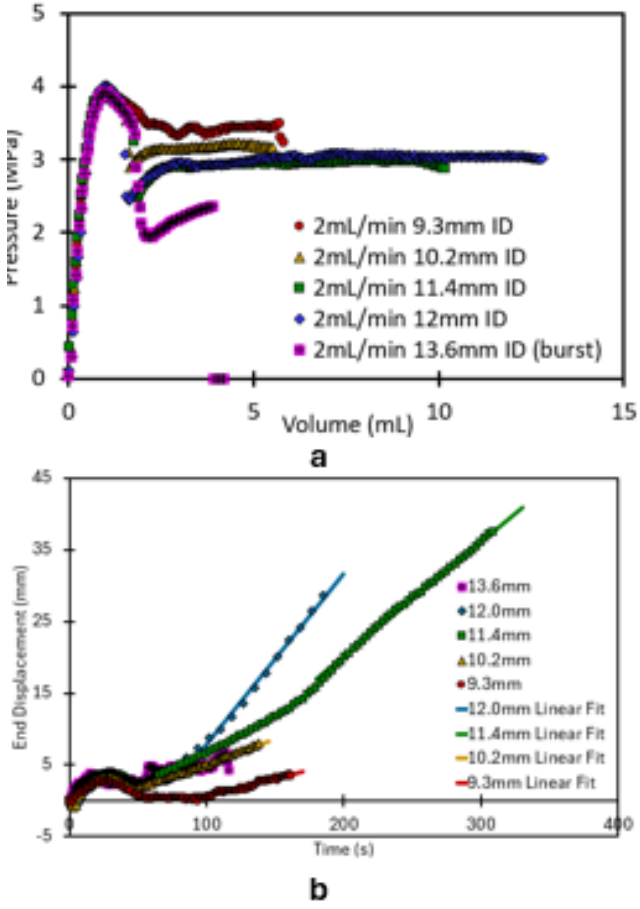

Figure 5.14 a. Comparing pressure-volume relations to limiter size. No significant changes in peak pressure were observed but increasing the limiter size reduced the propagation pressure. b. End Displacement vs time. Once steady state propagation is reached, the curve is roughly linear.

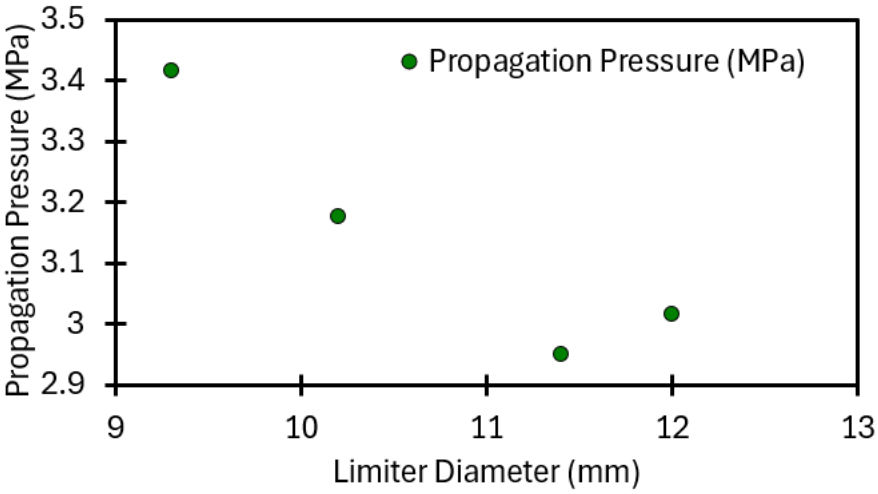

Figure 5.15 Propagation pressure vs limiter diameter.

As expected, the pressure before the peak was unaffected by limiter diameter as shown in Figure 5.14a since both measurements were taken before the tube contacted the limiter. However, the propagation pressure decreased (Figure 5.14a and Figure 5.15).

When cross-sections were taken the bulged section of each tube as seen in Figure 5.16, tubes inflated in larger limiters generally had thinner necked sections and smaller wall thickness to diameter ratios which supports the hypothesis that larger limiters reduce the propagation pressure due to wall thinning as seen in Figure 5.15 and Figure 5.17b. Cross-sections generally showed a distinct thick region and a thinner necked region although some tests had irregularities within the necked region as shown in Figure 5.16b and Figure 5.16f. This confirms that the tubes generally experienced stable circumferential necking with the addition of an external limiter.

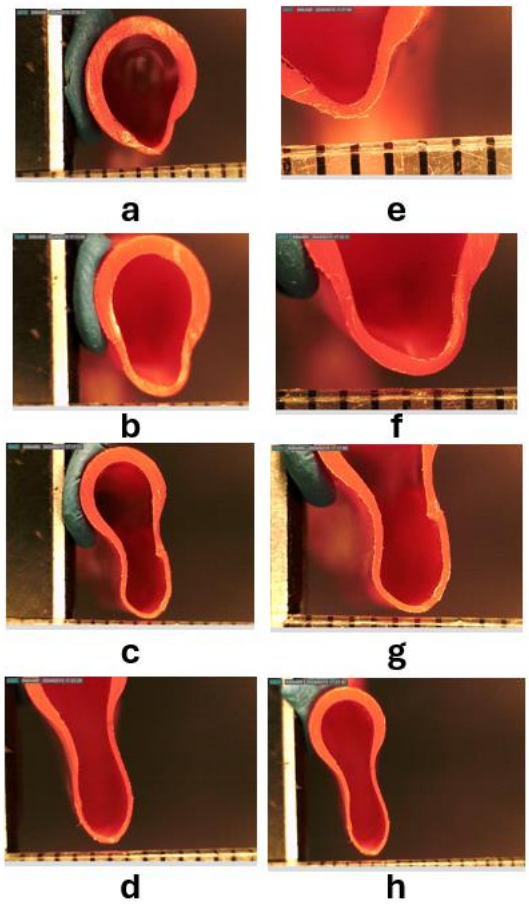

Figure 5.16 Cross sections of tubes inflated inside various limiter sizes. a. 9.3mm limiter. b. 10.2mm limiter. c. 11.4mm limiter. d. 12.0mm limiter. e-h. Zoomed in versions of a-d.

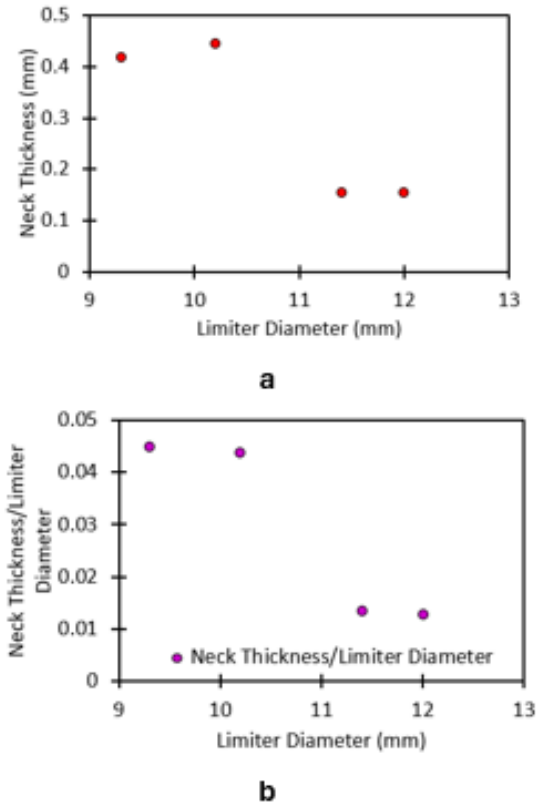

Figure 5.17 a. Thickness of necked region vs limiter diameter. b. Neck thickness to limiter diameter ratio vs limiter diameter.

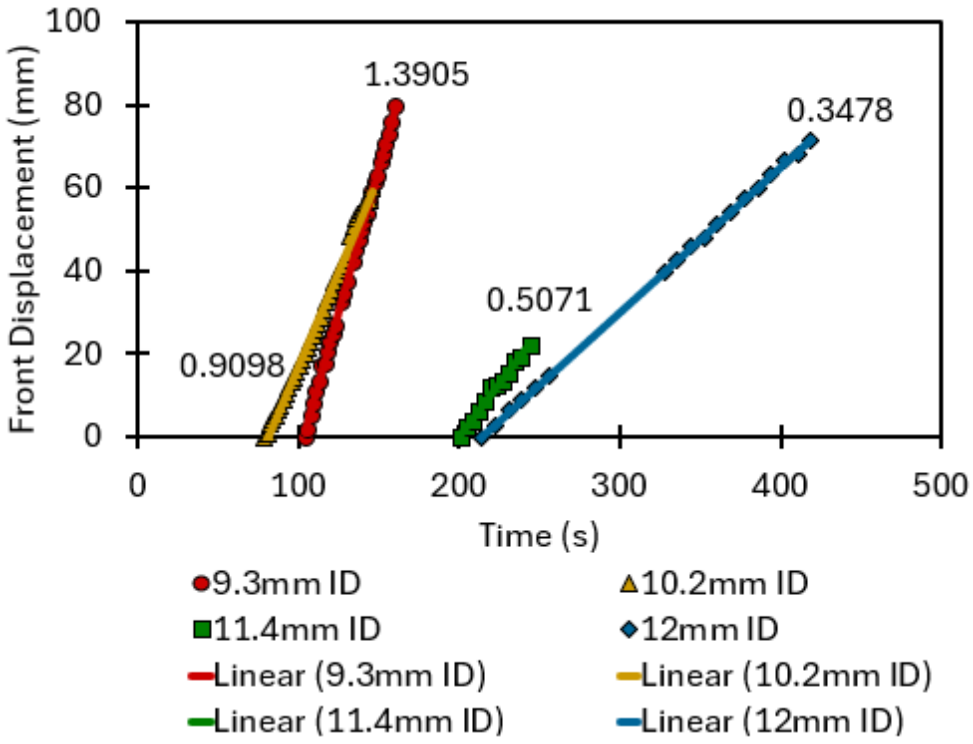

Figure 5.18 Propagation front displacement vs time since start of experiment. Slopes give propagation velocities. Increased limiter sizes resulted in lower velocities.

Propagation velocity also decreased with increased limiter size as shown in Figure 5.18. This agreed with the expectations and is likely the result of larger limiters causing the bulged sections of the tubes to have larger cross sectional areas. A larger cross sectional area within the bulged section would require more volume to force the bulge front to propagate the same amount of distance. Since the volumetric flow rate is the same between trials, this results in the bulge propagating at a slower rate.

Another observation is that the end displacements generally increased with increasing limiter size as shown in Figure 5.14b. This is partly due to the tubes inside larger limiters reaching higher volumes during propagation. Higher volumes are reached with larger limiters due to the larger diameters combined with no change in limiter length. However, the rate of increase in end displacement during steady propagation also increases with increasing limiter

diameter as shown in Figure 5.14b and Figure 5.19b. The cause of this is not known.

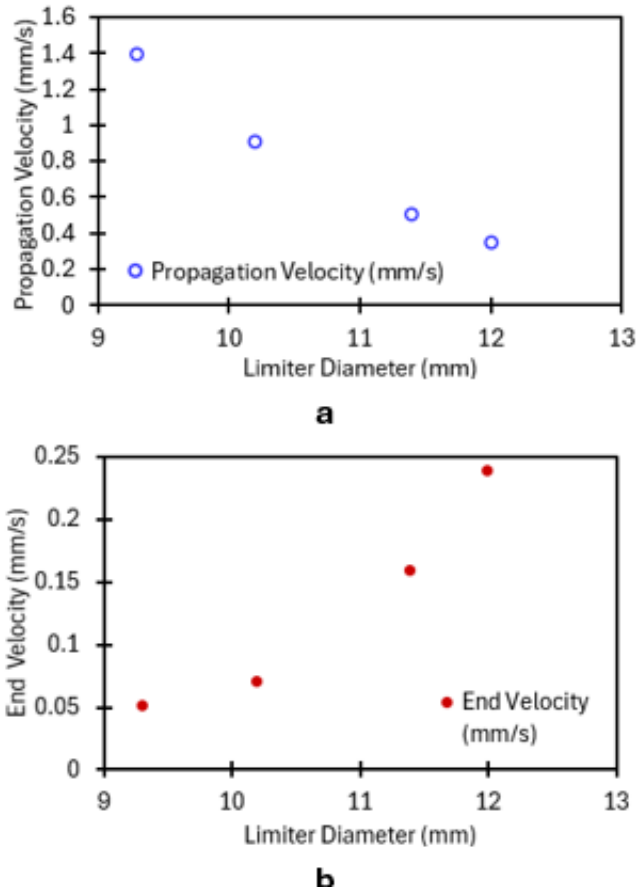

Figure 5.19 a. Propagation velocity and steady state end velocity vs limiter diameter. b. Estimated outer diameter of section without bulge vs limiter diameter.

The estimates for the unexpanded outer diameters during steady state propagation based on propagation velocity appeared reasonable for the 9.3mm, 10.2mm, and 11.4mm trials but not for the 12.0mm. The estimates for the 9.3mm, 10.2mm, and 11.4mm trials appeared reasonable since they implied that the unexpanded section was still experiencing some stretch due to the tube being pressurized. However, the unexpanded sections did not follow the expected pattern of decreasing with increased limiter diameter. This decrease was expected due to the lower propagation pressures associated with higher limiter diameters. Data from the 12.0mm tests estimated an unexpanded diameter below the diameter of the reference configuration which

implied contraction of that section. The contraction likely did not happen since the unexpanded section was still pressurized. This artifact was more likely to be caused by incorrect propagation velocity measurements or using invalid assumptions when estimating the unexpanded diameter.

The end displacements of the 9.3mm test were measured poorly resulting in few if any conclusions. The small axial stretches combined with the tube's angle changing during inflation made the end displacements difficult to measure in this set. This change in angle was neglected when measuring the end displacements since only displacements in the X direction were considered. This causes the tube to appear "shorter" when the angle is steeper and "longer" when the angle is shallower. The propagation velocity measurements were likely affected too but to a lesser degree.

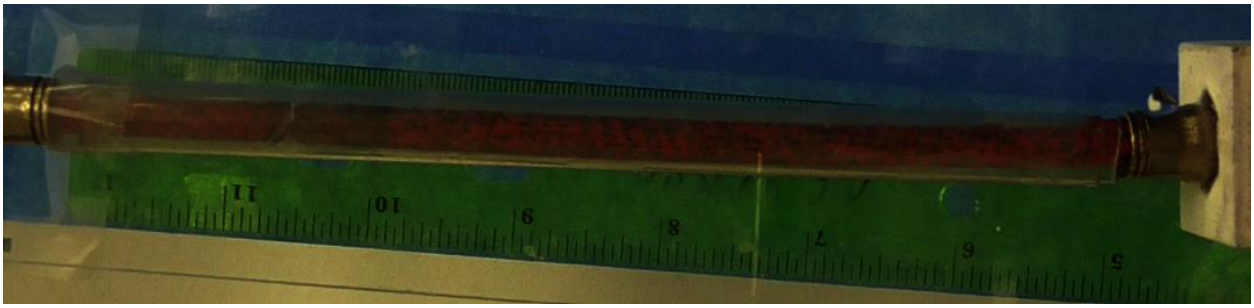

Figure 5.20 Displacement values will appear larger here due to the tube being nearly parallel to the x axis.

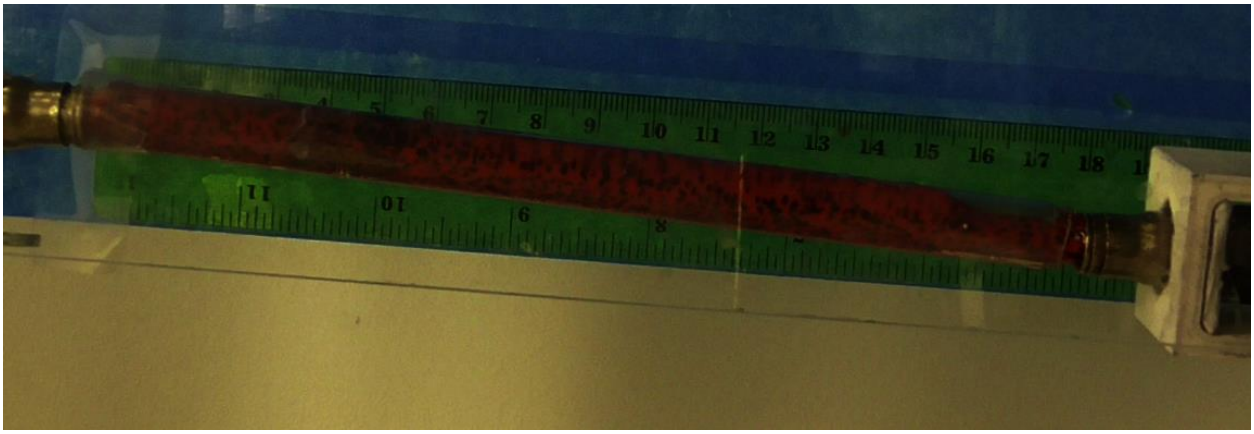

Figure 5.21 Displacement values will appear smaller here due to the tube being at an angle from the x axis.

5.6 Rate Dependence

Plastics often experience rate dependence and appear stiffer when deformed at higher rates. Many plastics also experience stress relaxation when under constant strain and creep when under constant stress. In these experiments, flow rate serves as a good proxy for strain rate since inflating the tube more rapidly causes a similar change in strain but over a shorter time. Previous literature shows that the yield strength of some viscoelastic materials increases with increasing strain rate [39] [40]. However, the behavior after yielding remained qualitatively similar in some plastics while appearing qualitatively different for others. For example, polycarbonate samples tested in uniaxial compression at a large range of strain rates had qualitatively similar yielding behavior despite the differences in yield strength [39]. In contrast, PMMA samples in compression had qualitatively different yielding behavior at different strain rates with higher strain rates showing more softening after yielding [39].

In the experiments here, flow rate acted as a proxy for strain rate. The flow rates chosen were 0.7mL/min, 2mL/min, and 6mL/min since each rate was roughly triple the previous one. This range of flow rates provided a wide range of strain rates while keeping experiment run times reasonable but slow enough to collect sufficient data points. The limiter diameter was kept constant at 10.2mm for all trials to keep the cross sectional area of the bulged section constant which means the propagation velocity should be proportional to the flow rate. Since higher flow rates result in higher strain rates and therefore higher yield strengths, it can be expected that the peak pressure should be higher with increasing flow rates. Assuming the general shape of the stress-strain curve does not change with strain rate the end displacements should follow similar trajectories with respect to volume and that the end velocities should be proportional to the flow rate.

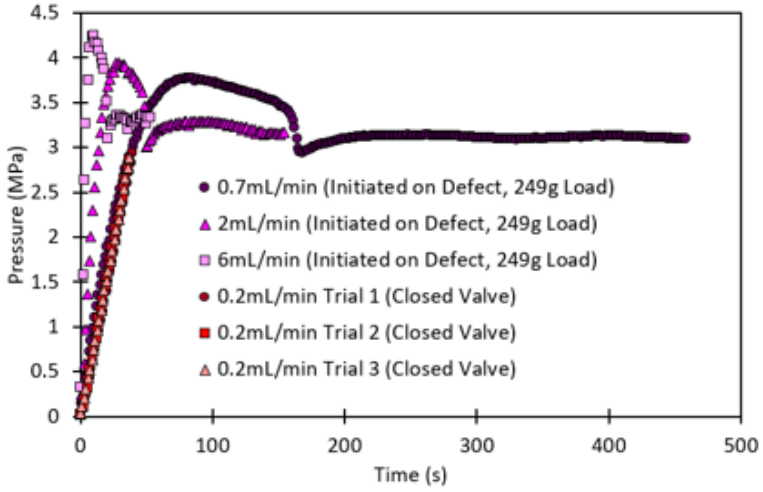

a

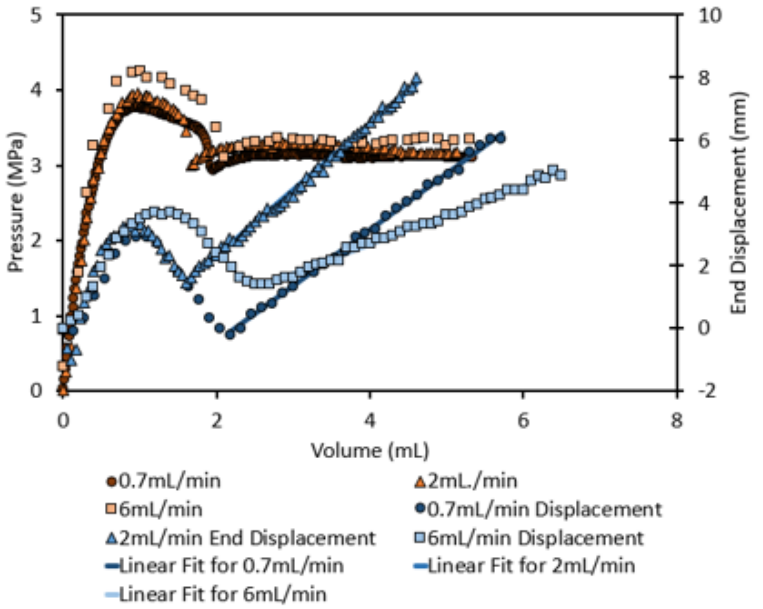

b

Figure 5.22 a. Raw pressure-time data for three 0.2mL/min closed valve trials and open valve trials at 0.7mL/min, 2 mL/min, and 6mL/min. b. Summary plot showing the pressure-volume and pressure-end displacement relations of the 0.7mL/min, 2mL/min, and 6mL/min open valve trials.

From Figure 5.22, it can be seen that changing the flow rate (and therefore the strain rate) has only modest effects on the pressure-volume curves and that the general shape of the curves remains the same. It can be seen that the peak pressure happens at almost exactly the same volume and that the steady state propagation pressure is similar regardless of strain rate. However, the peak pressure increases as the strain rate increases as seen in Figure 5.22 and Figure 5.23b.

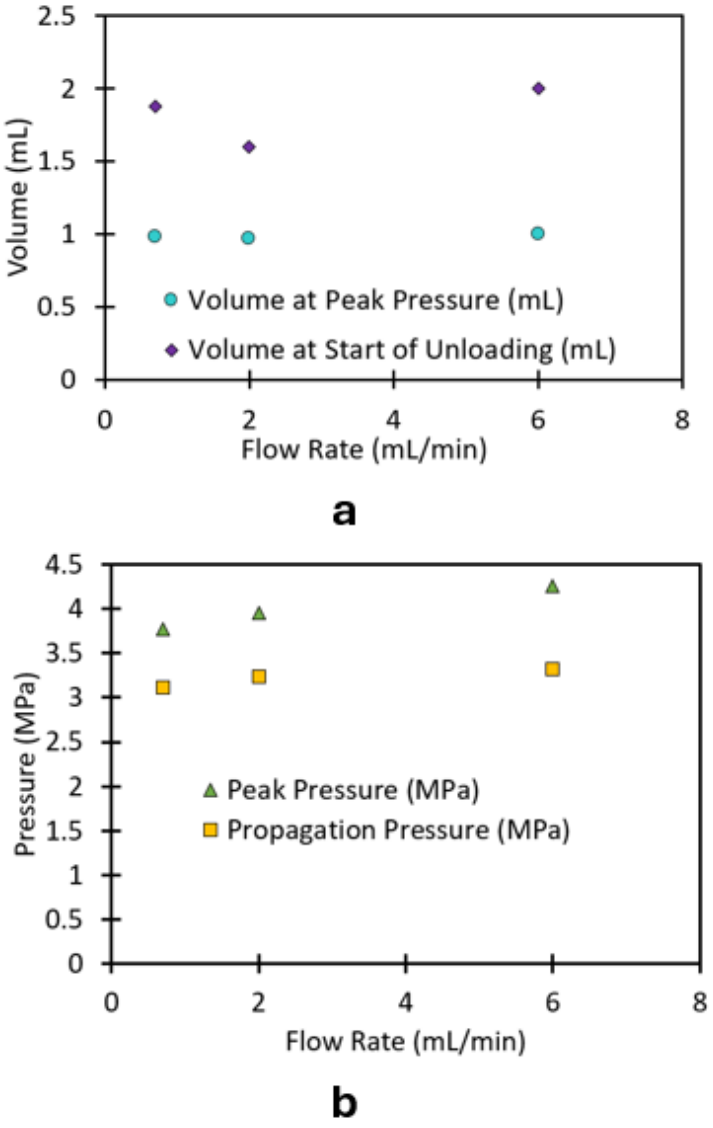

Figure 5.23 a. Volume at max pressure and volume at start of unloading versus flow rate. b. Maximum pressure versus flow rate and propagation pressure versus flow rate.

Tests also showed the propagation velocity to roughly triple when the flow rate is tripled. This is seen in Figure 5.24. This is expected as the bulge's volume increases at a nearly constant rate once steady state propagation is reached. Increasing the flow rate should proportionally

increase the rate at which the volume in the bulge increases during propagation since the cross sectional area of the bulge is the same regardless of the flow rate.

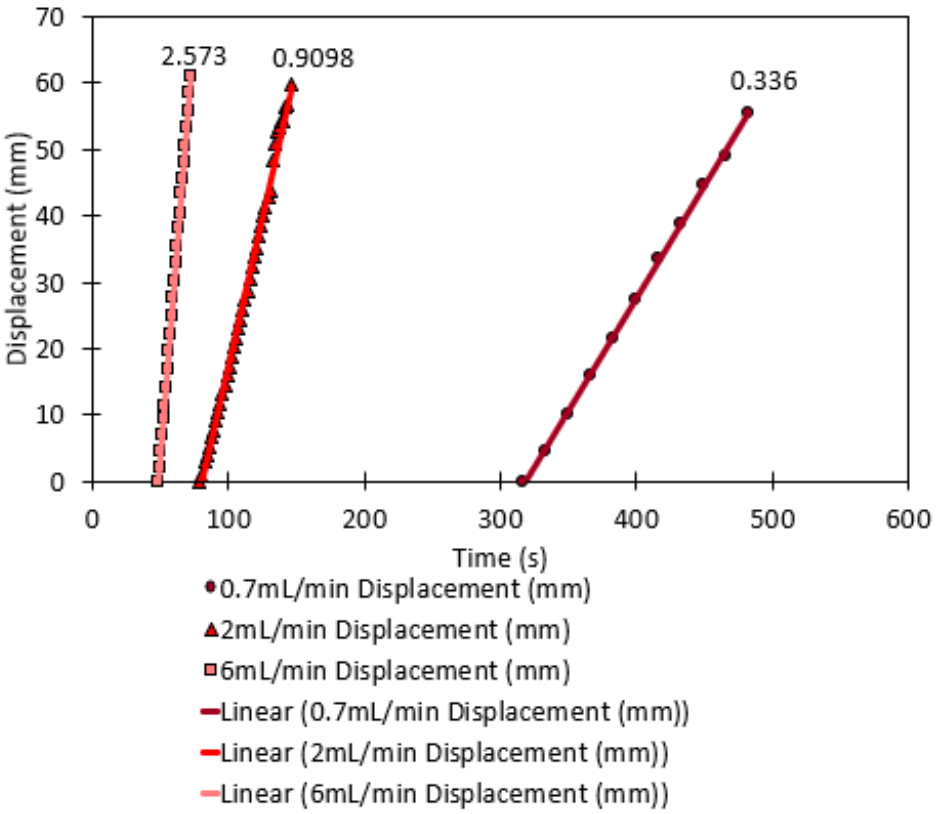

Figure 5.24 Propagation front displacement versus time since start of experiment for tests at 0.7mL/min, 2mL/min, and 6mL/min.

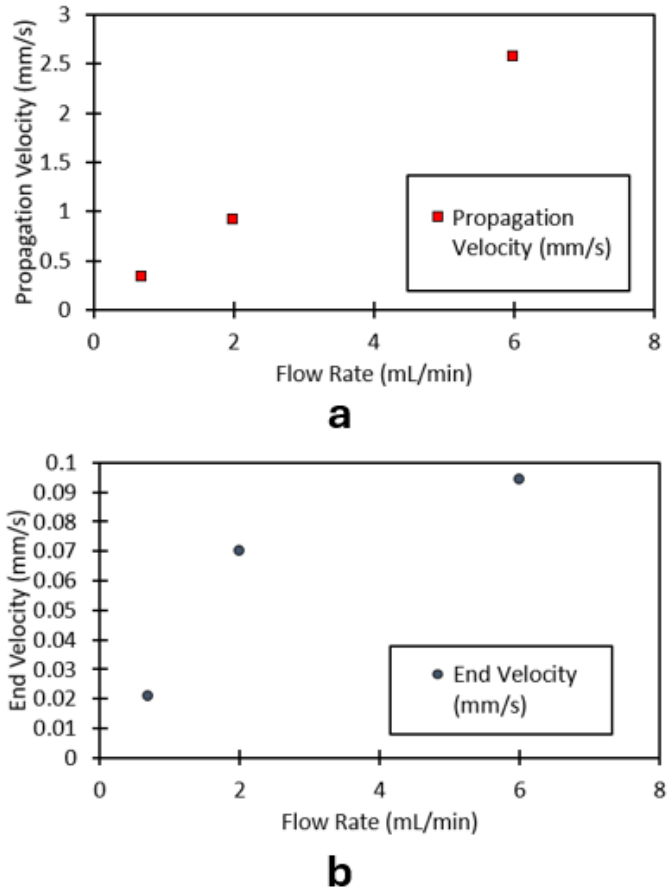

Figure 5.25 a. Propagation velocity vs flow rate. b. End velocity versus flow rate.

The data for the displacements and end velocities are shown below in Figure 5.25 and Figure 5.22b. Although the propagation velocities generally align with each other, end displacements behave differently. They all generally show a similar pattern where the tube lengthens initially, contracts when the bulge first appears, and lengthens again as the bulge propagates. As the strain rate increased, the tube contracted less. This was most apparent between the 0.7mL/min test and the 2mL/min test but was still noticeable when comparing the 2mL/min test to the 6mL/min test. The end velocity in the final linear regime roughly tripled as expected in between the 0.7mL/min and the 2mL/min trials but increased by less than 1.5-fold between the

2mL/min and the 6mL/min trials. It was also seen that the first local maximum in the displacement curve happened either during or slightly after the maximum pressure and the local minimum in the displacement curve occurred during or after unloading. It was also observed that increasing the flow rate resulted in a more gradual transition from the shortening to the lengthening portion of the data.

Due to the propagation pressures being similar regardless of flow rate, it is expected that the stresses and strains of the unexpanded sections are also similar. Since strain in the unexpanded trials is similar, one can expect the inner and outer diameters of the unexpanded sections to be independent of the flow rate. Minimal changes in the estimated unexpected diameters were calculated between each trial as shown in Figure 5.26. These results qualitatively agree with the above predictions.

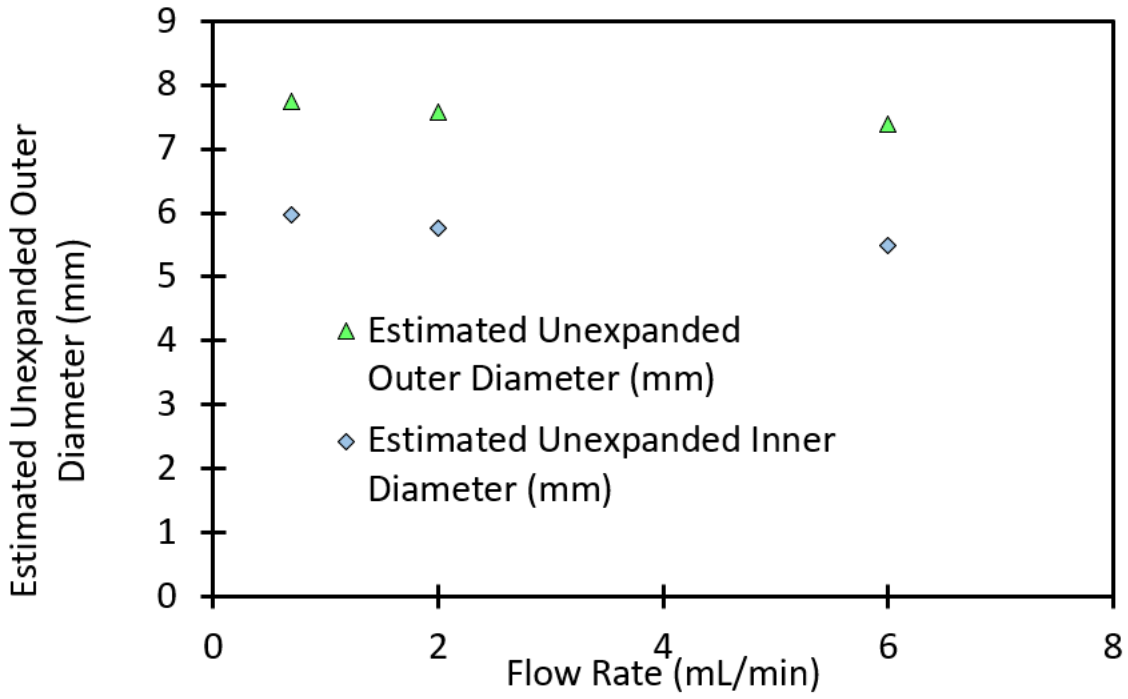

Figure 5.26 Estimated unexpanded outer and inner diameters versus flow rate from equation

5.7 Stable vs Unstable Propagation

Since the pressure reduces during stable propagation, it was hypothesized that this pressure may be lower than the rupture pressure of the tubes. Equivalently, we hypothesized that the non-axisymmetric propagating instabilities in constrained tubes, once started, may continued to propagate after the limiter was removed. To test this, a constant flow rate of 2mL/min was chosen and a limiter covering only a portion of the tube was used. A circumferential defect was added to trigger the formation of an instability in the section of the tube covered by the limiter. The constant flow continued to force the bulge to propagate and eventually escape the limiter.

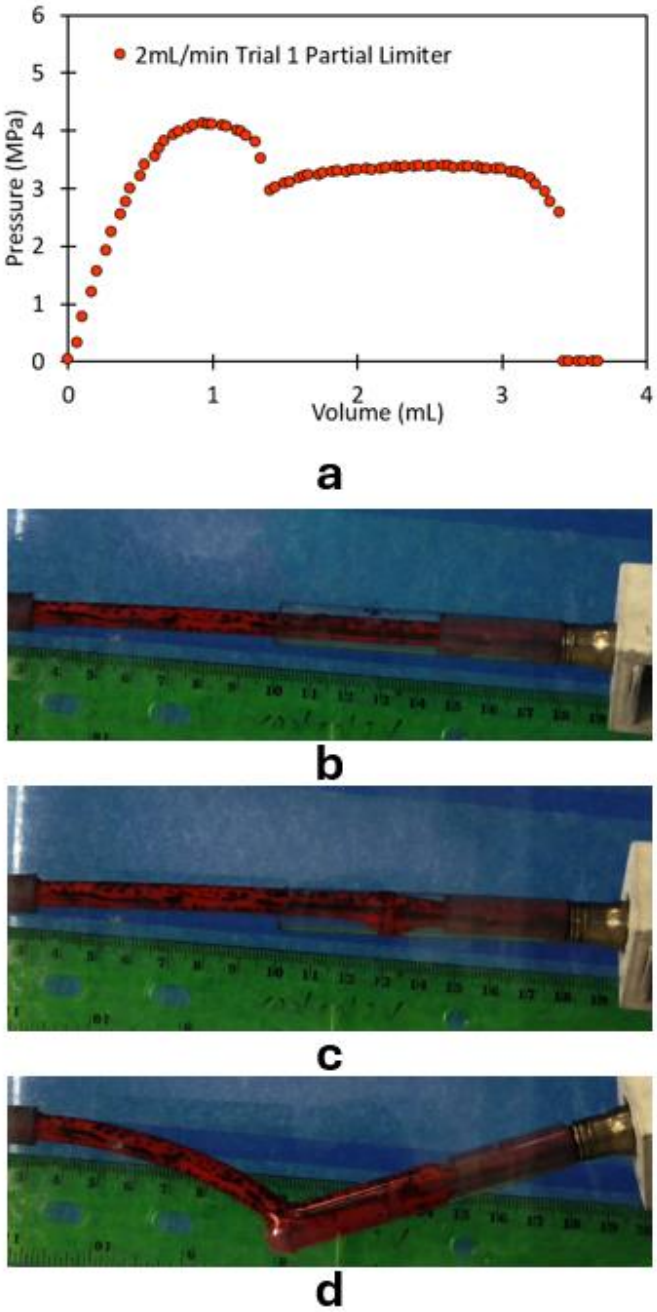

Figure 5.27 a. Pressure-volume and end displacement-volume relations for a tube where an instability was triggered inside a 10.2mm limiter and propagated past the limiter's exit. b. Setup with a 10.2mm limiter that covers part of the tube. c. Initiation of bulge within limiter. d. Bulge exiting limiter.

It was found (Figure 5.27d) that the propagation could not continue beyond the limiter. Propagation within the limiter had similar behavior compared to fully constrained tests and propagation lasted long enough for the pressure to level off. However, after exiting the limiter, the bulge started expanding further. The pressure dropped and rupture happened shortly after.

6.0 Conclusions and Future Research

6.1 Summary of Polyurethane Tube Tests

Based on the results of the tests done in Section 4.3, Section 4.4.2, Appendix A.6, and Appendix A.7, viscoelasticity has a significant effect on tube behavior. In Section 4.3, tests done at different flow rates found that viscoelasticity affects the absolute pressure values and tube profile although the shape of each curve remains largely unchanged. A similar pattern was seen in the uniaxial tensile tests in Appendix Figure 13. Interestingly, higher flow rates generally resulted in more uniform expansion but did not guarantee it. Also, the presence of a pressure maximum did not guarantee the formation of a bulge which contrasts with previous literature evaluating tubes with elastic models [5].

Other than viscoelasticity, strain-induced damage has a significant effect on bulging behavior. Even inflations to 1.5mL (considerably less than what is needed to cause permanent deformation) caused softening in future inflation cycles as seen in Figure 4.7. When inflated to volumes large enough to cause bulging but still below what is needed to cause permanent deformation, the bulged portion was exaggerated on the second inflation cycle along with a decrease in the end displacement. It is plausible to assume that the strain-induced damage was larger in the bulged section causing that section to deform more easily when re-inflated. The decrease in end displacement is likely due to the high amount of softening in the bulged section making deformation in the tangential direction more energetically favorable than deformation in the axial direction.

Once taken to even larger volumes, plasticity (permanent deformation) also comes into play. Under larger inflations, not surprisingly, the bulged sections had more visible plasticity after depressurization as shown in Figure 4.5. When the effects of plasticity and strain-induced damage were both present on the 15mL curve in Figure 4.7, a bulge was present during re-inflation but the pressure increased monotonically. This series of events cannot be explained through a purely elastic analysis [5].

6.2 Future Research on Polyurethane Tubes

Due to the limitations of the push-to-connect fittings used, the effect of large axial loads was not able to be studied here. Based on the inner diameter of the tubes tested and the typical values for the maximum pressures, the force exerted on the push-to-connect fittings was about 37N and was calculated as per equation **6-1**.

$$F_{max} = P_{peak}\pi R_2^2 \qquad \textbf{6-1}$$

In order for any external axial loads to have any significant effect, the applied loads had to have been on the order of at least 10N which would have caused the fittings to fail. Previous literature found that sufficiently large axial loads reduced the pressure needed to trigger the formation of an instability [5] [30]. This happened due to the axial load reducing the local pressure maximum. It is possible that polyurethane also experiences a lowering of the peak pressure with the application of a large axial load but experiments would need to be done to test this.

One other type of test that could be done in the future could be inflation testing but with displacement-controlled boundary conditions. Previous tests involving rubber tubes found that inflating rubber tubes with a fixed displacement resulted in bulge formation even in some cases where the tube would have expanded uniformly in the presence of a fixed axial load [20]. Also, the model showed that fixing the axial stretch to sufficiently high values prevented bulging which contradicts previous research showing that a higher fixed axial load lowered the pressure to initiate bulging [5] [30]. Analysis showed that this proposed model was accurate for elastic tubes with thickness to mean radius ratios of up to 1.2. This proposed model added the first two terms of a series describing the bending stiffness of the rubber tubes being tested which made the overall model more accurate for thicker tubes [20]. Adding bending stiffness to improve the accuracy of thick-walled predictions is intuitive since thicker walls have larger moments of inertia and are therefore harder to bend into shapes such as bulges when loaded.

From this previous research, testing polyurethane tubes with a fixed axial displacement could be done in multiple ways. Since bending stiffness has an impact on whether bulging occurs, changing the flow rate in a fixed displacement experiment could influence bulge formation since higher flow rates would generally result in more stiffness (including bending stiffness) due to viscoelastic effects. Also, it is possible that the critical axial displacement needed to stop bulging could depend on the strain-induced damage from previous cycles since it is possible that inflating to relatively small strains could still create nonuniform amounts of damage within the tube due to imperfections during the manufacturing process and that more heavily damaged regions could bulge on subsequent cycles. If the strain-induced damage is less uniform, it is possible that more axial stretch would be required to prevent bulging.

6.3 Summary from LDPE Tube Tests

For the uniaxial tensile tests, 2 tests run up to 300% nominal strain, the average yield strength was found to be 5.25MPa and the average elastic modulus was found to be 67.2MPa. Large amounts of plasticity were seen when pulled beyond 100% strain. No visible necking was seen when samples were pulled in the axial direction but necking was visible when samples were pulled in the tangential direction.

In the tests without external limiters, a rapid rise occurred initially and was followed by a peak which was then followed by a shallow drop in pressure. After the shallow drop, a bulge formed, causing a steep drop in pressure and rupture shortly afterwards. Yielding was found to start at the inner surface. Assuming ν=0.5, the pressure needed to initiate yielding was 1.6MPa and added volume needed to initiate yielding was 0.27mLand it was also found that assuming a lower Poisson's Ratio reduced the added volume needed to initiate yielding. However, the peak pressure (~4MPa) was significantly higher than the calculated yield pressure. The estimated elastic modulus from the calculated tangential stresses and strains was significantly higher (154MPa) when compared to the modulus from uniaxial tests. This implies either anisotropy in the samples or poor measurements. The tube's sequence of bulging and rupturing implies that there is enough strain hardening to prevent immediate rupture but not enough to force the bulge to propagate. An external limiter was then added to simulate a sudden increase in strain hardening in the circumferential direction.

As expected, limiter size had no significant impact on the peak pressure, volume at peak pressure, and elastic modulus since the processes that took place during the measurement of those properties all happened before the tube touched the limiter. However, limiter size did affect propagation velocity, propagation pressure, the wall thickness of the necked region, and the wall

thickness to diameter ratio of the necked region as shown in Figure 5.14, Figure 5.17, and Figure 5.18. The decrease in propagation velocity with increased limiter size made sense due to the conservation of volume while the reduction in propagation pressure made sense due to the decreasing wall thickness to diameter ratio in the necked region. Also, the lower wall thickness of the necked region with increased limiter size was expected since the neck was unstable before touching the limiter.

As expected, increasing the flow rate increased the maximum pressure due to viscoelastic effects. This was not surprising since higher flow rates result in higher strain rates and that viscoelastic materials tend to respond more stiffly at higher strain rates. Also, propagation velocity scaled nearly linearly with the volumetric flow rate which was expected since the tube was only allowed to expand in the axial direction after bulging. Despite the changes in propagation pressure and velocity, the general shape of each curve stayed the same. Finally, it was seen that triggering bulge formation within an external limiter and subsequently forcing the bulge to exit the limiter quickly resulted in rupture. This was one more piece of evidence that the tube necks unstably without the help of an external limiter.

6.4 Future Research on LDPE Tubes

One avenue of future research could be evaluating the effects of anisotropy. It is also possible that the LDPE tubes in the experiments here are anisotropic. Uniaxial tensile tests showed that necking occurred in the circumferential direction but not in the axial direction. Previous literature suggests that arteries with aneurysms have different amounts of anisotropy when compared to normal arteries and that collagen is less oriented in aneurysmal tissue [43] [44] [45]. This anisotropy may

take the form of stiffness, fracture strength, or strain hardening. In the example of arteries, aneurysmal tissue was found to have a higher tangential modulus to axial modulus ratio and a higher tangential failure stress to axial failure stress ratio [44] [45]. In LDPE tubes, anisotropy may be introduced by extrusion, drawing, or blowing [47] [48] [49]. Previous research shows that necking forces the polymer chains to line up in the direction of the maximum principal stress [49]. When biaxial tests were done on blown LDPE films, necking occurred when the maximum principal stress was not aligned with the polymer chains [49]. This was still true when the principal stresses were at a 2:1 ratio. This ratio may be applicable to the formation of instabilities in LLDPE tubes since thin-walled tubes experience a 2:1 ratio between the tangential and axial stresses and negligible radial stress.

One other future project could be creep tests. Previous research has been done on HDPE pipes experiencing a constant internal pressure [37] [38]. In HDPE pipes, holding the same pressure at a higher temperature resulted in a shorter lifespan. Higher internal pressures generally resulted in ductile failures and sometimes caused localized bulging before while rupture. However, lower pressures were more likely to cause a brittle fracture. Failure at very low pressures was caused by chemical degradation and rupture time was nearly independent of pressure [37]. Another study evaluated the effect of heating MDPE pipes with both ends constrained and evaluating the stress relaxation occurring when the pipes were held at the elevated temperature. It was found that heating a constrained tube caused a rise in stress proportional to the difference in current and initial temperature during heating. Afterwards, the stress dropped slightly and plateaued over thousands of minutes [36]. Stress relaxation tests at a constant temperature showed a plateau in stress with a magnitude of about half of the peak stress [36]. Both curves were qualitatively what one would expect from a viscoelastic material. In the future, creep tests involving constant pressure could be

done on LDPE tubes since the previous articles were limited to testing MDPE and HDPE [36] [37] [38]. Strain tracking could be done to evaluate how the tube deforms (including potential bulging) during the process and many tests could be done to plot rupture time vs pressure. Another possibility could be repeating the tests mentioned above but at different temperatures. These tests could be done to further study the viscoelasticity of LDPE as well as analyzing the response to pressure-controlled tests since the tests done so far here are all volume-controlled.

Yet another option could be the use of dead load tests similar to those in Figure 4.8b but with a constant internal pressure. These tests can also be run with different at different temperatures or with a fixed axial displacement. For these tests, it could be expected that higher temperatures would decrease the rupture time assuming a constant pressure while higher pressures would decrease the rupture time while assuming a constant temperature. The dead loads or fixed displacements would have to be chosen carefully since excessive loading would lead to permanent deformation before the tests start. Due to LDPE being softer, brittle fracture would be unlikely. When compared to polyurethane, the dead load test would be expected to have a faster response when compared to the polyurethane test in Figure 4.8b. This possible faster response is expected due to having a small viscoelastic effect which can be seen in Figure 4.6.

Appendix A Unconstrained Polyurethane Tubes

Appendix A.1 Reproducibility

Inflation tests on polyurethane tubes with an outer diameter of 1/4” and an inner diameter of 5/32” were inflated to set volumes and then deflated. As seen in Appendix Figure 1, the results had high reproducibility.

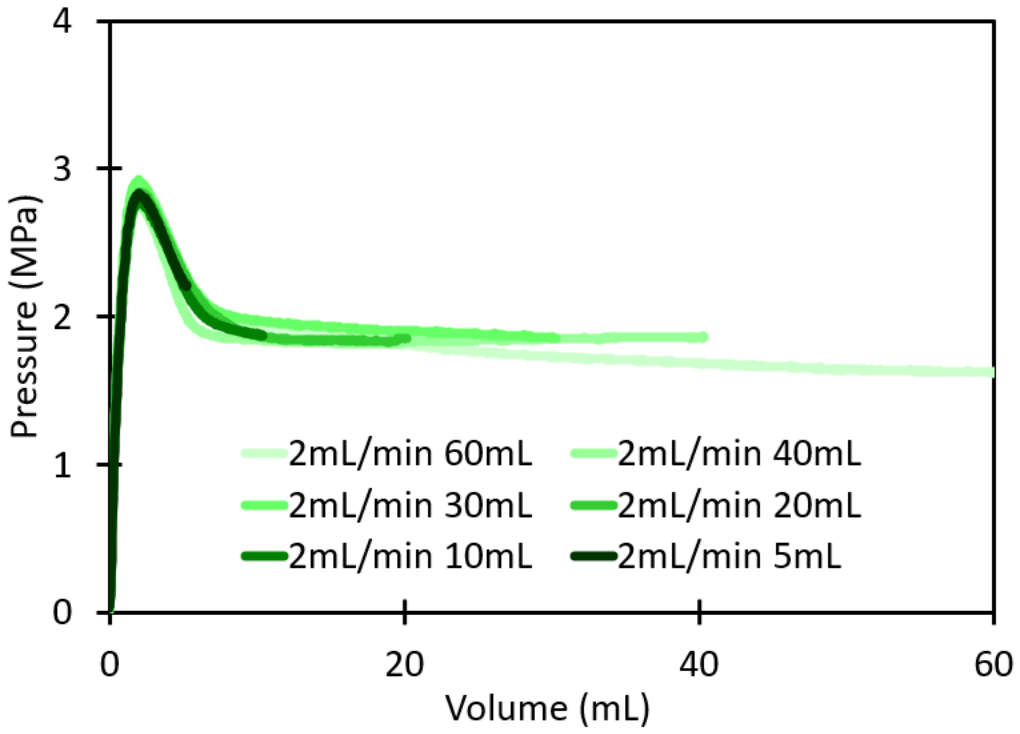

Appendix Figure 1 Pressure-volume relations for polyurethane tubes inflated at 2mL/min to a set volume.

Appendix A.2 3mL, Multicycle Inflation

Due to the softening caused by a single previous loading cycle shown in Figure 4.7 in the main document, further tests involving multiple loading cycles were done. A single tube was inflated at 2 mL/min to 3mL, and deflated, and reinflated 10 times while observing the pressure-volume relation, the profile of the tube, and the end displacement. The same experiment was done inflating to 6 mL volume and the results are shown in Appendix Figure 3.

In both cases, the pressure-volume plots show a reduction in the peak pressure with each cycle as shown in Appendix Figure 2 and Appendix Figure 3. Similarly, the end displacement (a measure of overall axial lengthening) also increased with each cycle. Although the greatest change occurs after the very first inflation, a small decrease in pressure continues to the tenth inflation. Appendix Figure 3c compares the profiles for the 6 mL inflation over 10 cycles to show how the bulge is accentuated with more cycles.

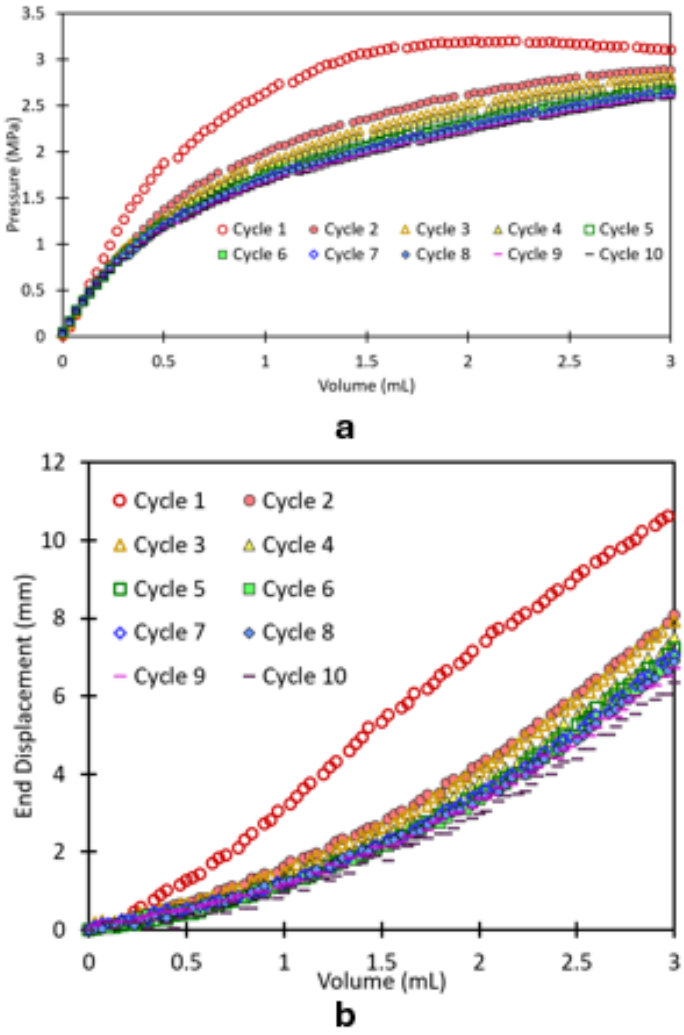

Appendix Figure 2 a. Pressure volume plots for each inflation cycle (inflate to 3mL). b. End displacement vs volume plots for each inflation cycle (inflate to 3mL).

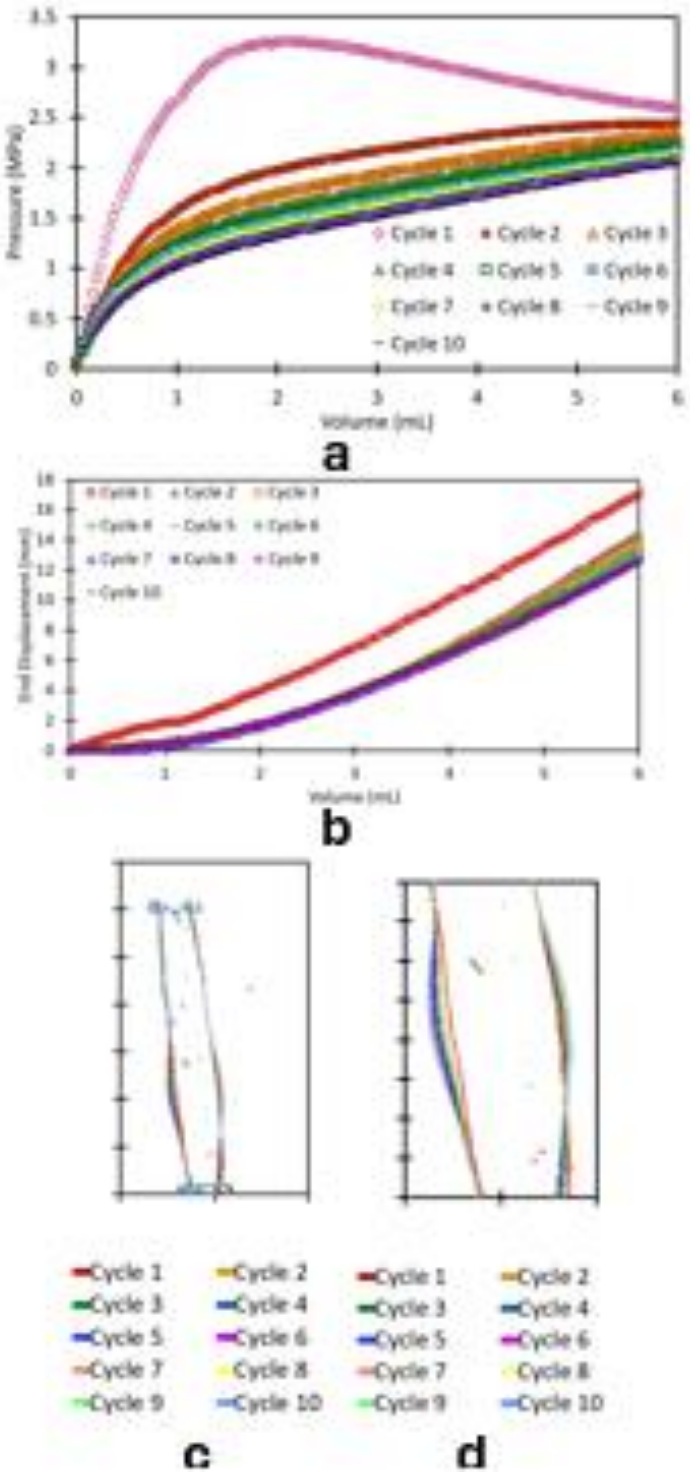

Appendix Figure 3 a. Pressure vs volume vs volume plots for each loading cycle (inflate to 6mL). b. End displacement vs volume plots for each loading cycle. c. Superimposed plots of

the final shape during each cycle of inflation for a polyurethane tube inflated repeatedly to 6 mL. d. Zoomed in view of the bulged section.

Appendix A.3 Strain-Induced Damage in Rubber Balloons

One experiment involving a rubber balloon was done by inflating it with air until a bulge formed and propagated for part of the length of the balloon. The balloon was deflated and reinflated so the bulge propagated along the entire balloon during the second cycle. This was done since the partial inflation during the first cycle caused strain-induced damage for the part of the balloon that experienced bulging while leaving the other part largely unaffected. Three coexisting diameters formed when the amount of inflation in the second cycle was sufficient to cause an instability but not sufficient to force the instability to propagate beyond the damaged section. The moderate diameter in this region was likely caused by softening due to the strain-induced damage from the previous loading cycle while also not experiencing propagation. The results can be seen in Appendix Figure 4.

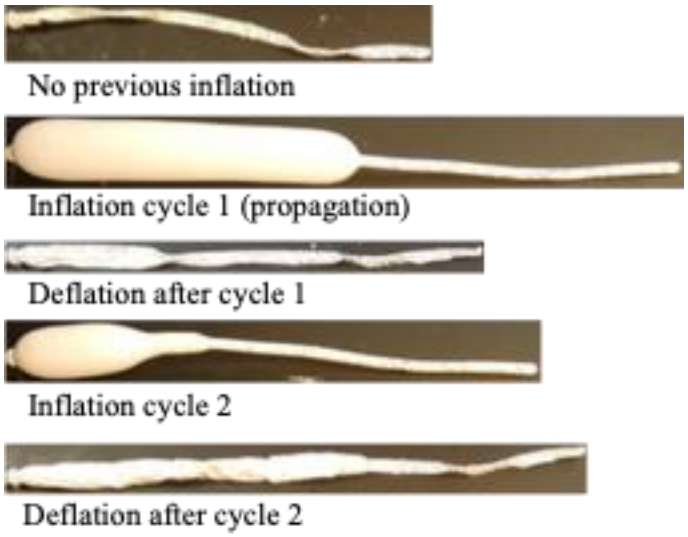

Appendix Figure 4 Partial inflation, deflation, and reinflation of a rubber balloon. The first cycle caused strain-induced damage on the part of the balloon that experienced large deformations due to bulging. During reinflation, three coexisting diameters were visible when the large bulge only covered part of the damaged section.

Appendix A.4 Engraved Defects

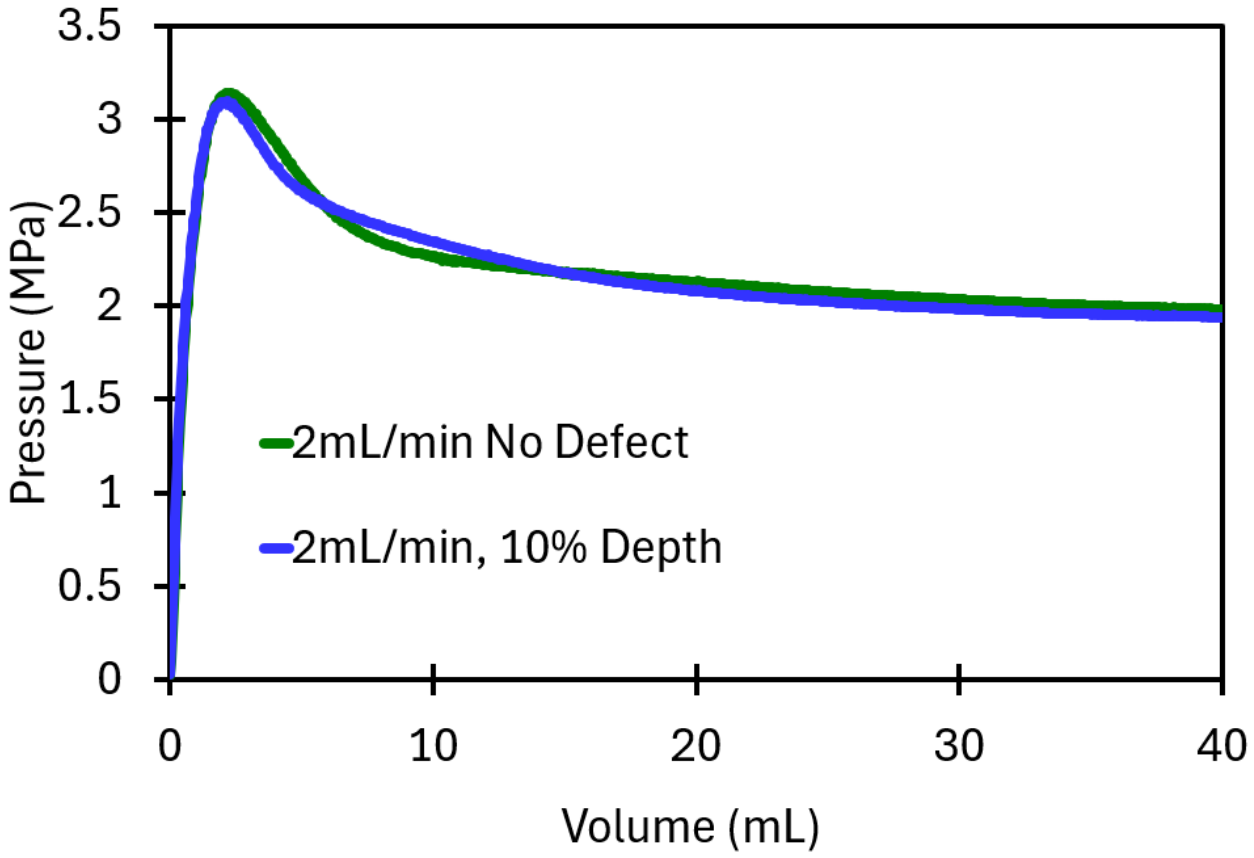

Appendix Figure 5 Pressure volume plots for unconstrained polyurethane tubes with at 2mL/min and 10mL/min.

Due to the theoretical pressure-volume curve (assuming hyperelasticity and uniform expansion) being nearly monotonic (Appendix Figure 6), one possible explanation for the appearance of multiple bulges is that the properties of the tube just happen to be on the borderline between uniform expansion and localization with propagation. A sketch a pressure-volume curve that is at the borderline between uniform expansion and bulge propagation is shown in Appendix Figure 6. One way to test this is to add a defect to force a single bulge initiation and see how the bulge behaves. If the multiple bulges are indeed due to the material properties being borderline

between a monotonic and a non-monotonic PV curve, the single bulge should form on the defect, and reduce the pressure. The bulge should then propagate axially with continued inflation.

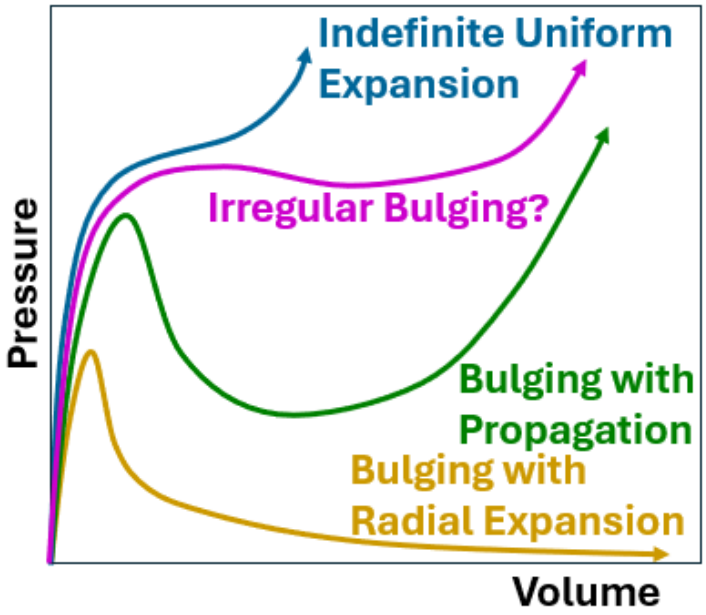

Appendix Figure 6 high, medium, low, and borderline-high strain hardening pressure-volume curves while assuming uniform expansion.

A LaserPecker LP2 Engraver 2 was used to create a defect on the polyurethane tubes. Each tube had one defect engraved in the circumferential direction to force axisymmetric bulging. When the defects were added, the behavior was qualitatively similar to that in the absence of bulges but some subtle changes happened. During inflation, the first bulge initiated on the defect consistently but it did not stop subsequent bulges from forming as seen in Appendix Figure 7e. The initial bulge also tended to be more pronounced compared to tubes without defects. Based on the lack of a propagating bulge from this test, the irregular expansion is likely not due to a borderline case between uniform expansion and a propagating bulge.

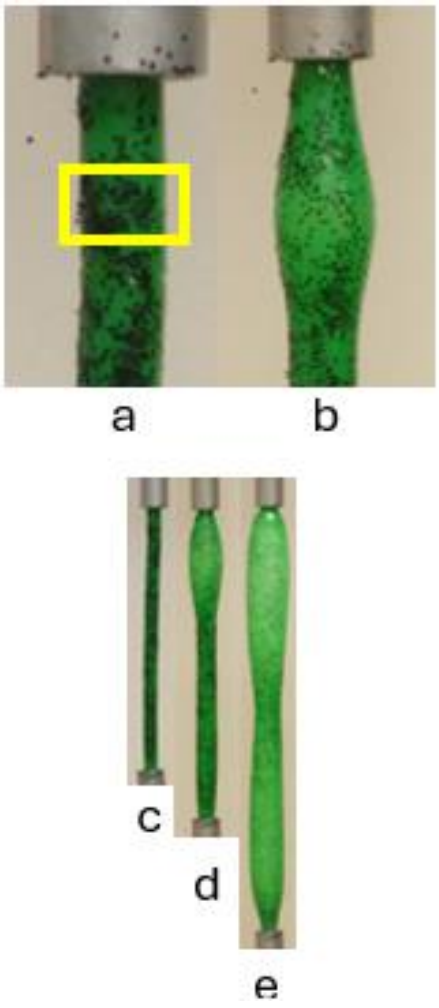

Appendix Figure 7 a. Laser-engraved defect. b. Zoomed in view of bulge initiating on defect. c. Zoomed out veiw of initial configuration. d. Zoomed out view of bulge initiating on defect. e. Second bulge forms later.

Appendix A.5 Varying Tube Geometry

Due to the possibility of tube geometry being a factor in instability formation, tubes with different diameters and wall thicknesses were also tested. Some of these dimensions were chosen to see

how the wall thickness to diameter ratio affects the behavior. Appendix Table 1 shows the chosen tube dimensions.

Appendix Table 1 tube geometries and maximum pressures

Tube outer diameter (in)	Tube inner diameter (in)	V_0 (mL)	P_{max} (MPa)
1/8	0.066	0.763	4.40
1/4	1/8	2.05	4.45
1/4	5/32	2.40	2.86
3/8	0.245	6.62	2.74

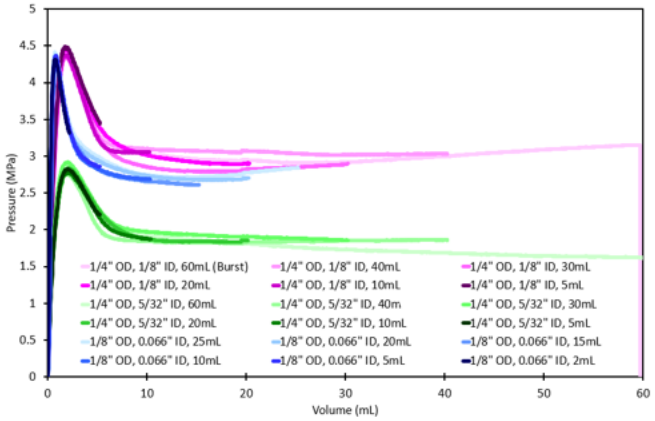

a

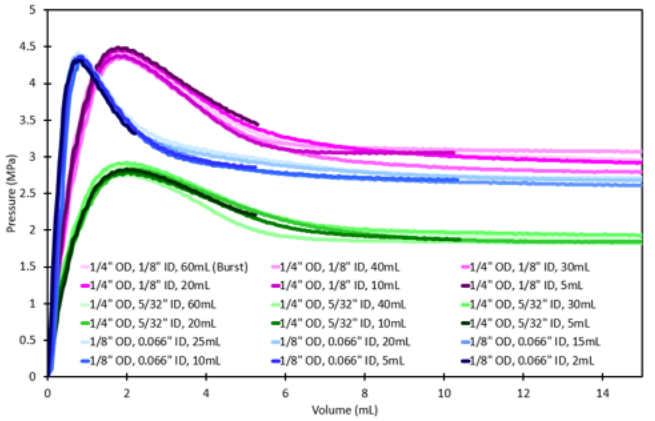

b

Appendix Figure 8 a. Pressure volume plots for polyurethane tubes with various diameters and various final volumes. b. Zoomed in version of part a.

As shown in the plots in Appendix Figure 8, increasing the wall thickness to diameter ratio increases the peak and steady state pressures. This is qualitatively consistent with most pressure vessel models for thin and thick-walled tubes. This also makes sense intuitively since the hoop stresses are smaller at each given pressure.

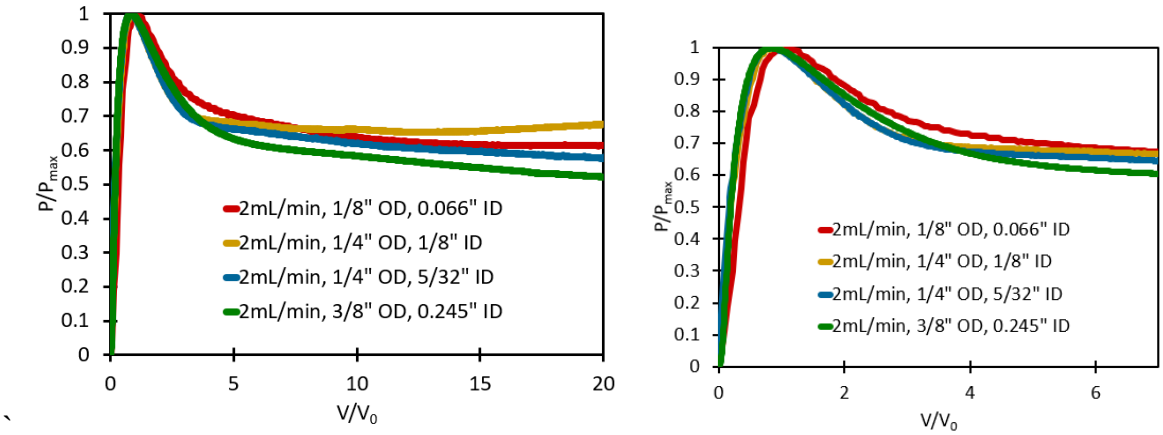

Appendix Figure 9 Normalized pressure vs normalized volume for polyurethane tubes of varying diameters.]

When the volume and pressure are normalized by V_0 (based on mean diameter) and P_{max} respectively, the pressure-volume curves collapse well especially at lower volumes. In the above graph, P_{max} is the maximum pressure of each plot and V_0 is the initial volume of each tube with the mean radius being used along with the initial length of the tube not constrained by any cuffs or connectors. Values for V_0 and P_{max} for each tube geometry are shown in Appendix Table 1. The variations between each test are likely due to the flow rate normalized by the initial volume increasing. This means that although the flow rate used in each set of experiments was the same, the tubes with smaller initial volumes experienced higher strain rates. This disparity leaves the possibility of the errors being caused by viscoelastic effects.

Appendix A.6 Relaxation Tests

Tests were done by inflating the tubes to set volumes and holding them at those volumes as shown in Appendix Figure 10a. These tests were done to test whether viscoelasticity or strain-induced damage were more important for causing the pressure (and therefore the wall stress) to reduce when the tube was held at a constant volume. At lower volumes, it was hypothesized that the decrease in pressure after stopping inflation would be small due to the tube being stiffer since damage effects are smaller. At higher volumes, the opposite was predicted. Although the degree of pressure loss was expected to be different at different volumes, there was expected to be some

pressure loss at all volumes due to viscoelastic effects. This pressure loss was expected to be sharpest right after pumping is stopped and approach a steady state value.

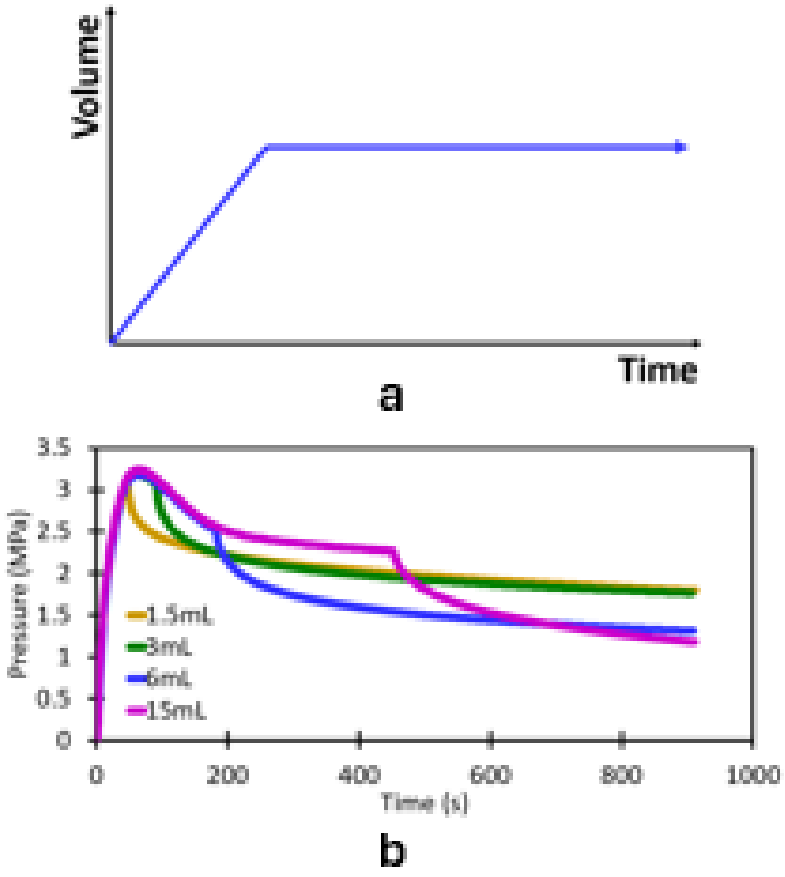

Appendix Figure 10 a. Volume curve for tubes in this experiment. Tubes are inflated to a set volume and held for a period of time afterwards. b. Pressure time plots of polyurethane tubes inflated to set volumes and held.

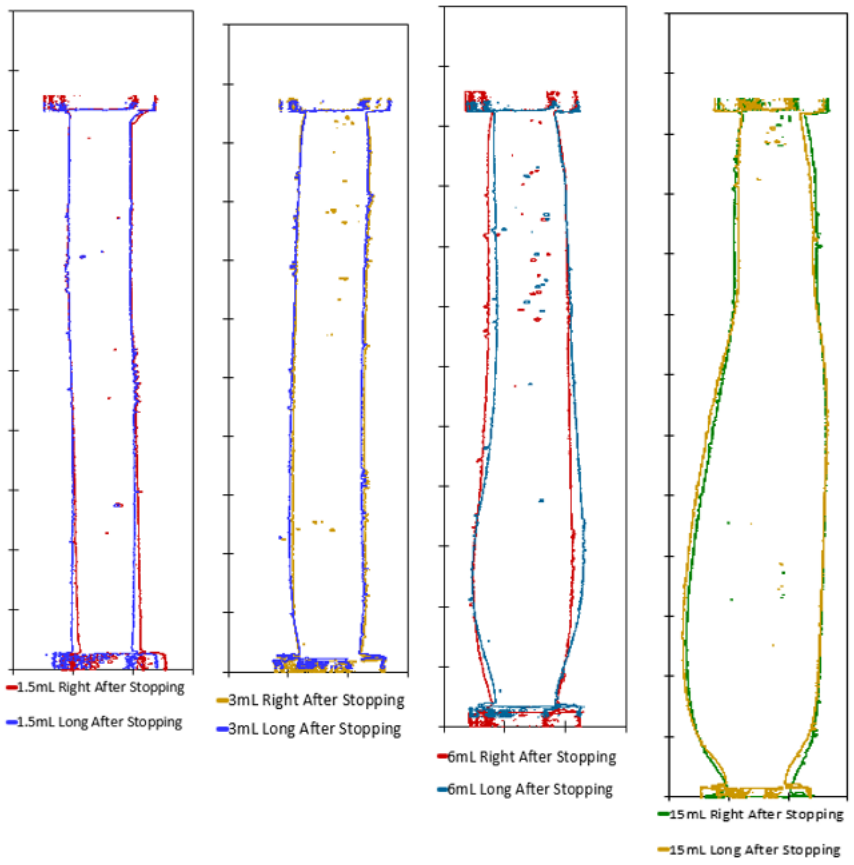

Appendix Figure 11 Superimposed outlines of polyurethane tubes being inflated to set volumes. One outline shows the tube right after inflation is stopped and the other outline shows the tube long after inflation is stopped.

These experiments involved inflating polyurethane tubes with a ¼" outer diameter and a 5/32" inner diameter to set volumes of 1.5mL, 3mL, 6mL, and 15mL and holding the tubes at those volumes for up to 850 seconds. A check valve was used for each test to prevent water from leaving the tube once inflation is stopped, keeping the volume constant after the completion of inflation. When the tubes were loaded to a set volume and held at that volume for extended periods of time,

the pressure decreased. This decrease is sharp at first but becomes more gradual as the time increases. However, it was seen that the decreases in pressure were large at all volumes. Image processing showed that when the tubes were held at a set volume, there were small changes in shape when the set volume was sufficiently high. When the set volume was high enough to show significant bulging, holding at that volume resulted in a slight exaggeration of the bulged section, a slight shrinkage of the lightly inflated section, and a slight shrinkage in total length. No significant changes in shape were observed when holding at lower set volumes. Due to the relatively large drop in pressure at all volumes, it can be said that viscoelasticity has a large effect on the mechanical behavior of the tubes. In contrast, the significant decrease in pressure at the smallest volumes suggests that strain-induced damage is not the main reason for the drop in pressure.

Appendix A.7 Supplementary Rate Effects Data

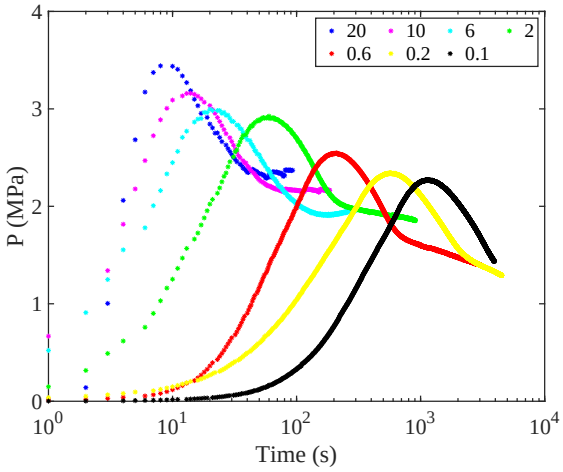

Appendix Figure 12 Same data as Figure 4.6 in the main paper, but with log(time) on the x-axis. Legend lists the various flow rate experiments listed in the legend (all in mL/min).

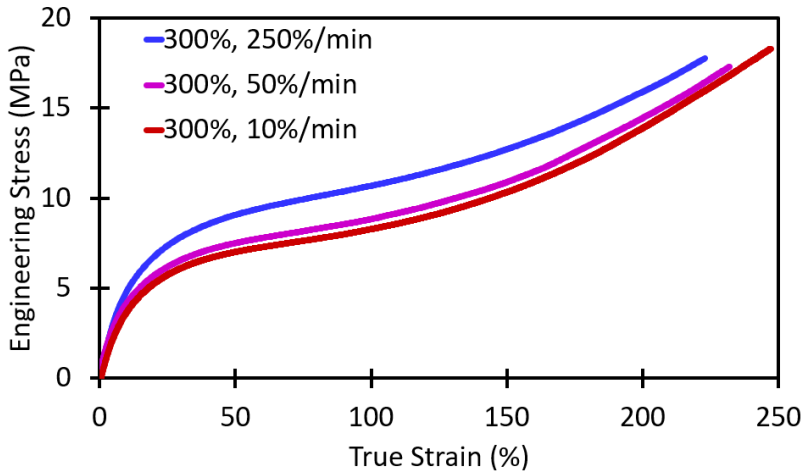

Appendix Figure 13 Uniaxial tests performed at nominal strain rates of 10%/min, 50%/min, and 250%/min.

Appendix B Supplemental LDPE Tube Data

Appendix B.1 Elastic Modulus vs Limiter Size

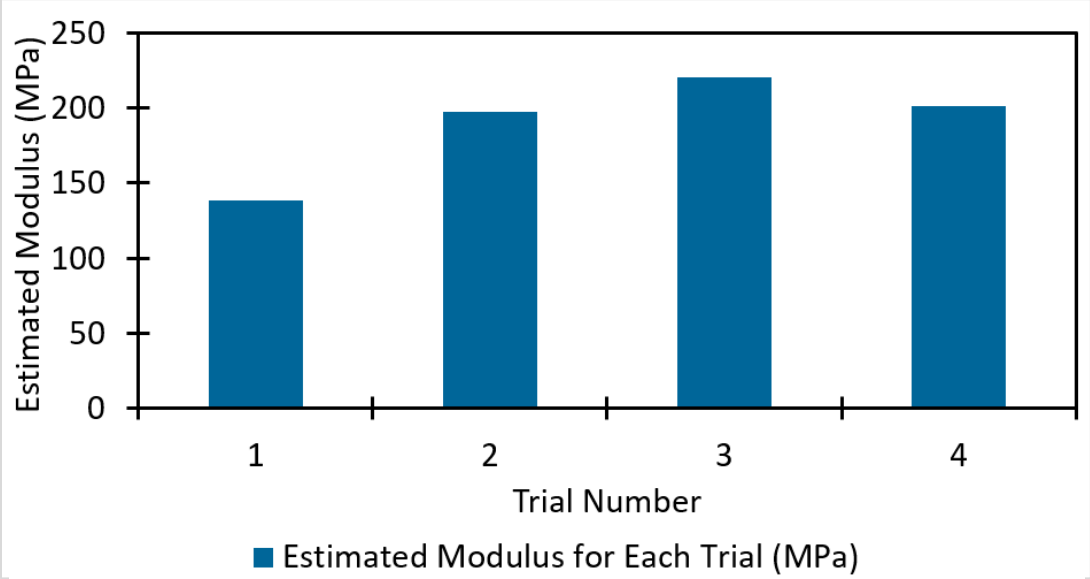

Appendix Figure 14 Estimated elastic modulus for trials run with a 12mm limiter diameter.

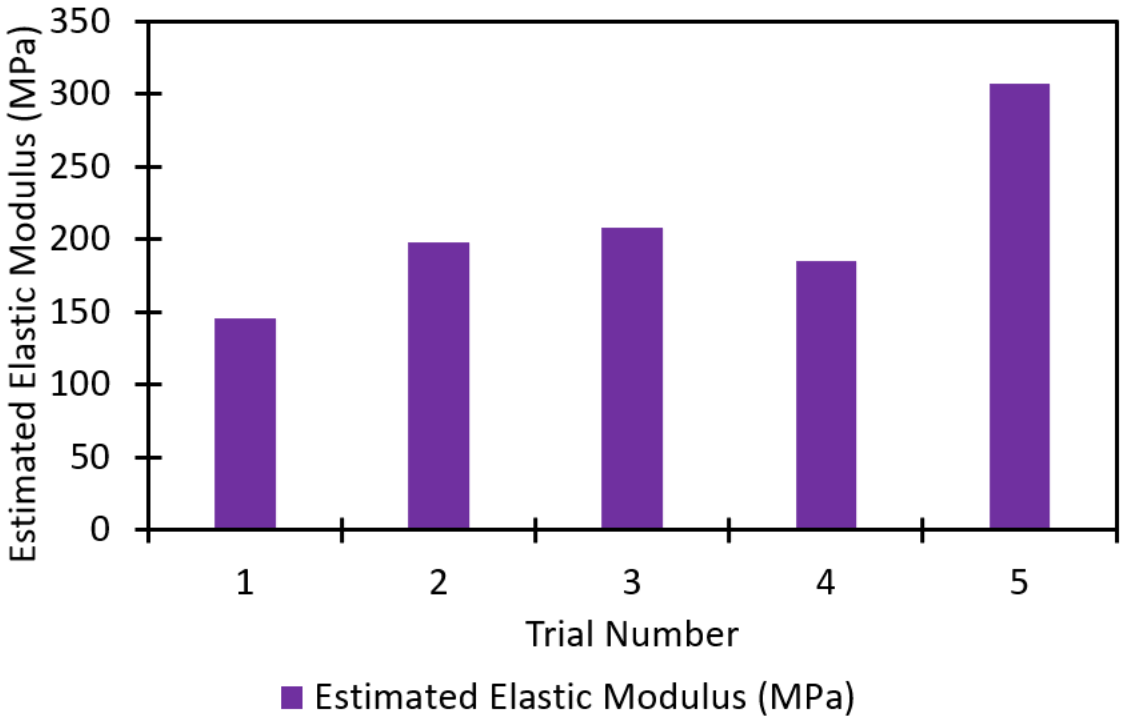

Appendix Figure 15 Elastic moduli for trials with an 11.4mm limiter diameter.

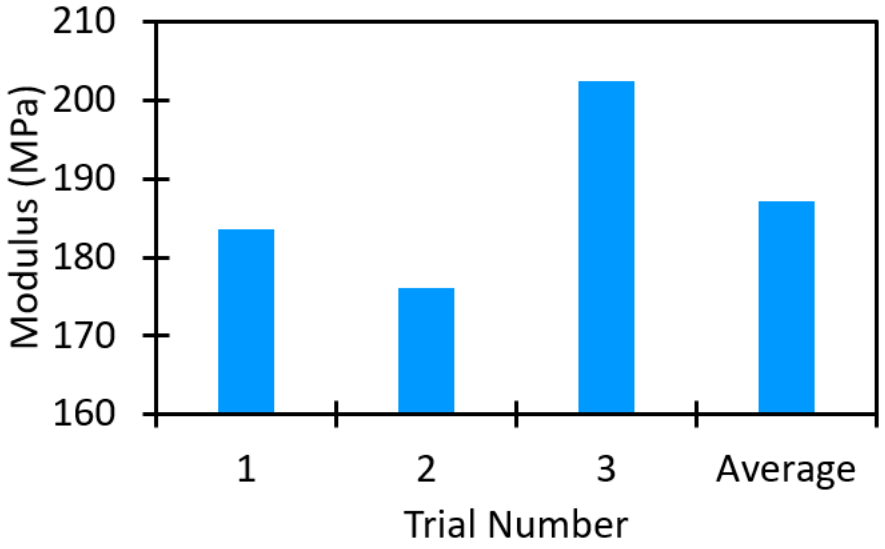

Appendix Figure 16 Estimated elastic moduli for trials with a 9.3mm limiter diameter.

Appendix B.2 Propagation Velocity and End Displacement at various Limiter Sizes

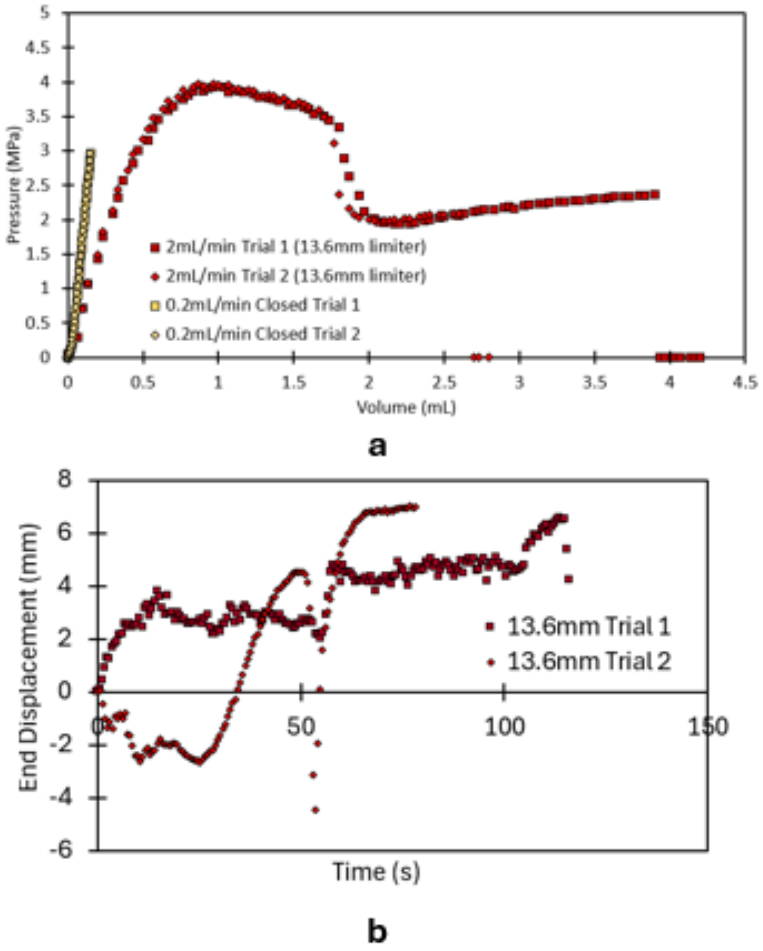

Appendix Figure 17 a. Pressure-volume relations for trials with a 13.6mm diameter limiter when compared to trials with a 10.2mm diameter limiter. b. End displacement vs time for the above

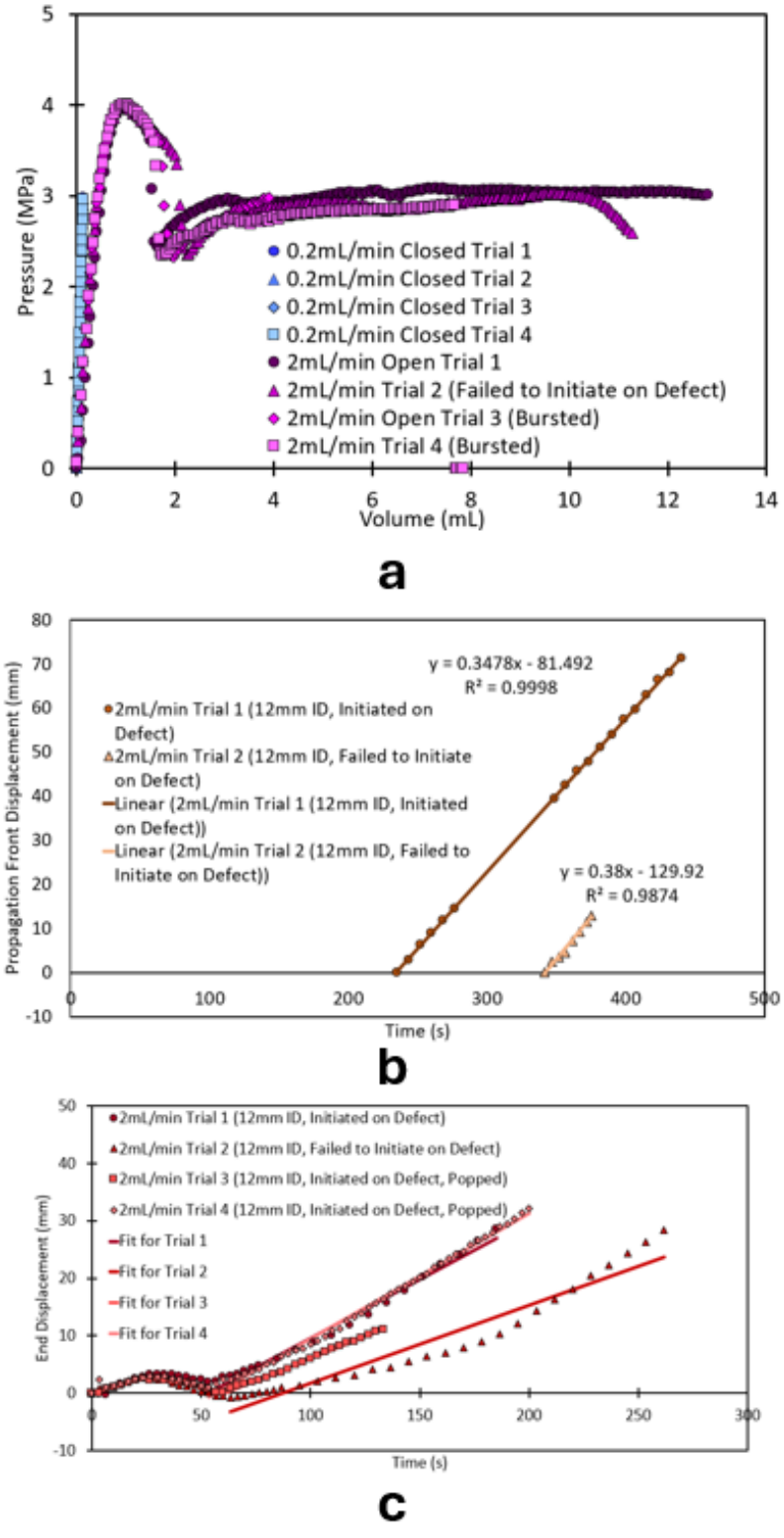

Appendix Figure 18 a. Pressure volume plots for LDPE tubes with a 12mm limiter run at 2mL/min. b. Propagation front displacement versus time for trials with a 12mm limiter

diameter. Slope indicates propagation velocity. c. End displacements for trials with a 12mm limiter diameter.

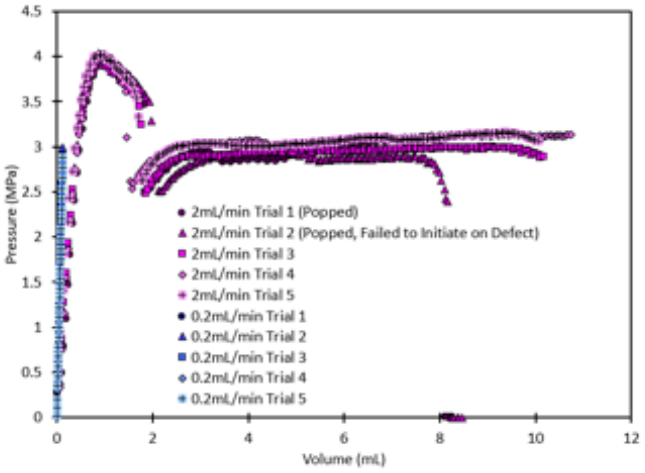
Pressure (MPa)
Volume (mL)
2mL/min Trial 1 (Popped)
2mL/min Trial 2 (Popped, Failed to Initiate on Defect)
2mL/min Trial 3
2mL/min Trial 4
2mL/min Trial 5
0.2mL/min Trial 1
0.2mL/min Trial 2
0.2mL/min Trial 3
0.2mL/min Trial 4
0.2mL/min Trial 5

a

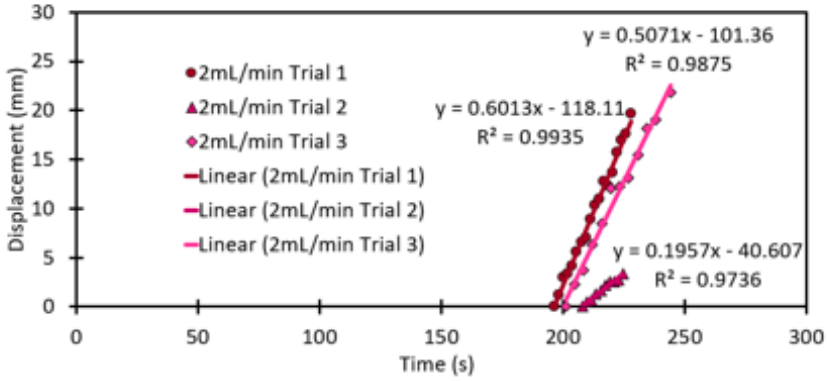
Displacement (mm)
Time (s)
2mL/min Trial 1
2mL/min Trial 2
2mL/min Trial 3
Linear (2mL/min Trial 1)
Linear (2mL/min Trial 2)
Linear (2mL/min Trial 3)
y = 0.5071x - 101.36
R² = 0.9875
y = 0.6013x - 118.11
R² = 0.9935
y = 0.1957x - 40.607
R² = 0.9736

b

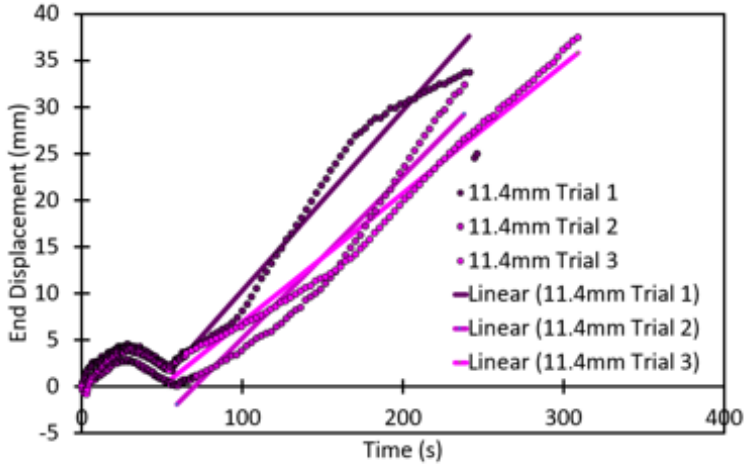
End Displacement (mm)
Time (s)
11.4mm Trial 1
11.4mm Trial 2
11.4mm Trial 3
Linear (11.4mm Trial 1)
Linear (11.4mm Trial 2)
Linear (11.4mm Trial 3)

c

Appendix Figure 19 a. Pressure-volume relations for trials with an 11.4mm limiter diameter. b. Propagation front displacements for trials with an 11.4mm limiter diameter. Slopes give propagation velocities. c. End dislacement vs time for 11.4mm trials.

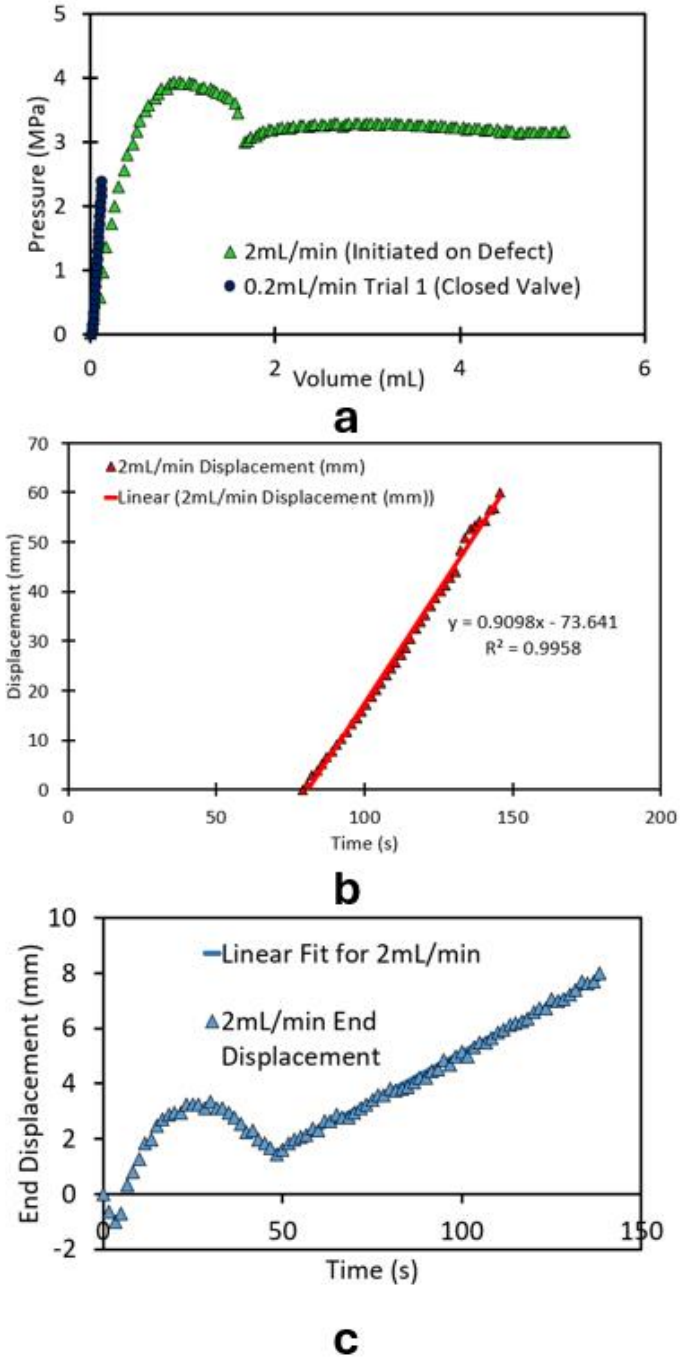

Appendix Figure 20 a. Pressure-volume plot for 10.2mm limiter test. b. Propagation front displacement vs time. c. End displacement vs time.

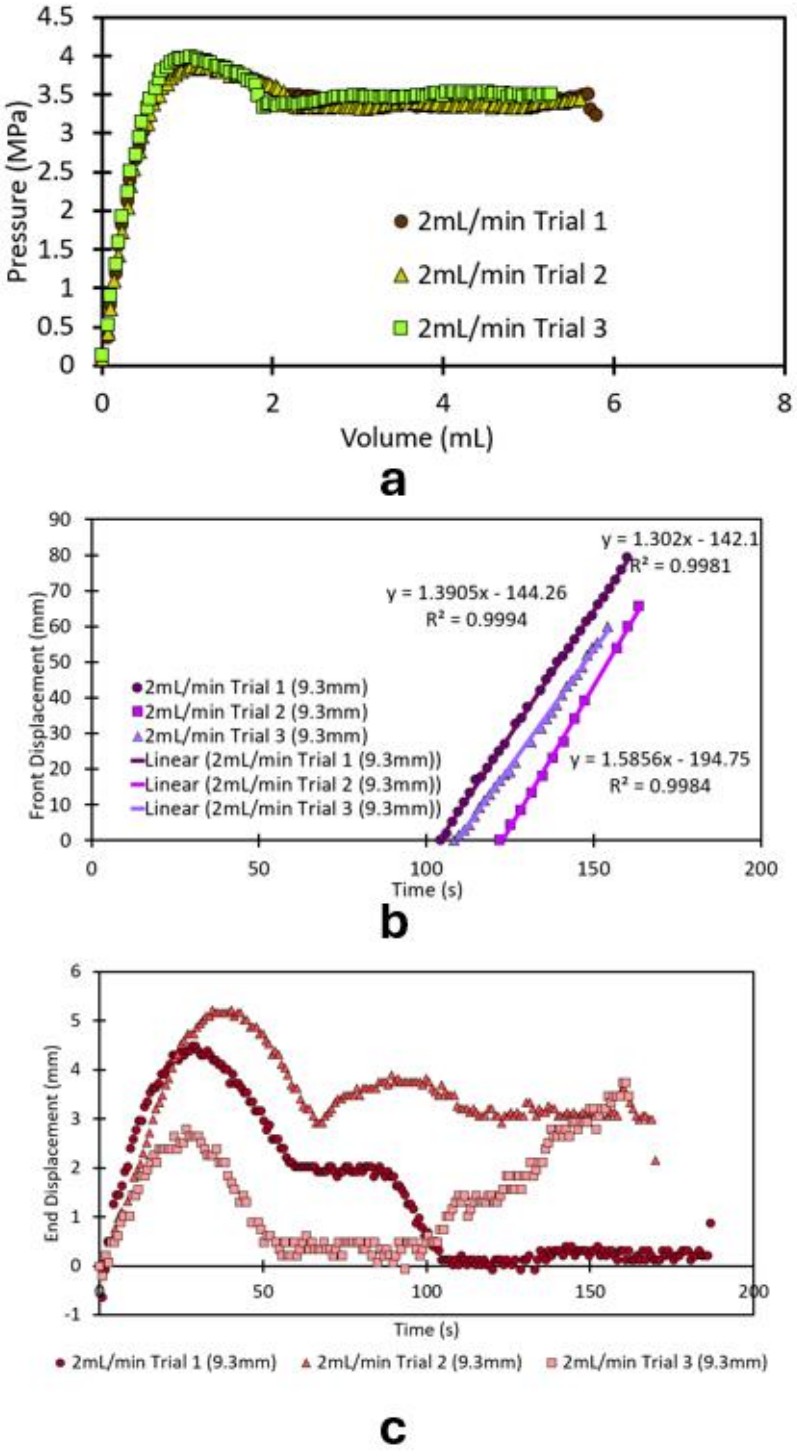

Appendix Figure 21 a. Pressure-volume relations for trials with a 9.3mm limiter diameter. b. Propagation front displacement (slope gives propagation velocity). c. End displacement vs time.

Bibliography

[1] Marthelot, J., Andrade-Silva, I., 2022, "Fabric-based star soft robotic gripper," *Advanced Intelligent Systems*, 2200435, pp. 1-9

[2] Hearn, Edwin John, 1997, *Mechanics of Materials 1*. Elsevier. 10.1016/B978-0-7506-3265-2.X5000-2

[3] Hearn, Edwin John, 1997, *Mechanics of Materials 2*. Elsevier. 10.1016/B978-0-7506-3266-9.X5000-8

[4] Moser, A. P., Folkman, S. 2008. *Buried Pipe Design, 3rd Edition,* McGraw Hill, New York.

[5] Kyriakides, S., Chang, Y., 1990, "On the inflation of a long elastic tube in the presence of axial load," *International Journal of Solids and Structures* 26(9-10): 975-991

[6] Kyriakides, S., Chang, Y., 1991, "The initiation and propagation of a localized instability in an inflated elastic tube," *International Journal of Solids and Structures* 27(9): 1085-1111

[7] Qinghua, Q., Xiaowei, X., Liu, Z., Feng, Q., and Neng, Z., 2022, "Research on YOLOX-based tire defect detection method," Proceedings of the 2022 6th CAA International Conference on Vehicular Control, Nanjing, China, October 28-30, 2022, DOI: 10.1109/CVCI56766.2022.9964564

[8] Larsson, M., Needleman, A., Tvergaard, V., Storakers, B., 1982, “Instability and failure of internally pressurized ductile metal cylinders,” *J. Mech. Phys. Solids* 30(3): 121-154, DOI: 10.1016/0022-5096(82)90020-5

[9] Hillmansen, S., Hobeika, S., Haward, R. N., and Leevers, P., S., 2004, “The effect of strain rate, temperature, and molecular mass on the tensile deformation of polyethylene,” *Polymer Engineering and Science* 40(2): 481-489, DOI:10.1002/pen.11180

[10] H. Alexander, “The tensile instability of an inflated cylindrical membrane as affected by an axial load,” *Int J Mech Sci*, vol. 13, pp. 87–95, 1970.

[11] W. L. Yin, “Non-uniform inflation of a cylindrical elastic membrane and direct determination of the strain energy function,” *J Elast*, vol. 7, no. 3, 1977.

[12] D. M. Haughton and R. W. Ogden, “Bifurcation of inflated circular cylinders of elastic material under axial loading-I. Membrane theory for thin-walled tubes,” 1978.

[13] A. D. Kydontefs, “Finite axisymmetric deformations of an initially cylindrical elastic membrane enclosing a rigid body,” *Q J Mech Appl Math*, 1968.

[14] A. D. Kydoniefs and A. J. M. Spencer, “Finite axisymmetric deformations of an initially cylindrical elastic membrane,” *Q J Mech Appl Math*, vol. 22, 1969.

[15] Y. Liu, Y. Ye, A. Althobaiti, and Y. X. Xie, “Prevention of localized bulging in an inflated bilayer tube,” *Int J Mech Sci*, vol. 153–154, pp. 359–368, 2019.

[16] Y. Ye, Y. Liu, and Y. Fu, “Weakly nonlinear analysis of localized bulging of an inflated hyperelastic tube of arbitrary wall thickness,” *J Mech Phys Solids*, vol. 135, 2020.

[17] Y. B. Fu, S. P. Pearce, and K. K. Liu, “Post-bifurcation analysis of a thin-walled hyperelastic tube under inflation,” *Int J Non Linear Mech*, vol. 43, no. 8, pp. 697–706, 2008.

[18] S. Kyriakides and Y.-C. Chang, “The initiation and propagation of a localized instability in an inflated elastic tube,” *Int J Solids Structures*, vol. 27, pp. 1085–1111, 1991.

[19] A. A. Alhayani, J. Rodríguez, and J. Merodio, “Competition between radial expansion and axial propagation in bulging of inflated cylinders with application to aneurysms propagation in arterial wall tissue,” *Int J Eng Sci*, vol. 85, pp. 74–89, 2014.

[20] Y. B. Fu, J. L. Liu, and G. S. Francisco, “Localized bulging in an inflated cylindrical tube of arbitrary thickness - The effect of bending stiffness,” *J Mech Phys Solids*, vol. 90, pp. 45–60, 2016.

[21] J. W. Pazin, F. Rouhani, and S. Velankar, “In preparation,” 2024.

[22] J. W. Pazin, “M.S. thesis Inelastic tube inflation,” Mechanical engineering department of University 0f Pittsburgh, 2024.

[23] M. Takla, “Non-symmetric bifurcation and collapse of elastic-plastic thick-walled cylinders under combined radial and axial loading,” *Marine Structures*, vol. 64, pp. 246–262, 2019.

[24] M. Takla, “Insight into elastic–plastic bifurcation of pressurized cylinders: Transition between bulging and necking; the line of catastrophic failure,” *Int J Mech Sci*, vol. 148, pp. 73–83, 2018.

[25] M. Takla, “Instability and axisymmetric bifurcation of elastic-plastic thick-walled cylindrical pressure vessels,” *International Journal of Pressure Vessels and Piping*, vol. 159, pp. 73–83, 2018.

[26] B. Lindgreen, V. Tvergaard, and A. Needleman, “Bulge formation and necking in a polymer tube under dynamic expansion,” *Model Simul Mat Sci Eng*, vol. 16, no. 8. 2008.

[27] L. P. Mikkelsen and V. Tvergaardd, “A nonlocal two-dimensional analysis of instabilities in tubes under internal pressure,” 1999.

[28] S. Kyriakides and Chang Yu-Chung, “On the inflation of a long elastic tube in the presence of axial load,” *International journal Solids Structures*, vol. 26, pp. 975–991, 1990.

[29] Z. Guo, J. Gattas, S. Wang, L. Li, and F. Albermani, “Experimental and numerical investigation of bulging behaviour of hyperelastic textured tubes,” *Int J Mech Sci*, vol. 115–116, pp. 665–675, 2016.

[30] S. Wang, Z. Guo, L. Zhou, L. Li, and Y. Fu, “An experimental study of localized bulging in inflated cylindrical tubes guided by newly emerged analytical results,” *J Mech Phys Solids*, vol. 124, pp. 536–554, 2019.

[31] L. Horný and M. Netušil, “How does axial prestretching change the mechanical response of nonlinearly elastic incompressible thin-walled tubes,” *Int J Mech Sci*, vol. 106, pp. 95–106,2016.

[32] D. M. Haughton and R. W. Ogden, “Bifurcation of inflated circular cylinders of elastic material under axial loading-II. Exact theory for thick-walled tubes,” *J. Mech. Phys. Solids*, vol. 27, 1979.

[33] S. Kyriakides and Y.-C. Chang, “On the inflation of a long elastic tube in the presence of axial load,” *Int J Solids Structures*, vol. 26, no. 9/10, pp. 975–991, 1990.

[34] R. W. Ogden, “Large deformation isotropic elasticity – on the correlation of theory and experiment for incompressible rubberlike solids,” *Proceedings of the Royal Society of London. A. Mathematical and Physical Sciences*, vol. 326, no. 1567, pp. 565–584, Feb. 1972.

[35] R. De Pascalis, W. J. Parnell, I. David Abrahams, T. Shearer, D. M. Daly, and D. Grundy, "The inflation of viscoelastic balloons and hollow viscera," in *Proceedings of the Royal Society A: Mathematical, Physical and Engineering Sciences*, Royal Society Publishing, Oct. 2018.

[36] Bilgin, O., Stewart, H., and O'Rourke, T. 2007, "Thermal and mechanical properties of polyethylene pipes," *Journal of Materials in Civil Engineering,* 19(12), 1043-1052, DOI: https://doi.org/10.1061/(ASCE)0899-1561(2007)19:12(1043)

[37] Krishnaswamy, R. 2005. "Analysis of ductile and brittle failures from creep rupture testing of high-density polyethylene," *Polymer,* 46(25), 11664-11672, DOI: https://doi.org/10.1016/j.polymer.2005.09.084

[38] Hamouda, H., Simoes-Betbeder, M., Grillon, F., Blouet, P., Billon, N., and Piques, R. 2001. "Creep damage mechanisms in polyethylene gas pipes," *Polymer*, 42(12), pp. 5425-5437, DOI: 10.1016/S0032-3861(00)00490-0

[39] Mulliken, A., D., Boyce, M., C. 2005. "Mechanics of rate-dependent elastic-plastic deformation of glassy polymers from low to high strain rates," *International Journal of Solids and Structures,* 43, pp. 1331-1356, DOI: https://doi.org/10.1016/j.ijsolstr.2005.04.016

[40] Hansen, U., Zioupos, P., Simpson, R., Currey, J., and D., Hynd, D. 2008. “The effect of strain rate on the mechanical properties of human cortical bone,” *Journal of Biomechanical Engineering,* 130(1): 011011, DOI: https://doi.org/10.1115/1.2838032

[41] Brady, T., E. and Yeh, G., S. 1971. “Yielding behavior of glassy amorphous polymers,” *Journal of Applied Physics,* 42, pp. 4622-4630, DOI: https://doi.org/10.1063/1.1659831

[42] Korkolis, Y., P. and Kyriakides, S. 2008. “Inflation and burst of anisotropic aluminum tubes for hydroforming applications, *International Journal of Plasticity,* 24(3), pp. 509-543. DOI: https://doi.org/10.1016/j.ijplas.2007.07.010

[43] Niestrawska, J., A., Viertler, C., Regitnig, P., Cohnert, T., U., Sommer, G., and Holzapfel, G., A. 2016. “Microstructure and mechanics of healthy and aneurysmatic abdominal aortas: experimental analysis and modeling,” *Journal of the Royal Society Interface,* 13: 20160620, DOI: https://doi.org/10.1098/rsif.2016.0620

[44] Vande Geest, J., P., Sacks, M., S., and Vorp, D., A. 2005. “The effects of aneurysm on the biaxial mechanical behavior of human abdominal aorta,” *Journal of Biomechanics,* 39, pp. 1324-1334, DOI: https://doi.org/10.1016/j.jbiomech.2005.03.003

[45] Sherifova, S., Sommer, G., Viertler, C., Regtnig, P., Caranasos, T., Smith, M., A., Griffith, B., E., Ogden, R., W., and Holapfel, G., A. 2019. “Failure properties and microstructure of healthy and aneurysmatic human thoracic aortas subjected to uniaxial extension with a focus on the media,” *Acta Biomaterialia*, 99, pp. 443-456, DOI: https://doi.org/10.1016/j.actbio.2019.08.038

[46] Robertson, A., M., Duan, X., Aziz, K., M., Hill, M., R., Watkins, S., C., and Cebral, J., R. 2015. “Diversity in the strength and structure of unruptured cerebral aneurysms,” *Annals of Biomedical Engineering,* 43(7), pp. 1502-1515, DOI: 10.1007/s10439-015-1252-4

[47] Gupta, V., B., Keller, A., and Ward, I., M. 1967. “The effect of crystallite orientation on mechanical anisotropy of low-density polyethylene,” *Journal of Macromolecular Science,* Part B, 2(1), pp. 139-146, DOI: 10.1080/00222346808212868

[48] Sabbagh, A., B., and Lesser, A., J. 1999. “On the phenomena of deformation and neck formation in LLDPE films subjected to uniaxial and biaxial loading conditions,” *Journal of Polymer Science Part B: Polymer Physics*, 37(18), pp. 2651-2663

[49] Smith, P., Lemstra, P., J., and Pijpers, P., L. 1982. “Tensile strength of highly oriented polyethylene. II. Effect of molecular weight distribution,” *Journal of Polymer Science: Polymer Physics Edition,* 20(12), pp. 2229-2241, DOI: https://doi.org/10.1002/pol.1982.180201206